MONTHLY NOTICES

OF THE

ROYAL ASTRONOMICAL SOCIETY

Vol. 112 No. 2 1952

Published and Sold by the

ROYAL ASTRONOMICAL SOCIETY

BURLINGTON HOUSE

LONDON, W. 1

Price Thirteen Shillings and Sixpence

NOTICE TO AUTHORS

1. *Communications.*—Papers must be communicated to the Society by a Fellow. They should be accompanied by a summary at the *beginning* of the paper conveying briefly the content of the paper, and drawing attention to important new information and to the main conclusions. The summary should be intelligible in itself, without reference to the paper, to a reader with some knowledge of the subject; it should not normally exceed 200 words in length. **Authors are requested to submit MSS. in duplicate. These should be typed using double spacing and leaving a margin of not less than one inch on the left-hand side. Corrections to the MSS. should be made in the text and not in the margin.** Unless a paper reaches the Secretaries more than seven days before a Council meeting it will not normally be considered at that meeting. By Council decision, MSS. of accepted papers are retained by the Society for one year after publication; unless their return is then requested by the author, they are destroyed.

2. *Presentation.*—Authors are allowed considerable latitude, but they are requested to follow the general style and arrangement of *Monthly Notices*. References to literature should be given in the standard form, including a date, for printing either as footnotes or in a numbered list at the end of the paper. Each reference should give the **name and initials** of the author cited, irrespective of the occurrence of the name in the text (some latitude being permissible, however, in the case of an author referring to his own work). The following examples indicate the style of reference appropriate for a paper and a book, respectively :—

A. Corlin, *Zs. f. Astrophys.*, **15**, 239, 1938.
H. Jeffreys, *Theory of Probability*, 2nd edn., section 5.45, p. 258, Oxford, 1948.

3. *Notation.*—For technical astronomical terms, authors should conform closely to the recommendations of Commission 3 of the International Astronomical Union (*Trans. I.A.U.*, Vol. VI, p. 345, 1938). Council has decided to adopt the I.A.U. 4-letter abbreviations for constellations where contraction is desirable (Vol. IV, p. 221, 1932). In general matters, authors should follow the recommendations in *Symbols, Signs* and *Abbreviations* (London : Royal Society, 1951) except where these conflict with I.A.U. practice.

4. *Diagrams.*—**These should be designed to appear upright on the page, drawn about twice the size required in print and prepared for direct photographic reproduction except for the lettering, which should be inserted in pencil. Legends should be given in the manuscript indicating where in the text the figure should appear.** Blocks are retained by the Society for 10 years; unless the author requires them before the end of this period they are then destroyed.

5. *Tables.*—**These should be arranged so that they can be printed upright on the page.**

6. *Proofs.*—Costs of alterations exceeding 5 per cent of composition must be borne by the author. Fellows are warned that such costs have risen sharply in recent years, and it is in their own and the Society's interests to seek the maximum conciseness and simplification of symbols and equations consistent with clarity.

7. *Revised Manuscripts.*—When papers are submitted in revised form it is especially requested that they be accompanied by the original MS.

Reading of Papers at Meetings

8. When submitting papers authors are requested to indicate whether they will be willing and able to read the paper at the next or some subsequent meeting, and approximately how long they would like to be allotted for speaking.

9. Postcards giving the programme of each meeting are issued some days before the meeting concerned. Fellows wishing to receive such cards whether for Ordinary Meetings or for the Geophysical Discussions or both should notify the Assistant Secretary.

MONTHLY NOTICES

OF THE

ROYAL ASTRONOMICAL SOCIETY

Vol. 112 No. 2

THEORETICAL LINE PROFILES FOR STARS OF P CYGNI TYPE

J. A. Rottenberg

(Communicated by C. S. Beals)

(Received 1951 November 26)

Summary

A simple model is set up of a star enclosed by an expanding envelope. The star is emitting a continuous spectrum and the envelope scatters radiation in the neighbourhood of a resonance frequency. The profiles which result from these assumptions are of the emission-line type. In varying degrees they show violet absorption borders, central reversals and occultation of the red edge, which are characteristic features of lines in P Cygni spectra.

The profiles are obtained by numerical solution of a pair of integral equations for the emissivity in the envelope and the flux of radiation from the system. The critical parameter for the appearance of central reversal is the ratio of expansion velocity to turbulent velocity in the envelope. ($v/v^* \sim 3$.) Noticeable occultation of the emission component sets in when the effective radii of envelope and star fall below the ratio $R_1/R_0 \sim 1{\cdot}25$.

For profiles in which the net energy in the line exceeds the underlying continuous spectrum, the Zanstra recombination cycle is introduced. The computed contours show, in addition to an increase in intensity of the emission components, an enhancement of the associated central reversal. In some cases this results in obscuring the violet absorption border.

The theoretically derived profiles encompass a wide range of lines, not only of P Cygni type but of some types of Be emission lines as well.

1. *Introduction*

The existence of an extensive atmosphere subject to large-scale motions is now widely accepted in interpreting the emission-line contours of early-type stars. Envelopes of this type have been postulated as early as 1904—by Halm in a paper read to the Royal Society of Edinburgh—and are now used in discussions of the spectra of planetary nebulae*, novae after outburst (**2**, **3**), Wolf–Rayet stars (**4**), and the stars of P Cygni class (**5**). Since these macroscopic motions are of a scale larger than can reasonably be ascribed to thermal agitation or turbulence, one infers that they take the form of a radial expansion. For planetary nebulae, novae and W–R stars this model satisfactorily explains most of the observed features.

* e.g. O. C. Wilson (1).

In the case of P Cygni lines, however, the profiles are often highly complex. Previous analyses of their features by straightforward application of a radially expanding atmospheric model, while successful for the simpler profiles, have for the more detailed ones seemed to require the introduction of a number of *ad hoc* assumptions concerning the acceleration of this motion at various heights in the envelope. In particular the often present "central reversals" have been taken as ground for inferring a sharp deceleration of flow high up in the envelope. Interpretations of this type* throw the burden of explanation on the mechanical aspects of the flow, without examining the necessity of the additional postulates.

The point of view adopted in this paper is that the contours of the emission lines can be explained in terms of simple, somewhat idealized systems, if a close rein is kept on the origin and destination of the radiation under discussion. General equations are set up and the profiles computed in a number of particular cases to show that the characteristic features of the complex P Cygni profiles are consequences of the coupling of the Doppler displacements (resulting from the radial expansion) with the *geometry* assumed in the model. Special assumptions about the velocity gradient are not required. It is however necessary to assign a significant role to resonance scattering, thereby making more precise the mechanisms of absorption and emission which operate to form a line contour.

2. *Atmospheric models and their mathematical idealization*

Failing any evidence to the contrary we make the obvious assumptions throughout the following that the stars with which we are dealing are each

(1) spherically symmetric systems in their physical and dynamical structure;

(2) describable by variables which are time-independent (that is, they are in a "steady state").

In view of the above assumptions the only mechanisms that one can now allow for producing an emission line are those which concentrate energy flux into specific frequencies by depletion—since radiation transfer is subject to energy conservation—of other frequencies of the energy spectrum. For an absorption line one has the reverse. There are two such frequency-changing processes which are recognized as being operative in the atmospheres of early-type stars:

(1) Matter, which absorbs and re-emits light in the same frequency but in different directions as seen from a frame of reference in which the matter is at rest, changes the frequency (as well as the direction) of a ray when the scattering is viewed by an observer with respect to whom the matter is in motion (**8**). This is the manner in which the Doppler effect enters our calculations.

(2) Absorption and re-emission by a process of photoelectric ionization and recombination convert radiation of high frequency into radiation of lower frequencies. This is the Zanstra mechanism (**9**), according to which (in the microscopic view) there is a strong probability of a quantum of radiant energy absorbed beyond the series limit reappearing after absorption in the form of quanta in the lines of the series—due to the possibility of electron capture at any excited level, followed by a sequence of cascade jumps down to the ground state. (One must of course admit the possibility of a similar conversion of quanta from lines of higher excitation into lines of lower excitation.)

* *vide*, e.g., (**6**) and (**7**).

These two processes are not mutually exclusive and there is no method as yet known for deciding when one or the other is *not* operative in the formation of a particular line. When, however, the equivalent width of the emission components of a complex line is greater than the equivalent width of the adjacent absorption components one may safely conclude that process (1) cannot provide an adequate explanation and that therefore process (2) must be at work. The mere existence of a small emission component alongside a deeper absorption component does not however in itself imply recombination, as has usually been assumed. Likewise, when the absorption component is well displaced to the violet or is greatly broadened one may infer that process (1) cannot be ignored.

For the representative case our simplified model takes the form of a perfectly absorbing body (bounded roughly by the reversing layer) which is radiating a continuous spectrum. We call this the star proper, or more simply the star. Enclosing the star we conceive of an expanding envelope, with arbitrary velocity gradient, and in which the ionization and excitation decrease radially outward from the reversing layer. The outermost regions of this envelope will be the ones chiefly active in resonance scattering; whereas the Zanstra mechanism, when it is operative, will be at work in the regions closer to the star. The distinction between these regions of operation is only qualitative, and at best poorly defined. The recombining region, when it exists at all, may be expected to overlap and blend into the scattering region. Again, the field of radiation from the star may be so intense that for a considerable distance outward from the inner boundary of the envelope the temperature of the electron–ion assemblage is so high that very little recombination takes place at all.

Clearly the simpler situation (1 above) is the one in which, *for the line concerned*, no new radiation of that frequency enters the stream beyond the surface of the star proper; that is to say, when there is no region of recombination. This case will be treated first and, as will be seen, the region of scattering will be idealized still further. The residual generality will still be sufficient to provide for most of the distinguishing characteristics in the typical P Cygni profile. The more complicated system, in which there is a recombining region lying between the surface of the star and the region of scattering, will be taken up at the end of the paper, and will be shown to yield P Cygni profiles in which the emission components are of great intensity relative to the absorption. The case of a purely recombining envelope, not enclosed by any region cool enough to permit resonance scattering, is probably more characteristic of the hotter Wolf–Rayet stars and will be given only passing reference here. The profiles for this latter case have already been derived, using comparatively simple methods (**2, 10, 11, 12**).

The tracing of the alterations in a given radiation field, in the course of its passage from the inner boundary of the envelope out to a distant observer, is *properly* a problem of solving an equation of transfer (**8**) subject to the appropriate boundary conditions, velocity distribution and structural symmetry. However, the difficulties encountered in treating even the case of plane-parallel stratification, in the lowest approximation of directional dependence and velocity gradient (**13, 14**), have been considerable. For the more involved case of a spherically symmetric envelope they would be well-nigh insurmountable. In order to avoid having to treat a transfer problem, and yet preserve the significant effect of scattering by a moving medium, we shall suppose that the envelope may be

treated as *geometrically* very thin although remaining optically dense. Thus let κ_ν be the scattering coefficient per unit mass for frequency ν, $\rho(r)$ the density at distance r from the centre, R' the interior radius of the envelope and R'' the exterior radius. Then the optical thickness in the *radial direction* is

$$\tau_\nu = \int_{R'}^{R''} \kappa_\nu \rho(r)\, dr. \tag{1}$$

We assume that this quantity remains finite as we compress the envelope into a thin shell, $R' \to R'' = R$. Consequently, for a ray making an angle $\cos^{-1}\mu$ with the normal to the R' surface, the optical thickness

$$\int_{R'}^{R''} \kappa_\nu \rho(r)\, ds, \qquad ds = \frac{r\, dr}{[r^2 - R'^2(1-\mu^2)]^{1/2}}$$

becomes in the limit

$$\tau_\nu/\mu \tag{2}$$

as $R' \to R''$. This is simply the expression for the optical thickness in any direction of a laminar medium. In like fashion, if $B_\nu(r)$ be the emissivity (Ergiebigkeit) at a point in the envelope, the intensity of the emergent ray, which is given by*

$$\int_{r=R'}^{R''} B_\nu(r) \exp\left\{-\int_{r'=r}^{R''} \kappa_\nu \rho(r')\, ds'\right\} \kappa_\nu \rho(r)\, ds,$$

becomes, in the approximation $R' \to R''$,

$$B_\nu(R) \int_{r=R'}^{R''} \exp\left\{-\int_{r'=r}^{R''} \kappa_\nu \rho(r')\, ds'\right\} \kappa_\nu \rho(r)\, ds$$
$$= B_\nu(R)\{1 - \exp[-\tau(\nu)/\mu]\}. \tag{3}$$

By a consistent use of this limiting process we can take account of directional dependence in a manner more adequate to our purposes than would be provided by the traditional approximation of an outward and an inward beam. *The approximation of a thin shell need not be given a literal interpretation:* R can be considered as an effective "mean radius" for even an extended envelope.

Apart from its control over directional variation of the specific intensity, the general equation of radiative transfer incorporates another important relationship which we must be careful to retain even though we dispense with the transfer equation itself; namely, the energy conservation law. Its application will provide us with the necessary equations for calculating our contours.

3. *Profiles based on the scattering mechanism*

3.1. *The integral equations of the problem.*—Consider a perfectly absorbing body of radius R_0 (see Fig. 1 *a*) radiating in all frequencies with specific intensity F. Let it be enclosed by a "thin shell" (in the sense above) of radius R_1 in which matter is moving radially outwards with velocity v; and let the optical depth for a ray normal to the shell be τ_ν as in (1), ν being the frequency as seen by an observer moving along with the matter in the shell. If $I(\nu, \mu)$ be the intensity of a ray striking the shell at an angle $\cos^{-1}\mu$ to the normal, with apparent frequency ν, then by use of (2) $I \exp[-\tau(\nu)/\mu]$ is the fraction of the ray transmitted without suffering any scattering (Fig. 1 *b*); hence

$$I(\nu, \mu)\{1 - \exp[-\tau(\nu)/\mu]\} \tag{4}$$

---

* *cf.*, e.g., S. Chandrasekhar, *Radiative Transfer*, p. 9, equation (50), Oxford, 1950.

is the amount of the ray which *is* scattered. The total flux of radiation thus lost in scattering by all rays which cross from the inner to the outer face of the shell is therefore

$$\int_{+} I(\nu,\mu)\{1-\exp[-\tau(\nu)/\mu]\}\mu\, d\omega = 2\pi\int_0^1 I(\nu,\mu)\{1-\exp[-\tau(\nu)/\mu]\}\mu\, d\mu \qquad (5)$$

per unit area, where the + sign indicates that the integration is to be carried over the half sphere subtended by unit surface element on the outer face of the shell.

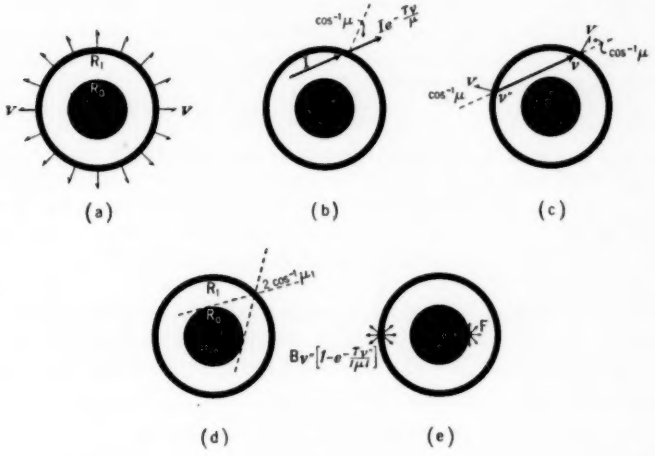

FIG. 1.

Let $B(\nu)$ be the emissivity of matter in the shell. (Again ν is the apparent frequency.) Then, according to (3), the intensity of a ray emerging with direction $\cos^{-1}\mu$ is*

$$B(\nu)\{1-\exp[-\tau(\nu)/\mu]\}, \qquad (6)$$

and in consequence the energy flux out of the shell is

$$\int B(\nu)\{1-\exp[-\tau(\nu)/|\mu|]\}\,|\mu|\,d\omega. \qquad (7)$$

The integration here is to be carried over the whole unit sphere of solid angle $\int d\omega = 4\pi$, since the emission as a result of scattering will emerge from both the inner and outer faces of the shell. Formula (7) can be integrated out to give

$$2\pi\int_{-1}^{1} B(\nu)\{1-\exp[-\tau(\nu)/|\mu|]\}\,|\mu|\,d\mu = 2\pi B(\nu)[1-2E_3(\tau_\nu)]. \qquad (8)$$

The exponential integral of order n is defined as

$$E_n(x) \equiv \int_1^\infty \exp(-tx)\frac{dt}{t^n}. \qquad (9)$$

* This expression is the limb " darkening " law for a thin shell. Note that in point of fact it makes the limb of the disk $\mu=0$ brighter than the centre $\mu=1$ in the ratio $1:\{1-\exp[-\tau(\nu)]\}$. The brightness of the limb is of course one of the striking features in photographs of planetary nebulae where the condition of a thin shell is well approximated.

If there are no sources or sinks of radiation within the shell, then the energy lost from the star's radiation field in unit area of the shell by scattering (5) must equal* the amount emitted by the shell (8); thus:

$$2\pi B(\nu)[1-2E_3(\tau_\nu)]=2\pi\int_0^1 I(\nu,\mu)\{1-\exp[-\tau(\nu)/\mu]\}\mu\,d\mu. \tag{10}$$

Now the radiation striking the inner surface of the shell can, in this system, come only from other portions of the shell or from the central star itself. A ray judged as having frequency ν and angle $\cos^{-1}\mu$ to the normal by an observer moving with the scattering material (that is to say, radially outwards with velocity v) would be judged by an observer at rest at the centre of the star as making an angle $\cos^{-1}\mu$ with the normal to the shell, and as having frequency ν'. Since $\nu'-\nu$ is due to the Doppler shift,

$$\nu'=\nu[1+\mu v/c], \tag{11}$$

in which c is the velocity of light. Similarly an observer stationed at the point on the other half of the shell where the continuation of the same ray strikes the shell again would judge the frequency as being ν'', if he participates in the local motion, where†

$$\nu''=\nu'[1+\mu v/c]=\nu[1+2\mu v/c]. \tag{12}$$

See Fig. 1 *c*.

Rays making an angle with the normal at the point of incidence whose cosine falls between 1 and $[1-(R_0/R_1)^2]^{1/2}\equiv\mu_1$ originate at the surface of the central star (see Fig. 1 *d*). The latter has been assumed to be radiating with intensity F in all frequencies and directions (Fig. 1 *e*), so

$$I(\nu,\mu)=F, \qquad \mu_1<\mu\leqslant 1. \tag{13}$$

For all other directions of incidence the rays originate on the shell, the intensity being given by (6) and the frequency by (12), so

$$\begin{aligned} I(\nu,\mu)&=B(\nu'')\{1-\exp[-\tau(\nu'')/\mu]\}\\ &=B(\nu[1+2\mu v/c])\{1-\exp[-(1/\mu)\tau(\nu[1+2\mu v/c])]\}, \quad 0<\mu\leqslant\mu_1. \end{aligned} \tag{14}$$

If (13), (14) be substituted into (10) there results an integral equation

$$\begin{aligned} B(\nu)[1-2E_3(\tau_\nu)]=&\int_{\mu_1}^1 F\{1-\exp[-\tau(\nu)/\mu]\}\mu\,d\mu\\ &+\int_0^{\mu_1} B(\nu[1+2\mu v/c])\{1-\exp[-(1/\mu)\tau(\nu[1+2\mu v/c])]\}\\ &\times\{1-\exp[-\tau(\nu)/\mu]\}\mu d\mu \end{aligned} \tag{15}$$

for the determination of the emissivity $B(\nu)$.

Once $B(\nu)$ is determined, the combined flux leaving the system of star plus envelope in any frequency is known. Apart from an amplitude factor this combined flux is the spectrum contour. The flux is the sum of contributions from:

(i) the star as seen through the forward face of the envelope,

(ii) the back half of the shell as seen through the forward half, and

(iii) the forward half, or what is usually called the disk.

* In equation (10) we have equated the energy in each frequency separately. That is to say we assume coherence. Since the frequency referred to as ν is always that judged by the scatterer, this represents no departure from standard procedure. However, see references (**15, 16**).

† Second-order terms in (v/c) are of course ignored throughout.

After escaping from the outer surface of the envelope the radiation suffers no redistribution in frequency or direction and the flux can therefore be evaluated at any surface enclosing the system of star and envelope. It is most convenient to take for this purpose the outer surface of the *shell* and judge frequencies in a frame of reference at rest with respect to the *star*; from there outward the inverse-square dilution law holds. Quantitatively (i) is given by

$$2\pi\int_{\mu_1}^{1} F\exp\{-(1/\mu)\tau(\nu[1-\mu v/c])\}\mu\,d\mu, \tag{16}$$

where, in the integrand, F is the intensity of the ray as it leaves the surface of the star and $\exp\{(-1/\mu)\tau(\nu[1-\mu v/c])\}$ is the fraction of this which traverses the shell without scattering. The optical path length $(1/\mu)\tau(\nu[1-\mu v/c])$ is that which the scatterer would apply to a ray which originated at the stellar surface with frequency ν. Similarly (ii) is given by

$$2\pi\int_{0}^{\mu_1} B(\nu[1+\mu v/c])\{1-\exp[-(1/\mu)\tau(\nu[1+\mu v/c])]\} \times\exp\{-(1/\mu)\tau(\nu[1-\mu v/c])\}\mu\,d\mu. \tag{17}$$

The first two factors in the integrand are together the intensity (6) of the ray leaving the shell with frequency $\nu[1+\mu v/c]$ as seen there, but with frequency ν as seen in the chosen stationary frame. The factor $\exp\{(-1/\mu)\tau(\nu[1-\mu v/c])\}$ has the same significance as in the expression for (i). Lastly, (iii) is given by

$$2\pi\int_{0}^{1} B(\nu[1-\mu v/c])\{1-\exp[-(1/\mu)\tau(\nu[1-\mu v/c])]\}\mu\,d\mu, \tag{18}$$

following the same reasoning as for (ii); but here no factor for absorption is required since the radiation is already outside the shell. If (16), (17) and (18) be summed one obtains the expression for the spectrum contour, apart from a multiplicative constant,

$$\begin{aligned}\mathscr{F}(\nu) = F&\int_{\mu_1}^{1}\exp\{-(1/\mu)\tau(\nu[1-\mu v/c])\}\mu\,d\mu\\ &+\int_{0}^{\mu_1} B(\nu[1+\mu v/c])\{1-\exp[-(1/\mu)\tau(\nu[1+\mu v/c])]\}\\ &\qquad\times\exp\{-(1/\mu)\tau(\nu[1-\mu v/c])\}\mu\,d\mu\\ &+\int_{0}^{1} B(\nu[1-\mu v/c])\{1-\exp[-(1/\mu)\tau(\nu[1-\mu v/c])]\}\mu\,d\mu.\end{aligned} \tag{19}$$

3.2. *The form of solution of the integral equations.*—Equations (15) and (19), which are now the fundamental equations of the problem, take on a neater form if the frequency of each point in the spectrum is measured as displacement from the normal frequency of the resonance line in units of the Doppler shift produced by a velocity v equal to the velocity of expansion of the envelope. Set

$$y=\frac{\nu-\nu_0}{\nu_0}\,\frac{c}{v}\quad\text{or}\quad \nu=\nu_0(1+yv/c), \tag{20}$$

wherein ν_0 is the frequency of the "normal" line centre. Then $\tau(\nu)$, $B(\nu)$, $\mathscr{F}(\nu)$ become functions $\tau^*(y)$, $B^*(y)$, $\mathscr{F}^*(y)$. In the expression $\tau(\nu[1-\mu v/c])$, for example,

$$\nu[1-\mu v/c]=\nu_0(1+yv/c)(1-\mu v/c)=\nu_0[1+(y-\mu)v/c]; \tag{21}$$

hence

$$\tau(\nu[1-\mu v/c])=\tau^*(y-\mu).$$

No confusion will result if the asterisks are dropped, it being understood that henceforth the unit of frequency is always (20), unless the contrary be specifically indicated. The normal line centre corresponds to $y=0$. Equations (15), (19) become respectively

$$B(y)[1-E_3(\tau(y))] = F\int_{\mu_1}^{1}\{1-\exp[-\tau(y+2\mu)/\mu]\}\mu\,d\mu + \int_0^{\mu_1} B(y+2\mu)\{1-\exp[-\tau(y+2\mu)/\mu]\}\{1-\exp[-\tau(y)/\mu]\}\mu\,d\mu, \tag{22}$$

$$\mathcal{F}(y) = F\int_{\mu_1}^{1}\exp[-\tau(y-\mu)/\mu]\mu\,d\mu + \int_0^{\mu_1} B(y+\mu)\{1-\exp[-\tau(y+\mu)/\mu]\}[\exp-\tau(y-\mu)/\mu]\mu\,d\mu + \int_0^{1} B(y-\mu)\{1-\exp[-\tau(y-\mu)/\mu]\}\mu\,d\mu. \tag{23}$$

Given the parameter μ_1 and the function $\tau(y)$, equation (22) can be solved for $B(y)$ and the result used in (23) to determine $\mathcal{F}(y)$. Clearly the method of solution will have to be numerical.

Its appearance to the contrary notwithstanding, (22) is a very simple equation. For any value of y the right-hand side of the equation involves only values of $B(y+2\mu)$ in which $y+2\mu>y$, since the integrand contains the factor μ while B is always finite. (*Note the absence of the equality sign.*) Thus the emissivity at any frequency is *explicitly* given by the emissivity in frequencies further to the violet.* This is a consequence of the fact that each scattering particle in the envelope is receding from all other particles in the system.† The determination of $B(y)$, for large positive y first, is therefore indicated.

Assume for y large that $\tau(y)\to 0$. (The optical depth falls off to zero outside the resonance line.) Then on the left-hand side of (22) the factor $[1-2E_3(\tau(y))]$ is of order 2τ. The first integral on the right-hand side is of order $F(1-\mu_1)\tau$ whereas the second integral is of order τ^2. For y large, therefore,

$$B(y)\to \tfrac{1}{2}F(1-\mu_1). \tag{24}$$

Thus in calculating B as a function of y one need only start the integration of (22) sufficiently far in the violet for the last integral on the right to be negligible in view of the accuracy desired. (24) can be used in the integral to estimate its magnitude. Then the right-hand side of (22) can be evaluated at successive values y_i of y as one moves towards the red end of the line. The spacing of the points y_i at which $B(y_i)$ is determined can be chosen to maintain the ease and accuracy of the numerical integrations involved in the *succeeding* evaluations. In equation (23) the last two integrals are each of order τ whereas the first one on the right-hand side is of order $F\int_{\mu_1}^{1}\mu\,d\mu$. For y large, therefore,

$$\mathcal{F}(y)\to \tfrac{1}{2}F(1-\mu_1^2) \tag{25}$$

or

$$\mathcal{F}(y)\to(1+\mu_1)B(y). \tag{26}$$

* This necessity of proceeding in one direction is a recurrent feature in problems of a moving atmosphere. For example, in reference (**13**), the integration must be started at the violet end. If it is begun at the red end the solution remains indeterminate.

† If the envelope were contracting the red frequencies would determine the violet ones. The velocity v in (20) would then be negative.

In view of the arbitrariness of the multiplicative factor mentioned in the paragraph following equation (15) above, it will be convenient to arrange that

$$\tfrac{1}{2}F(1-\mu_1^2)=1, \tag{27}$$

so that according to (25) the profile of the line rejoins the continuous spectrum with the value unity.

It is necessary now to assign the function $\tau(y)$. According to (1), when $R'\to R''=R$,

$$\tau_\nu \to \kappa_\nu \int_{R'}^{R''} \rho(r)\,dr;$$

hence

$$\tau(y)=(\text{constant})\kappa(y). \tag{28}$$

When a resonance line is broadened by thermal agitation or turbulence, the absorption (read: *scattering*) coefficient is given by (17),

$$\kappa_\nu=(\text{constant})\,.\,\exp\left\{-\left(\frac{\nu-\nu_0}{\nu_0}\,\frac{c}{v^*}\right)^2\right\}, \tag{29}$$

where the most probable velocity

$$v^*=\sqrt{(v_0^2+v\tau^2)},$$

of an atom in the Maxwell distribution, is the resultant of the thermal and turbulent velocities. In the frequency units (20) here employed, (29) becomes

$$\kappa(y)=(\text{constant})\exp(-\beta^2y^2) \tag{30}$$

and consequently (28) gives

$$\tau(y)=\tau(0)\exp(-\beta^2y^2), \tag{31}$$

where the new parameter

$$\beta=v/v^* \tag{32}$$

is the ratio of the directed velocity (radially outward) to the most probable random velocity (relative to the local rest frame) of the atoms comprising the material. For increasing velocities of expansion the turbulent velocity must be expected to increase too, so that the parameter is unlikely to take on extreme values.*

3.3. *The profiles for a range of values v/v^*.*—The parameter μ_1 which appears in the equations (22), (23) measures the ratio of the radius R_0 of the nuclear star to the effective radius R_1 of the envelope (Fig. 1*d*):

$$\mu_1=\sqrt{[1-(R_0/R_1)^2]}. \tag{33}$$

In this section we let $\mu_1\to 1$, which gives the case of a point star, postponing to the next section consideration of the changes produced by $\mu_1\neq 1$.

When $\mu_1\to 1$, subject to condition (27), the first integrals on the right of (22), (23) become respectively

$$F\int_{\mu_1}^1 \{1-\exp[-\tau(y)/\mu]\}\mu\,d\mu \to \{1-\exp[-\tau(y)]\}F\int_{\mu_1}^1 \mu\,d\mu \to \{1-\exp[-\tau(y)]\}$$

and (34)

$$F\int_{\mu_1}^1 \exp[-\tau(y-\mu)/\mu]\mu\,d\mu \to \exp[-\tau(y-1)]F\int_{\mu_1}^1 \mu\,d\mu \to \exp[-\tau(y-1)]. \tag{35}$$

* The profiles obtained below indicate values of β of order 3, when the velocity of expansion is $\sim$ 200 km/sec. Not all the width in v^* is necessarily due to turbulent velocity in our method of thin shells. The assumed velocity of expansion v of the envelope is only an average: any gradient in v would be mixed up with the turbulent width.

Consequently the equations to be solved become, for $\mu_1 = 1$,

$$B(y)[1 - 2E_3(\tau(y))] = \{1 - \exp[-\tau(y)]\} + \int_0^1 B(y+2\mu)\{1 - \exp[-\tau(y+2\mu)/\mu]\}\{1 - \exp[-\tau(y)/\mu]\}\mu\, d\mu, \quad (36)$$

$$\mathscr{F}(y) = \exp[-\tau(y-1)] + \int_0^1 B(y+\mu)\{1 - \exp[-\tau(y+\mu)/\mu]\}\exp[-\tau(y-\mu)/\mu]\,\mu\, d\mu + \int_0^1 B(y-\mu)\{1 - \exp[-\tau(y-\mu)/\mu]\}\,\mu\, d\mu. \quad (37)$$

The limiting values (24), (25) are given by

$$B(y) \to \tfrac{1}{2}, \qquad \mathscr{F}(y) \to 1, \quad (38)$$

for y large and positive. The equations (36), (37), (38) have been numerically integrated, after setting $\tau(0) = 1$ in (31), for three values of v/v^*: $\beta = 1, \sqrt{10}, 10$. The results are shown in Tables I, II, III, and $\mathscr{F}(y)$ is plotted for these three cases in Fig. 2. The scales of the *drawings* have been chosen to keep the turbulent

TABLE I

y	B_p	B_s	B	$\mathscr{F}_0$	$\mathscr{F}_1$	$\mathscr{F}_2$	$\mathscr{F}$
2·0	0·518	0·001	0·519	0·692	0·001	0·074	0·767
1·8	·532	·003	·535	·590	·002	·118	·711
1·6	·558	·006	·564	·498	·004	·174	·675
1·4	·588	·012	·600	·427	·005	·232	·663
1·2	·626	·021	·647	·383	·006	·284	·673
1·0	·670	·035	·705	·368	·007	·324	·699
0·8	·714	·049	·763	·383	·010	·349	·741
0·6	·754	·065	·819	·427	·015	·357	·798
0·4	·784	·084	·868	·498	·025	·356	·878
0·2	·803	·106	·910	·590	·044	·337	0·971
0·0	·810	·134	·944	·692	·075	·304	1·071
−0·2	·803	·169	·972	·789	·118	·260	1·167
−0·4	·784	·209	0·993	·869	·170	·210	1·248
−0·6	·754	·253	1·007	·926	·223	·160	1·309
−0·8	·714	·298	1·011	·962	·268	·114	1·344
−1·0	·670	·336	1·006	·982	·295	·076	1·352
−1·2	·626	·360	0·986	·992	·303	·045	1·341
−1·4	·588	·363	·950	·997	·281	·024	1·301
−1·6	·558	·339	·896	0·999	·232	·012	1·242
−1·8	·532	·293	·825	1·000	·170	·005	1·175
−2·0	0·518	0·231	0·750	1·000	0·112	0·002	1·114

width the same throughout (constant v^*); whereas the unit of frequency used in the *tables* is such that for each profile the expansion velocity gives unit Doppler displacement ($v = 1$). Equations (36), (37) may be written symbolically as

$$B(y) = B_p(y) + B_s(y),$$
$$\mathscr{F}(y) = \mathscr{F}_0(y) + \mathscr{F}_1(y) + \mathscr{F}_2(y).$$

Here $B_p(y)$ is the contribution to the emissivity which arises from initial or *primary* scattering of the star's emission, and $B_s(y)$ is that from scattering of the diffuse or *secondary* radiation (that is, rays coming from other parts of the envelope). $\mathscr{F}_0(y)$, $\mathscr{F}_1(y)$, $\mathscr{F}_2(y)$ are the contributions to the resultant profile which were listed

respectively as (i), (ii), (iii) in the paragraph (*q.v.*) following equation (15). These functions have also been tabulated in order to show the relative importance at each frequency of the various components.

TABLE II

y	B_p	B_s	B	$\mathcal{F}_0$	$\mathcal{F}_1$	$\mathcal{F}_2$	$\mathcal{F}$
2·0	...	...	...	1·000	...	0·000	1·000
1·8	...	...	...	0·998	...	·000	0·998
1·6	...	...	...	·973	...	·001	0·974
1·4	...	...	...	·816	...	·011	0·828
1·2	...	...	...	·512	...	·054	0·566
1·0	0·500	...	0·500	·368	...	·146	0·514
0·8	·503	...	·503	·512	...	·224	0·736
0·6	·524	0·000	·524	·816	...	·236	1·052
0·4	·615	·001	·615	·973	0·000	·180	1·153
0·2	·746	·007	·753	0·998	·001	·114	1·113
0·0	·810	·027	·836	1·000	·014	·064	1·078
−0·2	·746	·060	·806	...	·076	·028	1·104
−0·4	·615	·116	·731	...	·170	·005	1·174
−0·6	·524	0·157	0·682	...	·235	0·000	1·235
−0·8	·503	...	...	...	·225	...	1·225
−1·0	0·500	...	...	...	·157	...	1·157
−1·2	...	...	...	...	0·074	...	1·074

TABLE III

y	B_p	B_s	B	$\mathcal{F}_0$	$\mathcal{F}_1$	$\mathcal{F}_2$	$\mathcal{F}$
1·3	...	...	...	1·000	...	...	1·000
1·2	...	...	...	0·982	...	0·000	0·982
1·1	...	...	...	·692	...	·008	0·700
1·0	...	...	...	·368	...	·045	0·412
0·9	...	...	...	·692	...	·087	0·779
0·8	...	...	...	0·982	...	·086	1·068
0·7	...	...	...	1·000	...	·085	1·085
0·6	...	...	...	...	...	·077	1·077
0·5	...	...	...	...	...	·072	1·072
0·4	...	...	...	...	...	·063	1·063
0·3	0·500	...	0·500	...	...	·052	1·052
0·2	·518	0·000	·518	...	...	·039	1·039
0·1	·670	·001	·671	...	0·000	·020	1·020
0·0	·810	·001	·811	...	·002	·008	1·009
−0·1	·670	0·000	·670	...	·018	·001	1·019
−0·2	·518	...	·518	...	·039	0·000	1·039
−0·3	0·500	...	0·500	...	·052	...	1·052
−0·4	...	...	...	...	·063	...	1·063
−0·5	...	...	...	...	·072	...	1·072
−0·6	...	...	...	...	·077	...	1·077
−0·7	...	...	...	...	·085	...	1·085
−0·8	...	...	...	...	·086	...	1·087
−0·9	...	...	...	...	·045	...	1·045
−1·0	...	...	...	...	0·008	...	1·008

From Fig. 2 it will be noticed that the profiles are characterized by an absorption component to the violet of the line centre. Since we arranged for conservation of energy absorbed and re-emitted, and since we gave the star no cross-section for capture of radiation scattered by the shell (point star), it was assured that there would therefore also be emission components of total equivalent width equal to the equivalent width of the absorption component. (This provides a

convenient check of the accuracy of the profiles.) What was perhaps unexpected was that for values of β not much greater than unity the re-emission components—one from the forward face of the envelope, $\mathcal{F}_2(y)$ above, the other from the rear of the envelope $\mathcal{F}_1(y)$—would begin to separate so as to give an apparent "reversal" which falls almost exactly at the line centre. That is to say, as a result of the presence of the scattering shell a portion of the flux in the neighbourhood of a resonance line reaches the observer after having been redirected by the shell. The energy built up in this scattering envelope has a maximum, which for the

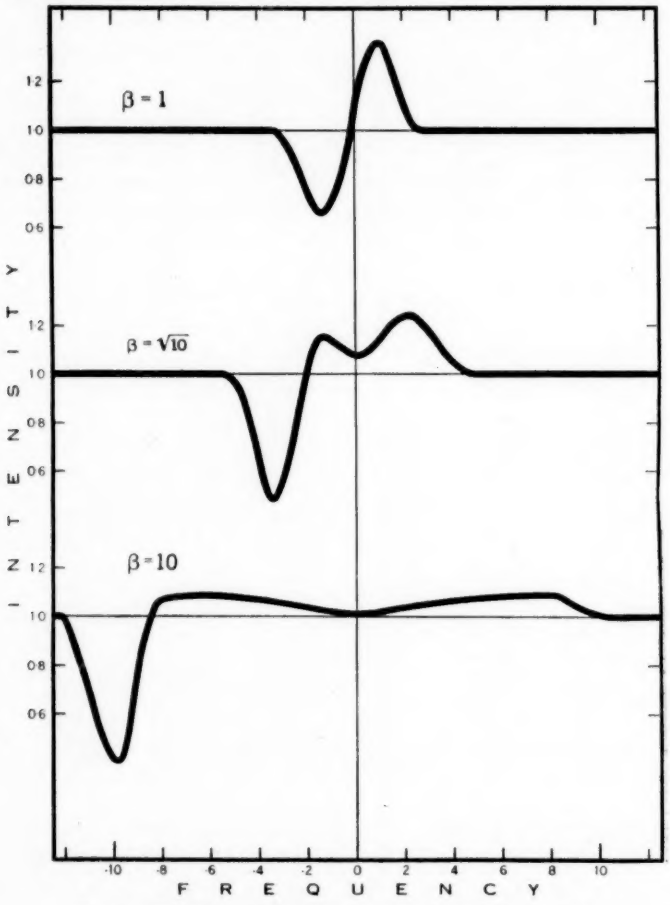

FIG. 2.—*Dependence of the profiles on the velocity ratio* $\beta = v/v^*$. *v is the velocity of expansion and v^* is the "most probable random" velocity.*

forward half of the shell falls at a frequency to the violet and for the rear half of the shell falls at a frequency to the red of the normal frequency, as judged by a stationary observer.

3.4. *Effect of occultation on the calculated profiles.*—To investigate the effect on the profiles of a finite radius of the "perfectly absorbing" star—hence the

TABLE IV

y	B_p	B_s	B	$\mathcal{F}_0$	$\mathcal{F}_1$	$\mathcal{F}_2$	$\mathcal{F}$
2·0	...	...	...	1·000	...	...	1·000
1·8	...	...	...	0·999	...	0·000	0·999
1·6	...	...	...	·952	...	·001	0·953
1·4	...	...	...	·902	...	·012	0·914
1·2	...	...	...	·634	...	·061	0·695
1·0	...	...	...	·376	...	·157	0·533
0·8	...	...	...	·474	...	·243	0·716
0·6	...	...	...	·640	...	·253	0·893
0·4	0·672	0·000	0·672	·904	0·000	·193	1·097
0·2	·802	·007	·809	·989	·001	·122	1·112
0·0	·858	·031	·889	0·999	·014	·069	1·083
−0·2	·802	·080	·882	1·000	·082	·030	1·112
−0·4	·672	·149	·821	...	·177	·005	1·182
−0·6	·582	·200	·782	...	·203	0·000	1·204
−0·8	0·572	0·182	0·754	...	·149	...	1·149
−1·0	...	...	...	...	·065	...	1·065
−1·2	...	...	...	...	·015	...	1·015
−1·4	...	...	...	...	·002	...	1·002
−1·6	...	...	...	...	0·000	...	1·000
−1·8	...	...	...	...	...	...	1·000
−2·0	...	...	...	...	...	...	1·000

TABLE V

y	B_p	B_s	B	$\mathcal{F}_0$	$\mathcal{F}_1$	$\mathcal{F}_2$	$\mathcal{F}$
2·0	...	...	...	1·000	...	...	1·000
1·8	...	...	...	1·000	...	0·000	1·000
1·6	...	...	...	0·993	...	·002	0·995
1·4	...	...	...	·939	...	·013	0·952
1·2	...	...	...	·744	...	·067	0·811
1·0	...	...	...	·454	...	·169	0·623
0·8	...	...	...	·339	...	·255	0·593
0·6	...	...	...	·482	...	·270	0·752
0·4	0·745	0·000	0·745	·762	0·000	·207	0·969
0·2	·861	·005	·867	·942	·001	·130	1·073
0·0	·908	·027	·935	0·993	·019	·075	1·086
−0·2	·862	·060	·922	1·000	·084	·033	1·117
−0·4	·744	·124	·868	1·000	·138	·006	1·144
−0·6	·644	·182	·836	...	·126	0·000	1·126
−0·8	0·632	0·177	0·809	...	·064	...	1·064
−1·0	...	...	...	...	·016	...	1·016
−1·2	...	...	...	...	·002	...	1·002
−1·4	...	...	...	...	0·000	...	1·000
−1·6	...	...	...	...	...	...	1·000
−1·8	...	...	...	...	...	...	1·000
−2·0	...	...	...	...	...	...	1·000

TABLE VI

y	B_p	B_s	B	$\mathcal{F}_0$	$\mathcal{F}_1$	$\mathcal{F}_2$	$\mathcal{F}$
1·4	...	...	...	0·961	...	0·019	0·981
1·2	...	...	...	·930	...	·085	·915
1·0	...	...	...	·607	...	·197	·803
0·8	...	...	...	·430	...	·285	·715
0·6	1·000	0·000	1·000	·395	0·000	·302	·698
0·4	...	...	...	·541	...	·229	·771
0·2	...	...	...	·714	...	·143	·857
0·0	...	...	...	·834	...	·083	·917
−0.2	...	...	...	0·923	...	0·039	0·962

ability to occult part of the rear half of the envelope—equations (22), (23), (27) were integrated for three additional values of μ_1, namely 0·8, 0·6 and 0·0, with $\beta = \sqrt{10}$. The results are shown in Tables IV, V, VI, which should be compared with the corresponding one for $\mu_1 = 1$, $\beta = \sqrt{10}$ in Table II.

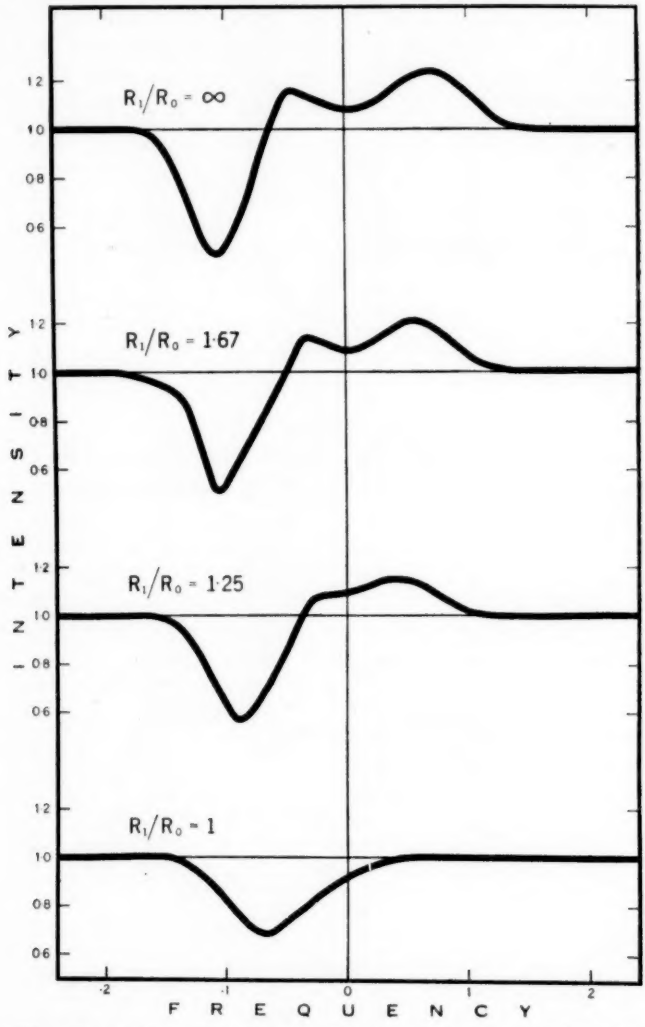

FIG. 3.—*Effect of occultation. R_0 is the radius of the star; R_1 is the mean radius of the envelope.*

For $\mu_1 = 0$ equations (22), (23), (27) simplify greatly: (22) becomes

$$B(y)[1 - 2E_3(\tau(y))] = F\int_0^1 \{1 - \exp[-\tau(y)/\mu]\}\mu\, d\mu$$
$$= \tfrac{1}{2}F[1 - 2E_3(\tau(y))],$$

and (27) gives $\frac{1}{2}F=1$; hence $B(y)=1$. When these values for F, B are substituted into (23) the contour follows:

$$\begin{aligned}\mathscr{F}(y) &= F\int_0^1 \exp[-\tau(y-\mu)/\mu]\mu\,d\mu + \int_0^1 B(y-\mu)\{1-\exp[-\tau(y-\mu)/\mu]\}\mu\,d\mu \\ &= 2\int_0^1 \exp[-\tau(y-\mu)/\mu]\mu\,d\mu + \int_0^1 \{1-\exp[-\tau(y-\mu)/\mu]\}\mu\,d\mu \\ &= \tfrac{1}{2} + \int_0^1 \exp[-\tau(y-\mu)/\mu]\mu\,d\mu.\end{aligned}$$

Since the integral in the last line above is always $\leqslant \frac{1}{2}$, the net effect of the two terms is an absorption line with no accompanying emission component.

The four curves for $\mathscr{F}(y)$ are shown in Fig. 3. The diminishing effect on the emission components, it will be seen, does not become noticeable until the occultation is well advanced.*

4. *Profiles based on the Zanstra mechanism*

4.1. *Emission from the recombining shell.*—According to the Zanstra–Menzel–Beals theory of emission in early-type stars, the energy appearing in lines of the Lyman and Balmer series is supplied from radiative frequencies beyond the head of the series. In the region immediately adjacent to the inner boundary of the envelope the radiation field is so intense that almost all the atoms are ionized.†

In this assemblage of ions and electrons, recombinations can take place. The probability p of the electron being captured directly into the ground state is, according to calculations by Cillié (**20**), only of order $\frac{1}{2}$. In the other $(1-p)$ captures the electron appears on an excited level and if undisturbed rapidly cascades down to the ground state, emitting at each jump a line quantum. On our assumption of steady state (of the gross physical variables) these recombinations cannot be permitted to upset the degree of ionization, so simultaneously the photoelectric ionization of an equal number of neutral atoms must be occurring. Thus, for each quantum $h\nu_0$ of radiation newly appearing in the line, a quantum $h\nu_e$ of energy greater than the ionization potential of the atom concerned has been lost to the radiation field in the ultra-violet.

If πS_e be the total flux of radiation emitted from the surface of the star in frequencies beyond the series limit, and $\pi S_e \exp(-\tau_1)$ be the flux in these same frequencies which escapes through the envelope (thereby defining τ_1), the energy lost by conversion in the envelope is represented by

$$\pi S_e[1-\exp(-\tau_1)]. \tag{39}$$

Since roughly one quantum $h\nu_0$ appears in the line for each quantum $h\nu_e$ lost in the ultra-violet continuum, the energy converted by the recombining region contributes

$$\pi S_e(\nu_0/\nu_e)[1-\exp(-\tau_1)] \tag{40}$$

to the flux in the immediate neighbourhood of ν_0. The precise distribution of this flux among the frequencies adjacent to ν_0 will be determined by various

* For $\mu_1=0{\cdot}6$ the radius of the nuclear star is already 0·8 of the radius of the shell. The last profile of the sequence, the one with $\mu_1=0$ in which occultation is complete, is the line produced in a plane atmosphere. This is the same profile arrived at by O. C. Wilson (**18**), and again by A. B. Underhill (**19**), whose discussions are restricted to moving plane atmospheres.

† Upwards of all but one in 10^6, in representative cases.

factors which ultimately determine the *shape* of each component (steepness of sides, flatness of top, etc.). We shall assume that apart from a uniform expansion of the envelope this distribution is mainly determined by the *random* motion of the atoms doing the emitting, so that the spectral variation of this additional flux can be written as

$$\pi F'(\nu) = \pi S_e \frac{\nu_0}{\nu_e} \frac{\tau_\nu'}{\int \tau_\nu' \, d\nu} [1 - \exp(-\tau_1)], \tag{41}$$

where τ_ν' is the optical thickness of the recombining region in frequency ν. That is to say, at any instant, the number of atoms capable of *absorbing* radiation of frequency ν is a direct measure of the number that have just arrived in that state by *emission* of radiation of that frequency. The flux in any frequency is also expressible in terms of the specific intensity emerging from unit area on the shell:

$$\pi F'(\nu) = \int I'(\nu, \mu) |\mu| \, d\omega, \tag{42}$$

where the integration is taken over both faces of the shell; that is, over the solid angle $\int d\omega = 4\pi$. To obtain the variation of $I'(\nu, \mu)$ with direction we again make the approximation that the recombining region is a thin shell of radius R_2. The dependence of $I'(\nu, \mu)$ on μ is then given by a formula analogous to (3). Making use of (41), (42) we find that its explicit expression is

$$I'(\nu, \mu) = \frac{S_e}{2} \frac{\nu_0}{\nu_e} \frac{\tau_\nu'}{\int \tau_\nu' \, d\nu} \frac{1 - \exp[-\tau'(\nu)/|\mu|]}{1 - 2E_3(\tau_\nu')} [1 - \exp(-\tau_1)]. \tag{43}$$

For the early-type stars no direct estimate of the flux outside the visible region can be made. The temperatures of these stars is obtained (**5**, **9**) by assuming that *all* the ultra-violet radiation is converted to line radiation. In the notation adopted here, this implies that

$$\tau_1 = \infty. \tag{44}$$

Further, in supposing that the actual physical state of the envelope can be approximated by two thin shells of different radii, one of which is characterized by the Zanstra emission process and the other by a process of scattering by a moving medium, we have inferentially supposed that the first is also characterized by a very high degree of ionization*, while the second is composed of a sufficiently high proportion of neutral atoms to maintain resonance scattering. In view of this separation of function we may, without stretching the approximation, assume that the recombining shell is so far ionized as to be transparent to radiation in the frequency of the line. Hence

$$\tau_\nu' \to 0. \tag{45}$$

Nevertheless $\tau_\nu'/\int \tau_\nu' \, d\nu$ can still be finite. (As, for example, with a coefficient of the form (31) when $\tau(0) \to 0$.) Let†

$$\frac{\tau_\nu'}{\int \tau_\nu' \, d\nu} \to \sigma(\nu). \tag{46}$$

---

* That this is compatible with equation (44) is admittedly open to argument.

† In this fashion we account for the possible non-coherence of the emitted radiation, as discussed by L. Spitzer (**15**). When one uses, as we shall, a coefficient of the form (31) to determine (46) the emission is distributed in frequency in the fashion postulated for planetary nebulae by H. Zanstra (**16**), Section 3.

With use of (44), (45), (46) the expression for the emergent intensity is considerably simplified. (43) becomes*

$$I'(\nu,\mu)=\frac{S_e\nu_0\sigma(\nu)}{4\nu_e|\mu|}\,. \tag{47}$$

4.2. *The equations for the two-shell model.*—If there is a recombining shell (in the sense of the preceding section) of radius R_2 lying between the star and the scattering shell, the right-hand side of equation (10) will involve not only the incident radiation given by (13) and (14) but also a term which measures the flux of energy scattered by unit area of the outer shell from rays which originated at the inner one.

The rays which originate at the forward face of the recombining shell R_2, and reach the scattering point, lie within a pencil whose extremes are the ray which is perpendicular to and the one which just grazes the R_2 shell. The cosines of the angles these rays make with the normal to the scattering shell R_1 fall in the range $1\geqslant\mu\geqslant\mu_2$. Those rays from the R_2 shell which by-pass the occulting star R_0, and traverse the forward face of the R_2 shell to reach the

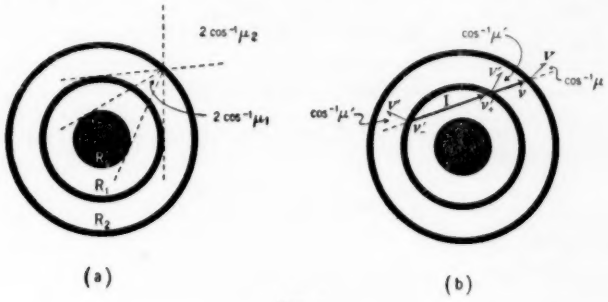

FIG. 4.

scattering point, lie within a pencil bounded by the ray which just grazes the star and the one which just grazes the R_2 shell. The corresponding cosines fall in the range $\mu_1\geqslant\mu\geqslant\mu_2$. (See Fig. 4 *a*.)

$$\mu_1=[1-(R_0/R_1)^2]^{1/2},\qquad \mu_2=[1-(R_2/R_1)^2]^{1/2},$$

where R_0, R_2, R_1 are respectively the radii of the star, the recombining shell, and the scattering shell. A ray, which strikes the R_1 shell at the angle $\cos^{-1}\mu$, leaves the R_2 shell at the angle $\cos^{-1}\mu'$, where

$$(1-\mu^2)=(1-\mu'^2)(1-\mu_2{}^2). \tag{48}$$

Matter in the R_2 shell may have a radial velocity, say v', of which one must take account. A ray which appears to the scatterer at R_1 to have frequency ν and direction μ seemed to the emitter at R_2 to have frequency ν' and direction μ', where (Fig. 4 *b*)

$$\nu'[1+\mu'v'/c]=\nu[1+\mu v/c], \tag{49}$$

$$\nu'[1-\mu'v'/c]=\nu[1+\mu v/c], \tag{50}$$

* Note that the singularity at $\mu=0$, introduced by letting $\tau_\nu'\to 0$ would make the radiation density $\frac{1}{2}\int I\,d\mu$ non-convergent if calculated on the above formula; that is to say, if the limit were taken first and the integration performed later. However, in our application we need only the flux $\int I\,\mu\,d\omega$, which remains well behaved, since μI in (47) is finite for all μ.

according as the ray is, respectively, from the approaching or the receding disk. If (49), (50) be written in the Doppler units (20), then a ray which appears at the R_1 shell to have frequency y will at the R_2 shell have had frequency y', where

$$y_+' = y + \mu - \gamma\mu' = y + m(\mu') - \gamma\mu',$$
$$m(\mu) \equiv [\mu^2(1-\mu_2^2) + \mu_2^2]^{1/2} \tag{51}$$
$$y_-' = y + \mu + \gamma\mu' = y + m(\mu') + \gamma\nu',$$

according as the ray is from the advancing or the receding disk. Here

$$\gamma = v'/v \tag{52}$$

is the ratio of the two expansion velocities.

Proceeding as in (4), (10), (14), we find that the flux in frequency y which, having originated at R_2, is scattered upon reaching R_1 is (omitting the 2π)

$$\int_{\mu_2}^{1} I'(y_+', \mu')\{1 - \exp[-\tau(y)/\mu]\}\mu\, d\mu + \int_{\mu_2}^{\mu_1} I'(y_-', \mu')\{1 - \exp[-\tau(y)/\mu]\}\mu\, d\mu. \tag{53}$$

If the variable of integration be changed according to formula (48), then (53) becomes

$$(1-\mu_2^2)\left\{\int_{m(\mu')=\mu_2}^{m(\mu')=1} I'(y_+', \mu')\{1 - \exp[-\tau(y)/m(\mu')]\}\mu'\, d\mu' + \int_{m(\mu')=\mu_2}^{m(\mu')=\mu_1} I'(y_-', \mu')\{1 - \exp[-\tau(y)/m(\mu')]\}\mu'\, d\mu'\right\}. \tag{54}$$

The intensity of the recombination emission has been written down in (47). In the present variables

$$I'(y', \mu') = \tfrac{1}{4} S_e \frac{\nu_0}{\nu_e} \frac{\sigma(y')}{|\mu'|}. \tag{55}$$

Thus (54) is given by

$$(1-\mu_2^2)\frac{S_e\nu_0}{4\nu_e}\left\{\int_0^1 \sigma(y_+')\{1 - \exp[-\tau(y)/m(\mu')]\}\, d\mu' + \int_0^{[(\mu_1^2-\mu_2^2)/(1-\mu_2^2)]^{1/2}} \sigma(y')\{1 - \exp[-\tau(y)/m(\mu')]\}\, d\mu'\right\}. \tag{56}$$

If y' is substituted from (51), and if it be agreed that the positive square root be always the one taken, then the above expression for the amount of new radiation scattered can be written as the single integral

$$\frac{S_e\nu_0}{4\nu_e}(1-\mu_2^2)\int_{-[(\mu_1^2-\mu_2^2)/(1-\mu_2^2)]^{1/2}}^{1} \sigma(y + m(\mu') - \gamma\mu')\{1 - \exp[-\tau(y)/m(\mu')]\}\, d\mu'. \tag{57}$$

This is the term to be added to the right-hand side of (15) in order to obtain the integral equation of the emissivity of the scattering shell in the two-shell model.

Proceeding in the same manner one finds, for the term to be added to the right-hand side of (19) to represent the flux of the emission from the recombining envelope which penetrates the outer shell without scattering, the expression

$$(1-\mu_2^2)\frac{S_e\nu_0}{4\nu_e}\int_{-[(\mu_1^2-\mu_2^2)/(1-\mu_2^2)]^{1/2}}^{1} \sigma(y - \gamma\mu') \exp\{-\tau[y - m(\mu')]/m(\mu')\}\, d\mu'. \tag{58}$$

Comparing (57) and (58) one can understand the significance of the component factors, of which one may have lost sight during the changes required to simplify them. The second factor in the integrand of (58) is the fraction of the original ray which penetrates the outer shell when it arrives there at an angle whose cosine is (*cf.* (48)) $\mu = m(\mu')$ and with a frequency which is y when judged in the

rest-frame of the star (as was agreed upon in the paragraph preceding equation (16)), but is $y-m(\mu')$ when judged by the scatterer. On the other hand, the first factor gives the strength of the emission along that ray in the same frequency y, but corrected now for the fact that the recombining shell, at which the ray originates, has velocity γ in units of the radial velocity of the outer shell and for the fact that the cosine of the angle made at this inner shell is μ'. In contrast, the first factor in the integrand of (57) has its frequency determined by the fact that the frame of reference for judging frequencies as y for use in equation (15) is taken to be that of the material at the scattering point (*cf.* the paragraph preceding equation (11)) and must therefore be adjusted by a term $m(\mu')$ to reduce it to the rest-frame of the star and by a term $\gamma\mu'$ to bring it to the rest-frame of the point and direction of emission. The second factor of the integrand of (57) is then the fraction of the ray momentarily absorbed by the scattering material when the frequency it sees is y and the cosine of the angle made with the normal is $\mu = m(\mu')$.

The addition of terms (57), (58) to our equations introduces a number of new parameters. The variation of these parameters so greatly increases the variety of profiles obtainable with our methods that an exhaustive investigation of all resultant types would run to exceedingly great length. We necessarily confine ourselves, therefore, to deriving the profiles for a few illustrative cases.

Since the effect of occultation on any profile is readily predictable, and has already been quantitatively investigated for the case of a single scattering shell, we shall restrict the calculations to point stars. Then the equations for the two-shell model are given by adding the terms (57) and (58), for $\mu_1 = 1$, to equations (36) and (37) respectively:

$$B(y)[1-2E_3(\tau(y))] = (1-\mu_2^2)\frac{S_c\nu_0}{4\nu_c}\int_{-1}^{1}\sigma(y+m(\mu)-\gamma\mu)\{1-\exp[-\tau(y)/m(\mu)]\}\,d\mu + \{1-\exp[-\tau(y)]\} + \int_0^1 B(y+2\mu)\{1-\exp[-\tau(y+2\mu)/\mu]\} \times \{1-\exp[-\tau(y)/\mu]\}\mu\,d\mu, \tag{59}$$

$$\mathcal{F}(y) = (1-\mu_2^2)\frac{S_c\nu_0}{4\nu_c}\int_{-1}^{1}\sigma(y-\gamma\mu)\exp\{-\tau[y-m(\mu)]/m(\mu)\}\,d\mu + \exp[-\tau(y-1)] + \int_0^1 B(y-\mu)\{1-\exp[-\tau(y-\mu)/\mu]\}\mu\,d\mu + \int_0^1 B(y+\mu)\{1-\exp[-\tau(y+\mu)/\mu]\}\exp[-\tau(y-\mu)/\mu]\mu\,d\mu. \tag{60}$$

4.3. *Profiles for the limiting case of small recombining shell.*—When the recombining shell is of radius small compared to the effective radius of the scattering shell (in this point star model) then (Fig. 4*a*) $\mu_2 = [1-(R_2/R_1)^2]^{1/2} \cong 1$. If one lets $\mu_2 \to 1$ in (58), (60), but in such a manner that $S_c(1-\mu_2^2) = S_c'$ remains finite, it is easily verified that these equations become identical with (36), (37) except for the first term on each right-hand side, where the factor

$$1 + \frac{S_c'\nu_0}{4\nu_c}\int_{-1}^{1}\sigma(y-\gamma\mu)\,d\mu = 1+\Sigma_\gamma(y), \tag{61}$$

representing the flux in frequency y of the star plus recombining envelope, replaces the unit flux (27) from the star alone.*

* When the combined flux (61) does not vary too rapidly with y the resultant profile $\mathcal{F}(y)$ will be reasonably well given by superimposing the corresponding contour of Section 3.3, $\mathcal{F}^*(y)$ say, on to the function $1+\Sigma(y)$; thus $\mathcal{F}(y) = \mathcal{F}^*(y)\,.\,[1+\Sigma'(y)]$.

The integration of the equations has been carried out for several choices of expansion velocity and turbulence in the recombining shell. The profile shown in Fig. 5 together with the values given in Table VII is the computed result for the case

$$\gamma = v'/v = 2, \qquad \beta' = v'/v'^{*} = 3, \qquad \beta = v/v^{*} = 3{\cdot}16; \tag{62}$$

that is, when the recombining shell is expanding twice as fast as the scattering shell ($v' = 2v$), and when the turbulent velocity in each shell is approximately a third of the associated expansion velocity ($v = 3{\cdot}16v^{*}$, $v' = 3v'^{*}$). The optical depth in the scattering envelope is again taken to be of the form of (31)

$$\tau(y) = \tfrac{1}{2}\exp(-\beta^2 y^2), \tag{63}$$

and a similar choice is made for the recombining envelope, in accord with (46).

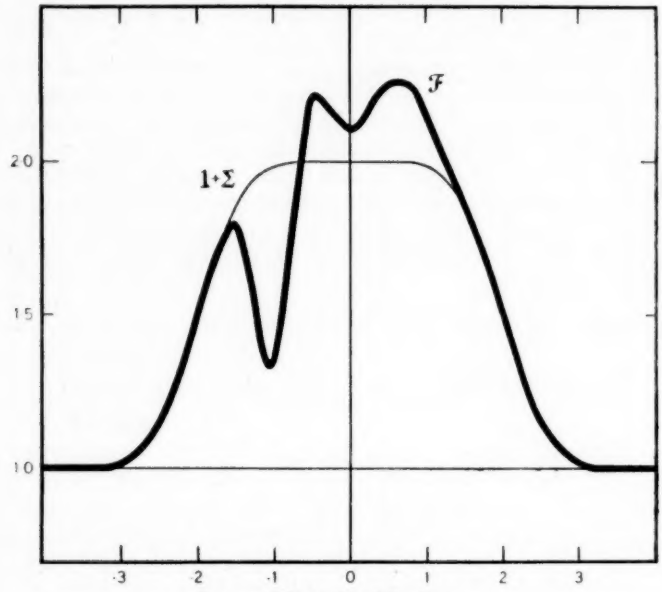

FIG. 5.—*The profile of Section 4.3.*
The star radiates the continuous spectrum 1. Σ is the flux due to recombination. As a result of scattering, a distant observer sees the line contour 𝓕.

The flat-topped, symmetrical contour (fine line in the figure, $1+\Sigma$ in the calculation) underlying this complex profile of P Cygni type is the shape the line would take if there were no scattering envelope. For then the emission from the recombining envelope (and from the continuous spectrum) would be the only visible feature. Flat tops indicate emission from an expanding medium of spherical shape. The effect of the scattering layer is to produce an absorption component, displaced to the violet in proportion to the velocity in the line of sight of the scattering atoms. Since the expansion velocity of the scattering material was taken, for this illustrated case, to be but half that of the recombining matter, the absorption attacks the emission profile where the latter is still quite intense. For radiative balance the energy thus absorbed must be re-emitted.

The energy reappears in the peaks on either side of the line centre, producing an apparent "central reversal".

4.4. *Profile when the shells coincide.*—When the recombining and scattering shells have the same effective radius, $\mu_2 \equiv [1-(R_2/R_1)^2]^{1/2}$. If the expansion velocity of matter in each shell is also the same, then $\gamma = 1$. This is the particular case we should have had, had we not made the distinction in Section 4.1 between recombining and scattering shells. The equations resulting from (59), (60) have been integrated with

$$\frac{S_c \nu_0}{2\nu_c}\,\sigma(y) = 10\tau(y) = 10\exp(-10y^2). \tag{64}$$

The results are shown in Table VIII and the profile in Fig. 6*a*. It will be noted that the rather large recombination flux adopted has almost entirely filled in the violet absorption border. However, the most striking feature of the profile is again the fact that the emissivity built up in the outer shell by the scattering process separates into two emission components leaving a deep "reversal" near the line centre. This may be seen from Fig. 6*b* where the contributions to the profile of starlight $\mathscr{F}_0'$, envelope emission $\mathscr{F}_0''$, and diffused light from the two faces of the scattering shell $\mathscr{F}_1+\mathscr{F}_2$ are separately shown.

TABLE VII

y	$1+\Sigma$	B_p	B_s	B	$\mathscr{F}_0$	$\mathscr{F}_1$	$\mathscr{F}_2$	$\mathscr{F}$
2·0	1·500	0·508	...	0·508	1·500	...	0·000	1·500
1·8	1·622	·522	...	·522	1·661	...	·000	1·661
1·6	1·802	·551	...	·551	1·778	...	·001	1·779
1·4	1·898	·599	...	·599	1·715	...	·010	1·726
1·2	1·955	·669	...	·669	1·399	...	·053	1·452
1·0	1·984	·750	...	·750	1·203	...	·151	1·354
0·8	1·995	·834	...	·834	1·427	...	·260	1·686
0·6	1·999	0·928	0·000	0·928	1·807	0·000	·259	2·066
0·4	2·000	1·079	·000	1·080	1·972	·001	·240	2·213
0·2	2·000	1·270	·006	1·276	1·998	·003	·150	2·151
0·0	2·000	1·433	·039	1·472	2·000	·025	·084	2·109
−0·2	2·000	1·296	·105	1·401	2·000	·110	·031	2·141
−0·4	2·000	1·137	·192	1·329	2·000	·227	·005	2·232
−0·6	1·999	1·030	·240	1·270	1·999	·257	0·000	2·256
−0·8	1·995	1·003	0·171	1·174	1·995	·254	...	2·249
−1·0	1·984	1·000	...	...	1·984	·165	...	2·149
−1·2	1·955	1·000	...	...	1·955	·063	...	2·018
−1·4	1·898	1·000	...	...	1·898	·013	...	1·911
−1·6	1·802	0·999	...	...	1·802	·001	...	1·803
−1·8	1·662	·997	...	...	1·662	·000	...	1·662
−2·0	1·500	0·992	...	...	1·500	0·000	...	1·500

The absorption line, produced in the $\mathscr{F}_0'$ curve at a displacement from the line centre corresponding to the velocity of the scattering shell, is the usual reversal of parallel light in passing through an absorbing medium. The attenuation of the symmetrical flat-topped contour Σ into the highly asymmetric $\mathscr{F}_0''$ is, however, quite striking, and shows to what extent the scattering-recombining shell is transparent to radiation from its opposite face. Frequencies to the red of $y = 0{\cdot}5$ escape almost completely. The diffuse emission as a result of scattering is, as we have now learned to expect, concentrated into two peaks with a minimum near the line centre.

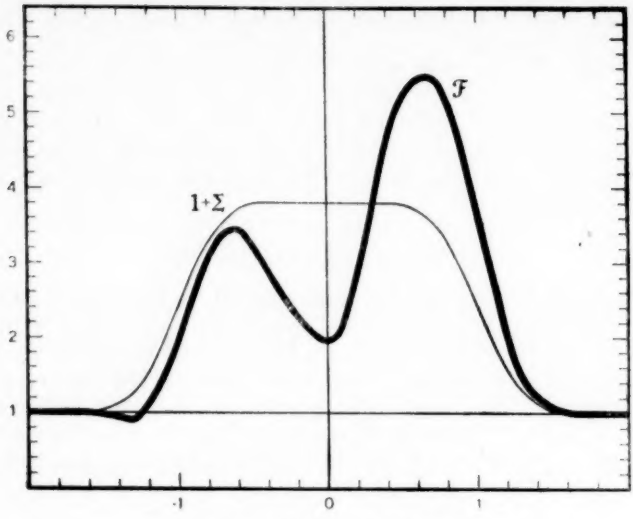

FIG. 6 *a.*—*The profile of Section 4.4.*
The star radiates the continuous spectrum 1. *Σ is the flux due to recombination. As a result of scattering, a distant observer sees the line contour* $\mathcal{F}$.

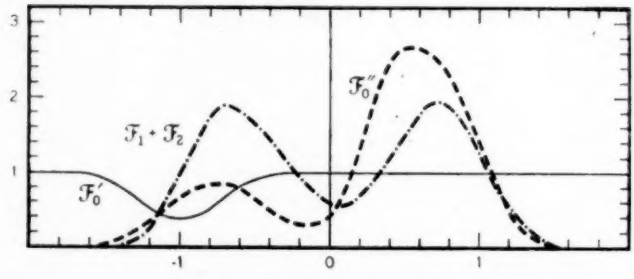

FIG. 6 *b.*—*The components of profile 6 a.*
The star, seen through the scattering envelope, provides the flux $\mathcal{F}_0'$. *The flux due to recombination gives the component* $\mathcal{F}_0''$, *when seen through the scattering envelope. Re-radiation by the envelope adds the contour* $(\mathcal{F}_1+\mathcal{F}_2)$.

The equivalent widths of the $\mathcal{F}$ and $1+\Sigma$ profiles are—within the limits of computational accuracy—equal.

4.5. *Profile for an intermediate case.*—Finally, in order to verify that no untoward effects intervene for choices of R_2 intermediate to the limiting cases $R_2=R_0$ and $R_2=R_1$ considered in Sections 4.3, 4.4, above, the integral equations ((59), (60)) were solved for $\sqrt{2}R_2=R_1$, $v'/v=\frac{1}{2}$:

$$\mu_1=1,\ F(1-\mu_1)=1,\ \mu_2=\frac{1}{\sqrt{2}},\ \sigma(y)\frac{S_c\nu_0}{2\nu_c}(1-\mu_2^2)=10\tau(y)=10\exp(-10y^2). \quad (65)$$

The values found for the various components are shown in Table IX and the profile in Fig. 7. The profile is of a familiar type.

TABLE VIII

y	$1+\Sigma$	B_p'	B_p''	B_s	B	$\mathcal{F}_0'$	$\mathcal{F}_0''$	$\mathcal{F}_1$	$\mathcal{F}_2$	$\mathcal{F}$
2·0	1·000	...	...	...	...	1·000	...	...	...	1·000
1·8	1·000	...	...	...	...	0·998	0·000	...	0·000	0·998
1·6	1·010	...	...	...	...	·973	·011	...	·002	0·986
1·4	1·105	...	...	...	...	·816	·091	...	·035	0·943
1·2	1·519	...	...	...	...	·512	·343	...	·265	1·120
1·0	2·401	0·500	0·000	...	0·500	·368	·641	...	0·980	1·988
0·8	3·282	·503	·050	...	·553	·512	·821	...	1·711	3·044
0·6	3·697	·524	0·419	0·000	0·944	·816	·784	...	1·817	3·417
0·4	3·792	·615	1·703	·001	2·318	·973	·490	0·000	1·453	2·916
0·2	3·801	·750	4·266	·010	5·026	0·998	·312	·001	0·958	2·270
0·0	3·802	·810	6·228	·100	7·138	1·000	0·396	·050	·535	1·981
−0·2	3·801	·750	5·564	·388	6·702	...	1·331	0·465	·236	2·916
−0·4	3·792	·615	4·734	0·886	6·235	...	2·461	1·186	·037	4·684
−0·6	3·697	·524	3·545	1·213	5·282	...	2·656	1·788	0·000	5·444
−0·8	3·282	·503	1·899	1·168	3·569	...	2·291	1·902	...	5·193
−1·0	2·401	0·500	1·280	0·908	2·688	...	1·399	1·315	...	3·714
−1·2	1·519	...	...	...	...	...	0·513	0·522	...	2·035
−1·4	1·105	...	...	...	...	...	·105	·115	...	1·220
−1·6	1·010	...	...	...	...	...	·01	·011	...	1·022
−1·8	1·000	...	...	...	...	...	·001	·000	...	1·001
−2·0	1·000	...	...	...	...	...	0·000	0·000	...	1·000

TABLE IX

y	$1+\Sigma$	B_p'	B_p''	B_s	B	$\mathcal{F}_0'$	$\mathcal{F}_0''$	$\mathcal{F}_1$	$\mathcal{F}_2$	$\mathcal{F}$
2·0	1·000	...	...	...	...	1·000	...	0·000	...	1·000
1·8	1·000	...	...	...	...	0·998	...	·000	...	0·998
1·6	1·000	...	...	...	...	·973	...	·001	...	0·974
1·4	1·000	...	...	...	...	·816	0·000	·014	...	0·830
1·2	1·005	...	...	...	...	·512	0·003	·055	...	0·569
1·0	1·071	0·500	...	...	...	·368	0·026	·158	...	0·552
0·8	1·504	·503	...	...	...	·512	0·198	·301	...	1·011
0·6	2·835	·524	...	...	...	·816	1·083	·635	...	2·534
0·4	4·770	·615	0·000	0·000	0·616	·973	3·024	·437	0·000	4·434
0·2	6·097	·750	0·017	·005	0·772	0·998	4·818	·314	·007	6·137
0·0	6·463	·810	0·225	·027	1·062	1·000	5·432	·233	·026	6·691
−0·2	6·097	·750	1·262	·062	2·073	...	5·097	·154	·081	6·332
−0·4	4·770	·615	3·100	·141	3·855	...	3·771	·035	·240	5·046
−0·6	2·835	·524	4·102	·321	4·947	...	1·834	0·000	·429	3·263
−0·8	1·504	·503	3·649	·436	4·587	...	0·503	...	·462	1·965
−1·0	1·071	0·500	...	0·297	...	...	0·071	...	·430	1·501
−1·2	1·005	...	...	...	...	...	0·005	...	·269	1·274
−1·4	1·000	...	...	...	...	...	0·000	...	·095	1·095
−1·6	1·000	...	...	...	...	...	...	...	·011	1·011
−1·8	1·000	...	...	...	...	...	...	...	·000	1·000
−2·0	1·000	...	...	...	...	...	...	...	0·000	1·000

Note that in setting $\sigma(y) \propto \tau(y)$, we have taken $v^\bullet = v'^\bullet$ and hence have adopted as turbulence ratio for the recombining shell

$$\beta' \equiv \frac{v'}{v'^\bullet} = \frac{v}{v^\bullet} \cdot \frac{v'}{v} = \beta\gamma, \tag{66}$$

a value which, when $\gamma = \frac{1}{2}$, gives half the value in the scattering shell. Emission after scattering from the rear and forward faces is not sufficiently displaced in frequency. As a consequence the profile fails to show central reversal.

It is interesting to contrast Tables VIII, IX. But for the presence of a scattering envelope the contours of Figs. 6 and 7 would have been similar: an emission profile $1+\Sigma$ symmetric about the line centre. In the model described by Table IX, however, not as much of the energy finds its way into emissivity β_2'', β_s of the scattering shell, because the latter is farther removed in position and velocity from the recombining shell than was the case for Table VIII.

5. *Conclusions*

5.1. *The contours and the physical model.*—In appraising the extent to which our assumptions about the principal *physical* features of a P Cygni type envelope are verified by the profiles, we can do no more at this stage than compare the calculated contours with the P Cygni type profiles considered as a *class.**

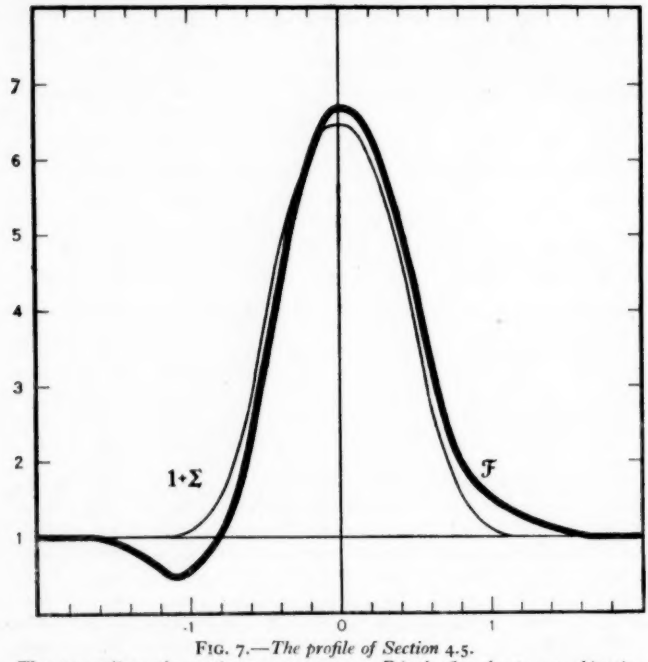

FIG. 7.—*The profile of Section* 4.5.
The star radiates the continuous spectrum 1. *Σ is the flux due to recombination. As a result of scattering, a distant observer sees the line contour* $\mathcal{F}$.

Relative to this more limited objective, the agreement between the calculated profiles and the observed ones is good. To illustrate this we reproduce a number of figures (Nos. 8–11) kindly provided by C. S. Beals from his publication "The Spectra of the P Cygni Stars" (**5**). The numbers appearing on the left of Figs. 8 and 9 give the type of profile according to Dr Beals' classification. For our purposes these are then representative observed profiles. Except for types II, VI, whose broad wings are indicative of Stark effect (which we have not attempted to take into account), each of these observed profiles has its mate among

* A quantitative analysis of the observed profiles of a particular star in terms of the parameters used in our calculations would require an investigation all its own. However, such an investigation appears entirely feasible.

the calculated profiles of Figs. 2, 3, 5, 6, 7 or among the profiles that may readily be interpolated from them.

Special attention should perhaps be drawn to one or two specific cases; for example, the remarkable parallelism of the Balmer series in HD 190603, Fig. 10, to the sequence of profiles showing the effects of occultation in Fig. 3. Also noteworthy is the similarity of the calculated profile in Fig. 6 with the observed hydrogen emission in Be spectra. Fig. 11 shows the Hα line in HD 218393. Despite the complexity of the latter profile it is readily seen that all its features can be accounted for by interpolating from the profile of Fig. 6 towards the profile of Fig. 7.

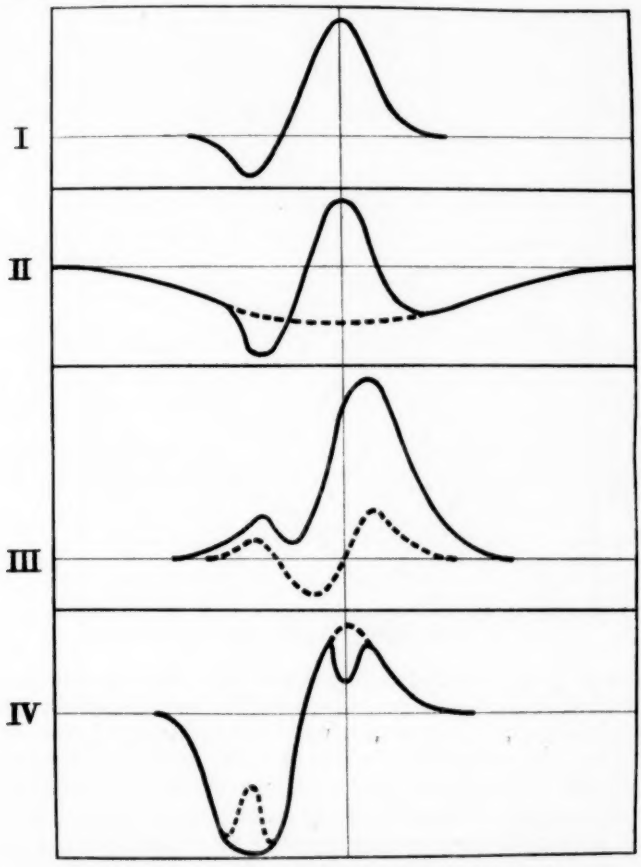

FIG. 8.—*Typical profiles of P Cygni-like stars. (After Beals.)*

Thus, as a class, the P Cygni stars come within the range of our model. This agreement with the observed profiles permits us to recast the assumptions about the model into assertions about these early-type stars.

(1) They are enclosed by an expanding atmosphere, whose outer regions are chiefly engaged in scattering. This is borne out by the *orientation* of absorption

and emission components in the spectral profiles: absorption minimum on the violet, emission maximum over the central-red frequencies. (When the latter is double, then the included minimum falls at the natural frequency of the line.)

(2) Since occultation is not a noticeable feature of the profiles the envelopes extend to at least 25 per cent in excess of the radius of the star proper.

(3) In addition, because in many of the profiles the equivalent width of emission exceeds that of absorption, the inner regions of the envelope must be emitting line radiation as a result of photoelectric ionization and recombination.

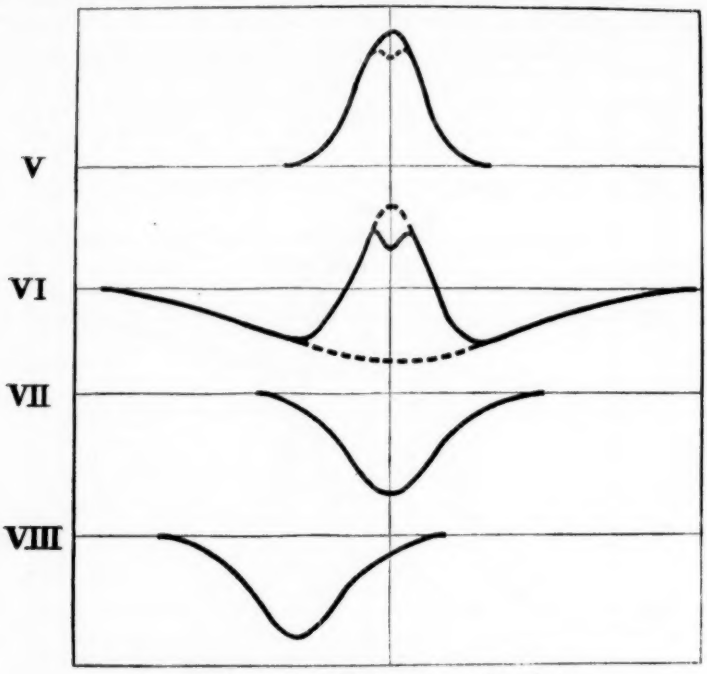

FIG. 9.—*Other profiles of P Cygni stars. (After Beals.)*

According to the analysis advanced in this paper, the oft-occurring "central reversal" is not primarily the result of absorption by matter with zero velocity in the line of sight. It is rather a consequence* of the fact that the average velocity of expansion is greater than the resultant of all non-uniform velocities in the envelope. These latter include the thermal velocities, turbulent velocity and any gradient or differential velocity present in the expansion. "Central reversals" arise in the computed profiles when the velocity of expansion exceeds the random velocities by a factor of order $\sqrt{10}$. This value provides a useful estimate of the velocity ratio in the envelopes of representative early-type stars. It is therefore noteworthy that the value thus found from the *line contours* agrees quite well with the value $2\sqrt{3}$ found for the same ratio by Chandrasekhar (**14**), who obtained his estimate from consideration of the *mechanical stability* under radiation pressure of an expanding planetary nebula.

* The reader is referred again to Fig. 6 *b*.

If the expansion in P Cygni-type envelopes is primarily produced by Lyman-α pressure on the hydrogen constituent, Chandrasekhar's calculation applies equally well here.* Consequently, the prevalence among P Cygni stars of profiles which are best fitted by a velocity of expansion at least three times the non-uniform velocities is not just a fortuitous fact. If the velocity of expansion were to fall below this value, with respect to the mean non-uniform velocity, pressures in the envelope would build up until the velocity increase became sufficient to restore equilibrium.

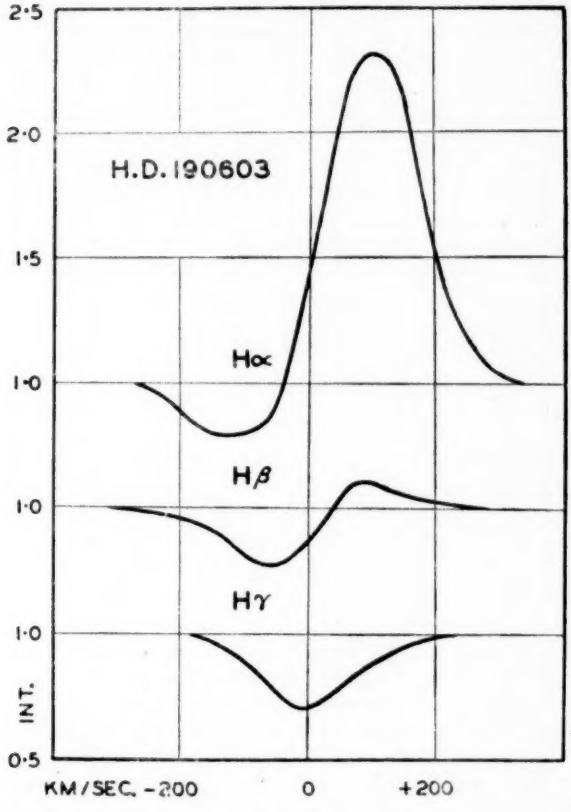

FIG. 10.

Although this interpretation of the velocity *ratio* is satisfactory, the *scale* of velocities is still to be explained. The observed displacements of the absorption components toward the violet imply expansion velocities of several hundred kilometres per second. Then, according to the equilibrium criterion, the corresponding non-uniform velocities must be of order one hundred kilometres per second. Indeed, the widths of the individual components themselves suggest a value of this order. But at temperatures around 25 000 deg. not more than

* The " thin shell approximation " that we have used replaces, in effect, the extended envelope by an equivalent planetary atmosphere.

twenty kilometres per second of this can be thermal velocity. Of course one would not have expected the expansion to be simply $\sqrt{10}$ times the thermal velocity, since an ejection velocity, produced solely by radiation pressure in the envelope, itself bespeaks a velocity gradient of comparable magnitude. And any velocity gradient itself contributes to the non-uniform velocities which widen the frequency range of the scattering coefficient. Still, it is difficult to see quantitatively why the expansion could not stabilize itself at smaller values than those observed. One cannot, it would seem, avoid having recourse to "turbulence" to provide the necessary breadth to the scattering coefficient. (An explanation in terms of the unexplained is not, however, very satisfactory.)

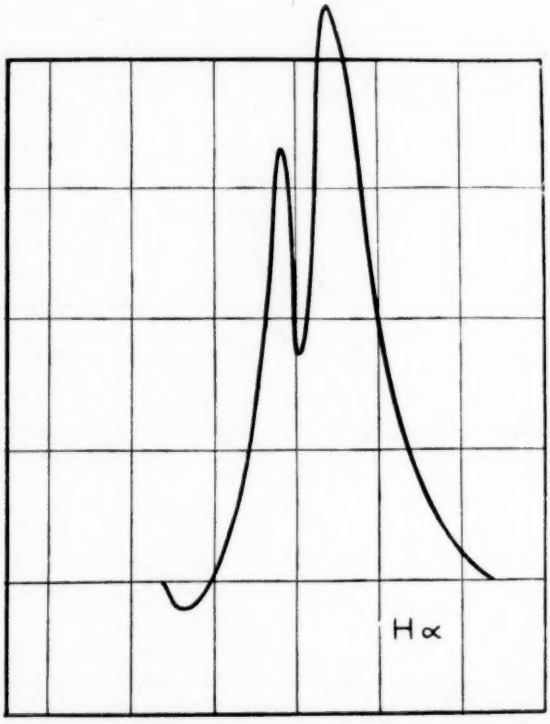

FIG. 11.—*The Hα line in HD 218393. (After Beals.)*

A point not emphasized in the previous paragraphs is the extent to which the choice of scattering coefficient determines the *shape* of each component, as distinct from the juxtaposition of emission and absorption components, in a complex line. Reference to the calculations, or a quick glance at the computed profiles, shows that each component and especially the wings show strongly the Gaussian form assumed in (29). Comparison with the observed profiles is in this respect also satisfactory. If reliance could be placed on the shapes of the components in the observed profiles being significantly free from instrumental distortion, it would be possible to conclude that the departures from uniform

motion (expansion) in the envelope are principally of the Gaussian or random type. To the extent that the non-uniform motions are a result of turbulence, or of non-coherence in the scattering (**15, 16**), this Gaussian form is understandable. But if the principal factor in broadening the scattering coefficient is the velocity gradient, the shape of the components should not be Gaussian.

The conclusion, that P Cygni atmospheres have an overall velocity of expansion approximately three times as great as their mean non-uniform velocities (whatever form these take), quantitatively supports Beals' radial ejection hypothesis. The above investigation has shown however that scattering (or re-emission after absorption) plays an important role in the outer regions of these atmospheres, where it acts to dam back the radiation from the inner regions until multiple scattering has altered the frequency of the radiation enough to permit escape. This makes it unnecessary to postulate any significant decelerations of the motions in this region in order to explain the central reversals, although such decelerations may be present.

5.2. *The computations.*—The correspondence of the computed profiles to the observed ones attests to the validity of the approximations necessarily made in order to derive them. Chief among these was the averaging process involved in treating the atmosphere or envelope as one or more thin shells. Mathematically this meant that the equation of transfer was given short shrift in order to concentrate on the boundary conditions of the problem. The importance of boundary conditions in problems of this sort was to a certain extent foreshadowed by Milne's classic treatment of the radiation problem in planetary nebulae (**21**).*

In introducing the method of approximation in Section 2, the only justification given for the process was its convenience. It was desired to study the consequences of a radiating system in which the several parts are moving with respect to one another and in which the occultation or obscuration of one part of the system by another may be significant. For this purpose it was necessary to have an adequate representation of the dependence of the radiation field on direction, particularly as required to relate the rays reaching one component of the system to the rays leaving another part. The traverse of the radiation field through the envelope is not of immediate concern, when one's interest is solely in the flux leaving the system and reaching the observer. All that one requires of the approximation is that it reproduce as well as possible the sum of radiation entering and leaving the various parts of the system in any one frequency; and this, as has been seen, can be accomplished without explicitly using the equation of transfer.

From a purely pragmatic view, then, the procedure adopted is the correct one for calculating profiles produced by an atmosphere in motion. The functional difficulties associated with using the integro-differential equation of radiation transfer are thereby avoided. Secondly, the effect of the boundary conditions on particular solutions can be interpreted easily in physical terms. Lastly, the two integral equations, for emissivity and flux, which form the basis of these calculations yield very readily to numerical computation.

There is some point now in enquiring why the "thin shell" provides a good approximation to an extended envelope *for the calculation of line contours.* If it were hypothetically possible to follow the trajectory of an individual light quantum as it leaves the photospheric surface, one could classify the quanta which reach

* See also (**14**).

the observer's recording apparatus in each frequency in the following fashion: (i) those whose trajectory is a single straight line (no scattering), (ii) those whose trajectory consists of two straight segments (single scattering), (iii) those whose trajectory consists of three straight segments (double scattering), etc. If one were to compare the numbers in corresponding classes when the envelope is regarded as a "thin shell" and when it is not, the numbers in (i) would be equal—by our definition of optical depth. In (ii) they can differ only as a result of velocity and density changing rapidly with depth in the extended envelope, and allowance was made for this in the "turbulent width" of the absorption coefficient. Or, in terms of the two segments of the trajectory which defines this class, there is no effective change introduced by variation in length of the segment which joins the photosphere to the scattering point. Not until class (iii) is reached does the "thin shell" description begin to depart from that of the extended envelope. The former gives an adequate accounting only of those quanta which traverse a considerable distance between scattering points and hence suffer a sizeable Doppler shift. Reference to Tables I, II, III shows however that singly scattered radiation B_s represents the greater part of the total scattered radiation density B. Small changes in the B_s columns will not noticeably change the contours.

It would be impossible to conclude this paper* without recording the author's indebtedness to Dr C. S. Beals, not only for suggesting the problems treated and making possible the progress of the work, but for his constant guidance through the observational material on P Cygni stars and its interpretation.

Dominion Observatory,
Ottawa:
1951 *November* 17.

References

(1) O. C. Wilson, *Ap. J.*, **111**, 279, 1950.
(2) B. P. Gerasimovič, *Zeits. f. Ap.*, **7**, 335, 1933.
(3) B. P. Gerasimovič, *Zeits. f. Ap.*, **10**, 154, 1935.
(4) C. S. Beals, *J.R.A.S. Can.*, **34**, 169, 1940.
(5) C. S. Beals, *Pub. Dom. Ap. Obs.*, IX, No. 2, 1950.
(6) C. S. Beals, *J.R.A.S. Can.*, **36**, 145, 201, 1942.
(7) O. Struve and P. Swings, *Ap. J.*, **96**, 475, 1942.
(8) W. H. McCrea and K. K. Mitra, *Zeits. f. Ap.*, **11**, 359, 1936.
(9) H. Zanstra, *Pub. Dom. Ap. Obs.*, **4**, 209, 1930; *Zeits. f. Ap.*, **2**, 1, 1931.
(10) C. S. Beals, *Pub. Dom. Ap. Obs.*, **6**, 111, 1934.
(11) S. Chandrasekhar, *M.N.*, **94**, 522, 1934.
(12) O. C. Wilson, *Ap. J.*, **80**, 259, 1934.
(13) S. Chandrasekhar, *Rev. Mod. Phys.*, **17**, 138, 1945.
(14) S. Chandrasekhar, *Ap. J.*, **102**, 402, 1945.
(15) L. Spitzer, *Ap. J.*, **99**, 1, 1944.
(16) H. Zanstra, *B.A.N.*, **11**, No. 401, 1949.
(17) A. Unsöld, *Physik der Sternatmosphären*, p. 159, Berlin, 1938.
(18) O. C. Wilson, *Ap. J.*, **82**, 233, 1935.
(19) A. B. Underhill, *Ap. J.*, **106**, 129, 1947.
(20) G. Cillié, *M.N.*, **92**, 820, 1932; **96**, 771, 1936.
(21) E. A. Milne, *M.N.*, **95**, 16, 1934.

* Thanks are due to the Mapping Section of the Hydrographic Survey of Canada for assistance with the drawings.

SELF-GRAVITATING STAR SYSTEMS. II

G. L. Camm

(Received 1951 December 4)

Summary

The general problem of the motion of a star system in the smoothed gravitational field which the system itself produces has been considered previously for the special case in which the stars are of equal mass. This restriction is now shown to be unnecessary. By a suitable definition of the velocity-distribution function the three equations which are involved in this problem can be written without any reference to the distribution of stars of different mass. The complexity of the problem is not affected by the increased generality.

For a star system with complete spherical symmetry the problem is reduced to solving a single non-linear partial differential equation. A number of special solutions have been obtained, including solutions which correspond to isothermal and polytropic gravitating gas-spheres. For three different models the variation of the projected density with radius has been found, and this is compared with observations of the variation of luminosity with radius in globular clusters. The best agreement is obtained in the case of a model which has never previously been considered, but which is essentially a modification of Plummer's model in which terms involving the angular momentum have been introduced.

---

1. *General theory of self-gravitating star systems with stars of different mass.*—The two-fold relationship between the velocity-distribution function of an isolated star system and the gravitational potential of the system itself has been pointed out in a previous paper on this subject (1). The generalized Boltzmann equation expresses the fact that changes of the velocity-distribution are controlled by the gravitational forces. The Poisson equation relates the gravitational potential and the mass-density which produces it. Finally the mass-density is obtained from the velocity-distribution function by integration over the velocity components. In the previous paper it had been supposed that the system consisted of stars of equal mass. This assumption is quite unnecessary. Obviously the results are unaffected if we assume, not that all the stars have the same mass, but that the average mass of a star is the same in all regions of the system. It now appears that, by a change in our definitions, we can formulate the problem in such a way as to include stars of very different masses, even when the distribution of masses is a function of position. Most fortunately, too, the change leaves the mathematical treatment quite unaffected.

As before, we adopt any convenient non-accelerated Cartesian frame of space-coordinates, x, y, z, and corresponding velocity components u, v, w. Then the mass-velocity-distribution function, $f(t, m, x, y, z, u, v, w)$, is such that the number of stars at time t which have masses between m and $m+dm$, which are in a volume $dx\,dy\,dz$, surrounding the point (x, y, z), and for which the velocity-components lie in the ranges, u to $u+du$, v to $v+dv$, w to $w+dw$, is $f\,.\,dm\,dx\,dy\,dz\,du\,dv\,dw$.

Again we assume that the gravitational forces can be derived from a potential function $\Omega(t, x, y, z)$. As a consequence, the Boltzmann equation now becomes

$$\frac{\partial f}{\partial t}+u\frac{\partial f}{\partial x}+v\frac{\partial f}{\partial y}+w\frac{\partial f}{\partial z}+\frac{\partial \Omega}{\partial x}\frac{\partial f}{\partial u}+\frac{\partial \Omega}{\partial y}\frac{\partial f}{\partial v}+\frac{\partial \Omega}{\partial z}\frac{\partial f}{\partial w}=0. \qquad (1)$$

From the definition of f, it is clear that $\rho(t,x,y,z)$, the mass-density, is given by the equation

$$\rho(t,x,y,z)=\iiiint mf(t,m,x,y,z,u,v,w)\,dm\,du\,dv\,dw, \tag{2}$$

where the integrations are over the entire ranges of m, u, v and w. Finally, from Poisson's equation we also have

$$\nabla^2\Omega=-4\pi G\rho(t,x,y,z). \tag{3}$$

The effect of non-uniform mass is removed if we define a function

$$F(t,x,y,z,u,v,w),$$

such that

$$F(t,x,y,z,u,v,w)=\int mf\,dm.$$

If we multiply (1) by m, and integrate over all m, we obtain

$$\frac{\partial F}{\partial t}+u\frac{\partial F}{\partial x}+v\frac{\partial F}{\partial y}+w\frac{\partial F}{\partial z}+\frac{\partial\Omega}{\partial x}\frac{\partial F}{\partial u}+\frac{\partial\Omega}{\partial y}\frac{\partial F}{\partial v}+\frac{\partial\Omega}{\partial z}\frac{\partial F}{\partial w}=0. \tag{4}$$

Similarly (2) can be written

$$\rho=\iiint F\,du\,dv\,dw. \tag{5}$$

Equations (3), (4) and (5) contain the essence of the self-gravitating problem, but do not refer to individual masses in any way. The mathematics of the previous paper is quite unaffected, except that the constant m is replaced by unity, and the function f which appears should be replaced by the function F, defined above.

It is not altogether surprising that the problem can be formulated without reference to the distribution of mass, for we are only concerned with the gravitational field of a smoothed-out distribution of matter. In such a field the acceleration of a star is independent of its mass. It is only when the effects of encounters are considered that stars of different masses experience different accelerations. It should be emphasized, of course, that in comparing theory and observation in this kind of investigation we usually compare the theoretical mass-density with either the number-density of observed stars, or the observed luminosity from a given element of volume.

2. *General theory for a spherical star system.*—The treatment of star systems with spherical symmetry introduces one more variable into the fundamental equation than in the problem of a system stratified in plane parallel layers. In the latter case there were only three variables, namely the time, one space coordinate and one velocity coordinate; in the spherical problem, however, there are two velocity variables, namely the velocity components along and perpendicular to the radius vector. It is convenient to take spherical polar coordinates, r, θ, ϕ, with the origin at the centre of the system. The corresponding components of velocity are Π, radially outwards, and Θ and Φ, the components transverse to the radius vector. Since complete spherical symmetry is assumed, the components Θ and Φ do not occur separately, but only in the combination $\Theta^2+\Phi^2$. It is therefore simpler to put $T=\Theta^2+\Phi^2$ (so that T is the square of the transverse speed), and to use T as the second velocity variable. The square of the angular momentum per unit mass is r^2T.

The integrated velocity-distribution function, F, now depends on the four variables, t, r, Π and T only. The function is defined in such a way that at time t the sum of the masses of all stars in an element of volume $d\tau$ at a distance r from the centre of the system which have radial velocity components between Π and $\Pi+d\Pi$, and which have transverse velocity components whose squares lie between T and $T+dT$, is $F(t,r,\Pi,T)\,d\tau\,d\Pi\,dT$. Thus F must satisfy an equation of continuity, namely

$$\frac{\partial F}{\partial t}+\Pi\frac{\partial F}{\partial r}+\frac{d\Pi}{dt}\frac{\partial F}{\partial \Pi}+\frac{dT}{dt}\frac{\partial F}{\partial T}=0.$$

The equations of motion are

$$\frac{d\Pi}{dt}=\frac{T}{r}-\frac{GM(t,r)}{r^2},$$

$$\frac{dT}{dt}=-\frac{2\Pi T}{r}.$$

In the first of these G is the gravitational constant and $M(t,r)$ is the total mass at time t inside the sphere of radius r. The equation of continuity now becomes

$$\frac{\partial F}{\partial t}+\Pi\frac{\partial F}{\partial r}+\left(\frac{T}{r}-\frac{GM}{r^2}\right)\frac{\partial F}{\partial \Pi}-\frac{2\Pi T}{r}\frac{\partial F}{\partial T}=0. \tag{6}$$

The mass-density, $\rho(t,r)$, is obtained from F by integration, so that we have

$$\rho(t,r)=\int_{T=0}^{\infty}\int_{\Pi=-\infty}^{+\infty}F(t,r,\Pi,T)\,d\Pi\,dT. \tag{7}$$

Lastly, Poisson's equation can be more simply written in the form

$$\partial M/\partial r=4\pi r^2\rho(t,r). \tag{8}$$

By a suitable change of variables it is possible to replace (6), (7) and (8) by a single partial differential equation. In effect we take the Fourier transform of F with respect to the variable Π, and the Laplace transform with respect to T. It is therefore convenient to define a function $M(t,r,s,p)$ by the equation

$$M(t,r,s,p)=4\pi\int_{x=0}^{r}\int_{T=0}^{\infty}\int_{\Pi=-\infty}^{+\infty}x^2F(t,x,\Pi,T)\exp(\mathrm{i}\Pi s-pT)\,d\Pi\,dT\,dx.$$

From the definition it will be seen that $M(t,r,0,0)$ is the same as $M(t,r)$, the mass at time t inside the sphere of radius r. It is also clear that

$$\frac{1}{4\pi r^2}\frac{\partial}{\partial r}M(t,r,s,p)=\int_{T=0}^{\infty}\int_{\Pi=-\infty}^{+\infty}F(t,r,\Pi,T)\exp(\mathrm{i}\Pi s-pT)\,d\Pi\,dT. \tag{9}$$

We now multiply (6) by $\exp(\mathrm{i}\Pi s-pT)$, and integrate with respect to Π and T. The following equations, all of which follow from (9), are required:

$$\iint\frac{\partial F}{\partial t}\exp(\mathrm{i}\Pi s-pT)\,d\Pi\,dT=\frac{1}{4\pi r^2}\frac{\partial^2 M}{\partial r\partial t},$$

$$\iint\Pi\frac{\partial F}{\partial r}\exp(\mathrm{i}\Pi s-pT)\,d\Pi\,dT=\frac{\mathrm{i}}{2\pi r^3}\frac{\partial^2 M}{\partial r\partial s}-\frac{\mathrm{i}}{4\pi r^2}\frac{\partial^3 M}{\partial r^2\partial s},$$

$$\iint\frac{\partial F}{\partial \Pi}\exp(\mathrm{i}\Pi s-pT)\,d\Pi\,dT=-\frac{\mathrm{i}s}{4\pi r^2}\frac{\partial M}{\partial r},$$

$$\iint T\frac{\partial F}{\partial \Pi}\exp(\mathrm{i}\Pi s-pT)\,d\Pi\,dT=\frac{\mathrm{i}s}{4\pi r^2}\frac{\partial^2 M}{\partial r\partial p},$$

$$\iint T\Pi\frac{\partial F}{\partial T}\exp(\mathrm{i}\Pi s-pT)\,d\Pi\,dT=\frac{\mathrm{i}}{4\pi r^2}\frac{\partial^2 M}{\partial r\partial s}+\frac{\mathrm{i}p}{4\pi r^2}\frac{\partial^3 M}{\partial r\partial s\partial p}.$$

With the aid of these equations, (6) is transformed, and after some simplification is written

$$\frac{\partial^2 M}{\partial r \partial t} + \frac{\partial^3 M}{\partial r^2 \partial s} - \frac{s}{r}\frac{\partial^2 M}{\partial r \partial p} + \frac{Gs}{r^2}\frac{\partial M}{\partial r} M(t, r, 0, 0) + \frac{2p}{r}\frac{\partial^3 M}{\partial r \partial s \partial p} = 0. \qquad (10)$$

This single equation is a necessary consequence of Poisson's equation and Boltzmann's equation. Conversely, any solution of (10) will lead, by application of the inverse Fourier and Laplace transformations, to functions F, ρ and Ω which satisfy equations (6), (7), (8). These will correspond to a possible physical model, if one condition is satisfied, namely that the function $F(t, r, \Pi, T)$ is non-negative.

It should be emphasized that this treatment completely disregards the possible effects of close encounters. At a later stage we shall have to consider how important encounters are in the physical systems to which the theory will be applied, but as there is no immediate likelihood of obtaining an exact solution which allows for encounters, we shall examine equation (10) for solutions, even though in each the gravitational field is really that of a smoothed-out distribution of matter.

3. *Some solutions of the steady-state problem: the isothermal model.*—The dynamical theory of spherical star systems has been studied quite extensively. Much of the early work is summarized by Martens in the introduction to his monograph on the subject (**2**). More recent contributions have been made by ten Bruggencate (**3**), Shiveshwarkar (**4**), Finlay-Freundlich (**5, 6**), and Kurth (**7, 8, 9**). Two fundamental results which reappear in the present paper are due to Plummer (**10**) and to Eddington (**11**). For the most part these papers produced solutions which were too general, either because they did not require that the gravitational potential was due to the system itself, or because they were based on the virial theorem, which is less restrictive than the combination of the Boltzmann and Poisson equations.

The aim of this present investigation is to find solutions of (10) which are as varied in type as possible. There seems to be no clear way of finding the general solution, and we therefore have to obtain particular solutions by the method of separation of the variables. If this is necessary, then the use of transforms yields no advantage, and we can combine (6), (7) and (8) by more direct methods. The experience gained in studying the stratified star system suggests that we attempt to find a function $F(t, r, \Pi, T)$ which satisfies the equations (6), (7) and (8), and which has the fairly general form

$$F = \frac{1}{4\pi r^2}\left\{\frac{\partial}{\partial r} M(t, r)\right\} . a(t, r) . b(t, r) . P\{\Pi a(t, r), Tb(t, r)\}. \qquad (11)$$

In this, a and b are functions of t and r, yet to be determined, and P is a function of $p(=\Pi a)$ and $q(=Tb)$, also to be determined. Without loss of generality we may assume

$$\int_{q=0}^{\infty}\int_{p=-\infty}^{+\infty} P(p, q)\, dp\, dq = 1.$$

It therefore follows that

$$\begin{aligned}\rho(t, r) &= \int_{T=0}^{\infty}\int_{\Pi=-\infty}^{+\infty} F\, d\Pi\, dT \\ &= \frac{1}{4\pi r^2}\frac{\partial M}{\partial r}\int_{q=0}^{\infty}\int_{p=-\infty}^{+\infty} P\, dp\, dq \\ &= \frac{1}{4\pi r^2}\frac{\partial M}{\partial r}.\end{aligned}$$

Thus the expression (11) gives a form for F which satisfies both (7) and (8). The expression for F is substituted in (6), which becomes an equation in t, r, p and q. By repeated differentiation we can separate the functions M, a, b and P, and so find each of them in turn, either exactly or else as the solution of a differential equation. The method is quite straightforward, but the labour of examining all the possibilities arising is extremely tedious. The conclusion of the matter is that there are only four solutions of type (11), and in none of them is the time explicitly involved. Consequently they all correspond to models in a steady state, and they are therefore of a special form in which F is solely a function of the two integrals of motion, namely the total energy per unit mass, $\frac{1}{2}(\Pi^2+T)-\Omega(r)$, and the square of the angular momentum per unit mass, r^2T. This result follows from a more general theorem due to Jeans (**12**), and has also been established for steady spherical systems by Shiveshwarkar (**4**).

The simplest of the four solutions is one for which

$$a^2=b=1/2h^2 \text{ (a constant)},$$

$$P=\pi^{1/2}\exp\{-(\Pi^2+T)/2h^2\}.$$

The mass-density is related to the gravitational potential by the formula

$$\rho=\rho_0\exp\{(\Omega-\Omega_0)/h^2\},$$

where ρ_0 and Ω_0 are the values of the density and the potential at the origin. Now we also have

$$d\Omega/dr=-GM/r^2,$$

from which it follows that

$$\frac{d}{dr}\left(r^2\frac{d\Omega}{dr}\right)=-G\frac{dM}{dr}$$

$$=-4\pi Gr^2\rho.$$

The potential function Ω must therefore satisfy the differential equation

$$\frac{1}{r^2}\frac{d}{dr}\left(r^2\frac{d\Omega}{dr}\right)=-4\pi G\rho_0\exp\{(\Omega-\Omega_0)/h^2\}. \qquad (12)$$

The actual form of F in this case is

$$F=(8\pi)^{-1/2}\rho_0h^{-3}\exp\{(2\Omega-2\Omega_0-\Pi^2-T)/2h^2\}.$$

Equation (12) is the equation satisfied by the gravitational potential of an isothermal gas sphere. It will be seen that the velocity-distribution is Maxwellian. This is likely to be the form ultimately taken up by a spherical system after a very large number of encounters have occurred. There is essentially only one solution of (12) which will satisfy the boundary conditions $\Omega=\Omega_0$ and $d\Omega/dr=0$ at $r=0$. (The second of these conditions merely expresses the fact that the gravitational attraction must vanish at the centre of the system. Models in which this attraction does not vanish at the centre have been considered by von Zeipel (**13**), but it seems unlikely that such models can correspond to a real situation.) In (12) it is convenient to write

$$\Omega=\Omega_0-h^2u, \qquad r=cx.$$

Thus the equation becomes

$$\frac{1}{x^2}\frac{d}{dx}\left(x^2\frac{du}{dx}\right)=\frac{4\pi G\rho_0c^2}{h^2}e^{-u}.$$

The constant c is at our disposal, and can be chosen so that

$$c^2 = h^2/4\pi G\rho_0.$$

This makes the equation completely dimensionless, and we have

$$\frac{1}{x^2}\frac{d}{dx}\left(x^2\frac{du}{dx}\right) = e^{-u},$$

with the initial conditions that u and du/dx vanish at $x=0$. This equation, originally studied by Emden (**14**), has more recently been considered for its astronomical implications by Chandrasekhar (**15**). It leads to a model of infinite radius and infinite total mass, which clearly will not correspond to a physical system. It may, however, represent the innermost part of a physical system, where the density is high. The general equation (10) applies equally well to a model where the form of velocity-distribution is fundamentally different in different regions—such as an isothermal core with an envelope satisfying quite a different law—but by restricting the form of solution to (11) we are prevented from finding such a combination.

4. *Eddington's model.*—The second solution of type (11) was originally obtained by Eddington (**11**), and is one in which a is constant, and $b = a^2(1+\alpha r^2)$, where α is a constant. The function P is of the form

$$P = Aq^{\mu}\exp\{-\tfrac{1}{2}(p^2+q)\}.$$

It is clearly necessary that the index μ is zero, for if μ were negative the function F would be infinite for $T=0$, so that at any point of the system there would be an infinite mass with a purely radial motion. Similarly, if μ were positive, there would be no particles with purely radial motion.

This solution leads to a relation between the density and the gravitational potential, namely

$$\rho = \frac{\rho_0}{1+\alpha r^2}\exp\{(\Omega-\Omega_0)/h^2\}.$$

Consequently the function Ω satisfies the equation

$$\frac{1}{r^2}\frac{d}{dr}\left(r^2\frac{d\Omega}{dr}\right) = -\frac{4\pi G\rho_0}{1+\alpha r^2}\exp\{(\Omega-\Omega_0)/h^2\}.$$

This replaces (12) and has, of course, the same boundary conditions. The change of variables previously used will not remove the constant α, so that a one-parameter family of solutions can be obtained. From the form of Eddington's distribution function it can be shown that there is no upper limit to the kinetic energy a star may have, and so there can be no "velocity of escape": the model cannot have a finite boundary. Thus it may be deduced that if the constant α is negative, the system is unlikely to correspond to a physical system. For if α is negative, $(1+\alpha r^2)$ will vanish for a finite value of r, and the density is infinite there.

If the constant α is zero, we recover the isothermal model previously considered. If α is positive, the solution corresponds to a model which has both an infinite radius and an infinite total mass. However, it differs from the isothermal model in two respects. The velocity-dispersion in the previous case was the same in all directions and at all points. In this modification, due to Eddington, the velocity-dispersion in the radial direction is the same at all points, but the dispersion of the transverse velocities decreases with increasing radius. Thus

there is star-streaming towards the centre at all eccentric points. Secondly, the two solutions differ in the way in which the density varies with radius for large values of r. In the isothermal model $\rho(r)$ is of order r^{-2} for large r, whereas in the modified form ρ is of order $r^{-2}(\ln r)^{-1}$. Thus the density tends to zero rather more rapidly, but not sufficiently rapidly to give a finite total mass.

5. *The polytropic model.*—A third type of solution of the form (11) is one in which $b=a^2$, and a is a function of r. The function P is now given by

$$P=q^{\lambda}(q+p^2+\text{constant})^{\mu}, \tag{13}$$

or

$$P=q^{\lambda}(\text{constant}-q-p^2)^{\mu}. \tag{14}$$

The arguments used in the previous section enable us to dismiss the cases in which $\lambda\neq 0$ as being inapplicable to a physical system. In the case $\lambda=0$ we shall certainly obtain a model of infinite radius unless we impose a finite limit on the energy. If we use the form (14) we can impose such a limit. In this case F is a function of the total energy only, and we have

$$F=A(2\Omega-\Pi^2-T)^{\mu}, \qquad \Pi^2+T\leqslant 2\Omega,$$

$$F=0, \qquad \Pi^2+T\geqslant 2\Omega.$$

Clearly the index μ must be positive, otherwise F becomes indefinitely large as (Π^2+T) approaches 2Ω. The function Ω vanishes at the boundary, and is positive inside it. The density is obtained directly from F, namely

$$\rho=A\iint(2\Omega-\Pi^2-T)^{\mu}\,d\Pi\,dT, \qquad (2\Omega-\Pi^2-T)\geqslant 0$$

$$=\frac{A\pi^{1/2}\mu\,!}{(\mu+\frac{3}{2})\,!}(2\Omega)^{\mu+3/2}.$$

In consequence of the Poisson equation, the function Ω must be a solution of the equation

$$\frac{1}{r^2}\frac{d}{dr}\left(r^2\frac{d\Omega}{dr}\right)=-\frac{4A\pi^{3/2}G\mu\,!}{(\mu+\frac{3}{2})\,!}(2\Omega)^{\mu+3/2}. \tag{15}$$

This can be simplified if we introduce the velocity-dispersion. By direct integration it will be found that

$$\overline{\Pi^2}=2\Omega/(2\mu+5), \qquad \overline{T}=2\overline{\Pi^2}.$$

Hence there is no star-streaming, and the velocity-dispersion is isotropic at all points, but it will decrease as r increases. If h^2 is the maximum value of $\overline{\Pi^2}$, attained at $r=0$, we have

$$2\Omega(0)=(2\mu+5)h^2.$$

It is now convenient to change variables in (15), putting

$$2\Omega=(2\mu+5)h^2\psi,$$

$$r=cx.$$

If we choose the constant c so as to satisfy the equation

$$c^2=(\mu+\tfrac{5}{2})\,!\,(\mu\,!)^{-1}A^{-1}\pi^{-1/2}(2\mu+5)^{-\mu-3/2}h^{-2\mu-1},$$

we find that (15) reduces to the form

$$\frac{1}{x^2}\frac{d}{dx}\left(x^2\frac{d\psi}{dx}\right)+\psi^{\mu+3/2}=0. \tag{16}$$

This is the familiar Emden equation for the equilibrium of a polytropic gas sphere (**14**). The polytropic index n is in our case the index $(\mu+\frac{3}{2})$. The boundary conditions are also those of Emden's problem, namely $\psi=1$, $d\psi/dx=0$ at $x=0$. From Emden's results we know that the star-system has a finite radius and finite mass if $n<5$, and that the radius is infinite but the total mass finite if $n=5$. In the case in which $n>5$, both radius and total mass are infinite. Effectively, therefore, there is a one-parameter family of solutions of type (14), with μ as the parameter.

The case $n=5$, $\mu=\frac{7}{2}$ is one for which (16) has an elementary solution, namely

$$\psi=(1+\tfrac{1}{3}x^2)^{-1/2},$$
$$\rho=\rho_0(1+\tfrac{1}{3}x^2)^{-5/2}.$$

This special case has been considered by Plummer (**10**), and was found to agree fairly well with the density distribution observed in globular clusters. This solution will be examined again in comparing these models with each other, and with observations.

The alternative form (13) is one in which no limit is placed on the total energy a star may possess. There may be stars with extremely high total energy, but it is reasonable to suppose that the number of stars of a given total energy tends to zero as the energy tends to infinity. This is arranged by taking as the distribution function

$$F=A(\Pi^2+T-2\Omega)^{-\mu}.$$

The index μ must be positive to ensure that $F\to 0$ as $T,\Pi\to\infty$. It is also necessary that Ω is everywhere negative, so that for all Π and T the function F remains finite. It is then found that

$$\overline{\Pi^2}=(-2\Omega)/(2\mu-5), \qquad \overline{T}=2\overline{\Pi^2}.$$

In order that the mean-square velocity should be finite, we require $2\mu>5$. Thus the velocity-dispersion at any point is isotropic, and since the absolute value of Ω increases with r, the velocity-dispersion also increases with the radius.

The differential equation satisfied by the potential function is analogous to (15). By a similar change of variables it can be reduced to the differential equation

$$\frac{1}{x^2}\frac{d}{dx}\left(x^2\frac{d\psi}{dx}\right)=\psi^{3/2-\mu}. \tag{17}$$

This is a polytropic equation with negative index. We know that the model is of infinite radius, and by considering (17) it can be shown that for large values of r, ρ is of order $r^{-2+\nu}$, where $\nu=4/(2\mu-1)$. Thus the density falls off more slowly than in the isothermal case, and for this reason we shall see that the solution under discussion does not correspond to a physical model.

6. *A modification of the polytropic model.*—The remaining solution of the special type (11) we have been considering is related to the polytropic model in the way that Eddington's is to the isothermal one. We have that $b=a^2(1+\alpha r^2)$, where α is a constant, but a is a function of r. As in the polytropic case, the function P takes one or other of the two forms (13) or (14). Again it is evident that the index λ must be zero. The function F is seen to be a power of a linear combination of the total energy and the square of the angular momentum. Solutions of this type have been considered by Kurth (**7**), though he has not exhausted all the possibilities of this model.

As before, to obtain a finite system it is necessary (though not sufficient) to take P to be of the form (14), so that F is given by the pair of equations

$$F = A(2\Omega - \Pi^2 - T - \alpha r^2 T)^\mu, \qquad \Pi^2 + T(1+\alpha r^2) \leqslant 2\Omega,$$

$$F = 0, \qquad \Pi^2 + T(1+\alpha r^2) \geqslant 2\Omega.$$

The index μ must be positive. The potential function Ω vanishes at the boundary, and is positive inside it. The density is obtained by direct integration, and comes out to be

$$\rho = A\pi^{1/2} \frac{\mu!}{(\mu+\frac{3}{2})!} \frac{(2\Omega)^{\mu+3/2}}{1+\alpha r^2}.$$

It therefore follows that Ω satisfies the differential equation

$$\frac{1}{r^2}\frac{d}{dr}\left(r^2 \frac{d\Omega}{dr}\right) = -\frac{4A\pi^{3/2}G\mu!}{(\mu+\frac{3}{2})!} \frac{(2\Omega)^{\mu+3/2}}{1+\alpha r^2}. \tag{18}$$

This can be simplified a little if we introduce ρ_0, the central density, and h^2, the maximum value of $\overline{\Pi^2}$, occurring at $r=0$. It is convenient to put $r=cx$, where $\alpha c^2 = \pm 1$, and also to put $\Omega = k\psi$. After substituting these new variables in (18), we obtain

$$\frac{1}{x^2}\frac{d}{dx}\left(x^2\frac{d\psi}{dx}\right) = -\left[\frac{8\pi G\rho_0 c^2 (2k)^{\mu+1/2}}{h^{2\mu+3}(2\mu+5)^{\mu+3/2}}\right] \frac{\psi^{\mu+3/2}}{1\pm x^2}.$$

The constant k can be chosen so as to make the quantity in square brackets numerically equal to unity, so that we finally have

$$\frac{1}{x^2}\frac{d}{dx}\left(x^2\frac{d\psi}{dx}\right) = -\frac{\psi^{\mu+3/2}}{1\pm x^2}. \tag{19}$$

The boundary conditions for (18) were $\Omega = \Omega_0 = h^2(\mu+\frac{5}{2})$ and $d\Omega/dr = 0$ at $r=0$. After the transformations made, the boundary conditions of (19) are

$$\psi = \psi_0 = h^2(\mu+\tfrac{5}{2})/k \quad \text{and} \quad d\psi/dx = 0 \quad \text{at} \quad x = 0.$$

Thus there are two parameters in the equation, the initial value ψ_0 and the index μ. There is the further complication that the constant α may be positive or negative. If α is positive, the denominator on the right-hand side of (19) is $(1+x^2)$; if α is negative, the denominator is $(1-x^2)$. It should also be pointed out that the right-hand side of (19) is proportional to the density. Consequently, if α is negative, ψ must have a zero for some x, $0<x<1$, otherwise the density will become infinite at $x=1$. The only part of the solution which is of interest is that part which lies between $x=0$ and the first zero of $\psi(x)$. The function ψ may have a mathematical existence beyond this point, but the density distribution to which this would correspond cannot influence the gravitational forces inside the critical radius. Further, since the density vanishes at this radius, there is no transfer of mass across the bounding sphere. For practical purposes, then, ψ decreases from ψ_0 to zero, and then remains zero for all larger values of x.

The velocity-dispersion for this model is found to be

$$\overline{\Pi^2} = 2\Omega/(2\mu+5), \qquad \overline{T} = 2\overline{\Pi^2}/(1+\alpha r^2).$$

Again it is evident that the sign of α makes a real difference. If α is positive, there is a radial star-streaming, as in Eddington's model; if α is negative, the dispersion is smaller in the radial direction than in any other.

Equation (19) has been solved numerically for $\mu=\frac{1}{2}$ and for $\mu=\frac{5}{2}$ (corresponding to polytropic indices $n=2$ and $n=4$), and with the constant α taken to be negative. It was found that the starting value ψ_0 had to be sufficiently large (i.e. α sufficiently small), otherwise ψ does not vanish before $x=1$, and so the density becomes infinite. The permitted values of α are in fact so small that the variation of ρ with radius is scarcely distinguishable from that found in the corresponding Emden polytropic model. The small difference which is found tends to make the density of the modified polytrope fall less rapidly near the centre and more rapidly in the outer regions. Thus the model is more like a polytrope of slightly lower index.

The special case $\mu=\frac{7}{2}$, $n=5$ has not been solved for negative α. We know that if α is zero the density tends to zero only as r tends to infinity. It therefore seems very improbable that the introduction of any negative value of α will cause ψ to vanish before $x=1$. No formal proof of this conjecture is offered, but experience with lower indices showed that ψ will vanish before $x=1$ only if α is sufficiently small, and we know that for $n=5$, if α is actually zero, ψ tends to zero only as x tends to infinity.

For very similar reasons it has not seemed profitable to investigate any models with $\mu>\frac{7}{2}$ and α negative. There is little likelihood that they will avoid infinite density at $x=1$.

Equation (19) has also been solved numerically for $\mu=\frac{1}{2}$, $\frac{5}{2}$ and $\frac{7}{2}$ (polytropic indices $n=2$, 4 and 5) and with various positive values of α. The differences from the Emden polytrope naturally increase with increasing α, but the nature of the solution does not change fundamentally. The models with $\mu=\frac{1}{2}$ and $\frac{5}{2}$ have finite radii; those with $\mu=\frac{7}{2}$ do not. The equation has not been examined for values of μ exceeding $\frac{7}{2}$.

There remains the modified polytrope with negative index; this is the case in which the distribution function is

$$F=A\{\Pi^2+T(1+\alpha r^2)-2\Omega\}^{-\mu}.$$

In this form there is no upper limit to the energy, so that μ must be positive, and the model is of infinite radius. It is therefore essential that the constant α should be non-negative.

The change of variables which gave rise to (19) now shows that the function Ω is a constant multiple of ψ, where ψ satisfies the differential equation

$$\frac{1}{x^2}\frac{d}{dx}\left(x^2\frac{d\psi}{dx}\right)=\frac{\psi^{3/2-\mu}}{1+x^2}.$$

This equation has not been examined in detail, but it is found that for large values of x the function ψ behaves like $(\ln x)^{1/(\mu-1/2)}$. It follows that the density will vary as $x^{-2}(\ln x)^{-\nu}$, where

$$\nu=(\mu-\tfrac{3}{2})/(\mu-\tfrac{1}{2}).$$

Consequently the density tends to zero rather less rapidly than in Eddington's modification of the isothermal model.

This model, like the polytropic model with the negative index (of which it is a modification), also has the peculiarity that the value of Π^2 tends to infinity with increasing radius.

7. ***A comparison of the four theoretical models.***—It is clearly important to compare in more detail the various models so far discussed. This can be done in a variety of ways for, in addition to the parameters μ and α (when they occur), each model contains two further parameters. These could be taken to be any two of the following quantities:—the central density, the radius, if finite, the total mass, if finite, and the velocity-dispersion at the centre. Since, however, the radius and the total mass are infinite in some cases, they are best excluded, and the most convenient parameters are found to be the central density, ρ_0, and an effective radius, a, at which the density falls to $\rho_0/10$. With these two parameters we can plot ρ/ρ_0 as a function of r/a for any model, and all the curves obtained will pass through the two points $(r/a=0, \rho/\rho_0=1)$ and $(r/a=1, \rho/\rho_0=0{\cdot}1)$.

The first comparison made is between the polytropic model for which $n=4$ and modifications of it when terms representing angular momentum are included. In this case the constant α can be positive or negative. The variation of density with radius is not given here, since the differences between the three models are very small in this respect. The difference between them, such as it is, shows that the polytropic model (denoted by *P*) has a slightly more extensive region of high density near the centre than the model modified with a positive parameter α (the model denoted by *M.P.*+), and a less extensive region than *M.P.*−. The difference can also be expressed by saying that *M.P.*+ shows a density distribution which is rather like an Emden polytrope which has an index a little greater than 4, whereas *M.P.*− gives a distribution like a simple polytrope of index a little less than 4.

In Table I some further comparisons are given for these three models. The dimensionless quantity αa^2 indicates the extent of the modification which distinguishes (18) from (15). The degree of central condensation is indicated by the ratio of the mass within the sphere of radius a, denoted by $M(a)$, to the total mass.

TABLE I

A comparison of three models of polytropic index 4. P is the Emden polytrope, M.P.− and M.P.+ are modifications

Model	*M.P.*−	*P*	*M.P.*+
αa^2	−0·0245	0	+0·0415
Radius/a	6·12	6·54	7·41
Total mass /$\rho_0 a^3$	1·882	1·883	1·868
$M(a)$/Total mass	0·574	0·577	0·580
$h^2/G\rho_0 a^2$ $(=\overline{\Pi^2}/G\rho_0 a^2)_{r=0}$	0·475	0·478	0·485
$(\overline{\Pi^2}/G\rho_0 a^2)_{r=a}$	0·265	0·269	0·275
$(\frac{1}{2}\overline{T}/G\rho_0 a^2)_{r=a}$	0·272	0·269	0·264

The table also gives the values of h^2, the velocity-dispersion at the centre, and in the last two lines the dispersion in the radial and transverse directions evaluated at $r=a$. In model *P* the velocity-distribution is spherical, but in *M.P.*− there is transverse star-streaming, and in *M.P.*+ the streaming is radial.

The differences between these three models appear from the table to be extremely small, but the differences in velocity-distribution are considerable for large r—though at such distances the density will be extremely low. For the

Emden polytrope (P) the velocity-ellipsoid is in fact everywhere a sphere, but for $M.P.-$ it becomes more oblate as we move farther from the centre of the system, and ultimately at the boundary the axes are in the ratio 1 : 1 : 0·29. On the other hand, the velocity-ellipsoid for $M.P.+$ becomes increasingly prolate, and the limiting ratio of the axes is 1 : 1 : 1·81.

It is to be remembered that all these three models are particular cases. The properties of P are determined once the index $n=4$ has been chosen, but in the two modified solutions the constant α is still at our disposal. The negative value of α chosen for $M.P.-$ is quite near the extreme limit when the denominator, $1+\alpha r^2$, in (18) vanishes at the zero of $\Omega(r)$. Thus the model $M.P.-$ is almost as different from P as any choice of α can make it. The case of $M.P.+$ is very different, since there does not appear to be any restriction on the size of α in this case. The results given in Table I for this model refer to a partieular solution which was determined after a value of ψ_0 particularly convenient for the numerical integration of (19) had been adopted. The choice of a smaller value of ψ_0 would have led to a larger α, and would presumably have increased the differences between P and $M.P.+$.

TABLE II

Comparisons between the isothermal model, Eddington's modification of it, Plummer's model, and a modification of it

Model	*I*	*M.I*	*Pl*	*M.Pl*
Radius		Density, $\rho(r)/\rho_0$		
$r/a=0{\cdot}0$	1·000	1·000	1·000	1·000
0·2	0·823	0·808	0·863	0·831
0·4	0·510	0·490	0·582	0·523
0·6	0·287	0·277	0·337	0·295
0·8	0·163	0·162	0·184	0·168
1·0	0·100	0·100	0·100	0·100
1·2	0·064	0·065	0·056	0·062
1·4	0·044	0·045	0·032	0·041
1·6	0·031	0·032	0·019	0·028
$M(a)/\rho_0 a^3$	0·939	0·917	1·052	0·959
$(\overline{\Pi^2}/G\rho_0 a^2)_{r=0}$	0·401	1·444	0·462	0·990
$(\overline{\Pi^2}/G\rho_0 a^2)_{r=a}$	0·401	1·444	0·292	0·833
$(\frac{1}{2}\overline{T}/G\rho_0 a^2)_{r=a}$	0·401	0·270	0·292	0·197
$(K.E./G\rho_0 a^2)_{r=a}$	0·601	0·992	0·438	0·614

The density distributions of these three models do not in fact seem to correspond very closely to observed density distributions in globular clusters. In Table II is given a more detailed comparison of four models, three of which have previously been suggested at various times as representing the observed density distributions. These are the isothermal model (denoted by I), the modification of it made by Eddington ($M.I$), the polytropic model of index $n=5$, suggested by Plummer and denoted here by Pl, and finally the modification of Plummer's model by the inclusion of angular momentum terms ($M.Pl$). This last model, it will be recalled, is one in which the constant α must be positive.

As before, the comparison is made between models with the same central density, ρ_0, and with the same radius a at which the density falls to $\rho_0/10$. All four models extend to infinity, and in all except Pl the total mass is also infinite.

The differences in density distribution are quite considerable; *Pl* has the most and *M.I* the least massive core, as is evident from the behaviour of $\rho(r)$ and also from the values of $M(a)$, the mass inside the sphere of radius a. Beyond $r=a$ the density falls off most rapidly in *Pl*, and least rapidly in *M.I*. This feature in which the density falls off more slowly in *M.I* than in *I* persists so far as the integration has been taken, but ultimately the position must be reversed, for it is known that in *I* the asymptotic behaviour of $\rho(r)$ is like r^{-2}, whereas in *M.I* it is like $r^{-2}(\ln r)^{-1}$.

Table II also brings out the radial star-streaming in *M.I* and *M.Pl*; it is quite marked even at $r=a$, which must be regarded as comparatively near the centre. In both these models the parameter α was chosen simply for convenience of numerical integration. It is clear that the values adopted are quite large enough to bring out the general effect of the extra-angular momentum terms.

Another remarkable difference revealed in Table II is the mean kinetic energy per unit mass. At the centre this is $\frac{3}{2}h^2$ or $\frac{3}{2}(\overline{\Pi^2})_{r=0}$; at radius a it is $\frac{1}{2}(\overline{\Pi^2}+\overline{T})_{r=a}$. This latter quantity is given in the last row of Table II. We see that, both at the centre and at $r=a$, the mean kinetic energy per unit mass is much greater in the two models in which angular momentum terms have been introduced. This is connected with the fact that in these two models the individual star orbits tend to be longer and thinner than the orbits in the original isothermal and Plummer models. (The elongated orbits are responsible for the radial star-streaming, since a star tends to move, for a large part of its orbit, in directions inclined at only small angles to the radius vector.) The high kinetic energy in *M.I* and *M.Pl* also has some bearing on the stability of these systems. Chandrasekhar has shown (**16**) that the effects of close encounters are much reduced if the mean kinetic energy is high, so that these models will be affected relatively slowly by close encounters in the central regions. It seems that the direct application of Chandrasekhar's formula will actually exaggerate the influence of encounters, as the formula was derived for a star field of more or less uniform density. However, in *M.I* and *M.Pl* many of the stars which pass through the central core move in orbits which extend to regions of low density, and only a small proportion of the stars move permanently in a region of high density.

8. *The projected density.*—For purposes of comparison with observation a knowledge of the theoretical space density is not of immediate value. What is observed is the projected density, $\nu(r)$, the total mass of stars in a cylinder of unit cross-section with its axis at a distance r from the centre of the cluster. This quantity is calculated from the space-density by means of the formula

$$\nu(r)=2\int_{x=r}^{\infty}\rho(x)\frac{x\,dx}{(x^2-r^2)^{1/2}}. \qquad (20)$$

For a model with a finite radius, $\rho(x)$ is identically zero beyond a certain fixed value of x ($x=c$, say), and the upper limit of the integral is effectively c. Clearly in this case ν is zero for all values of r greater than c.

There is some difficulty in comparing theoretical models which have an infinite radius with the observations on globular clusters which are obviously finite. There is, however, no reason why a globular cluster should not possess such a velocity-distribution for the greater part of its mass as would in theory belong to a cluster of infinite radius. The density-distribution of a cluster depends on its own gravitational field, and this is provided by the material nearest

the centre. That part of a cluster which in theory may exist at large radial distances does not contribute to the gravitational field nearer the centre. It is rather the reservoir from which are replaced the stars of large kinetic energy which move out from the central regions. If the reservoir is absent, then there will be a slow escape of stars of high energy.

An actual cluster is subject to the gravitational field of the galaxy to which it belongs, in addition to its own gravity. The external field will dominate the movements of all stars beyond a certain distance from the centre of the cluster, and therefore only the stars inside this boundary can properly be said to belong to the cluster. This fact is not allowed for in the elementary treatment of the dynamics of clusters, and consequently we cannot expect to obtain theoretical models which agree with the observed density distribution in the extreme outer regions. This is a great drawback to the method developed by Kurth (7). He assumes a law of density-distribution of the form $\rho \propto r^{-n}$, for sufficiently large values of r. Unfortunately the density in the outer regions of a cluster—where such a theoretical distribution is made to fit the observations—is only in part controlled by the field of the cluster itself.

In the present investigation the question of the finite or infinite radius is important in calculating the projected density. In practice the integral (20) is evaluated numerically up to some convenient upper limit of x, beyond which $\rho(x)$ has not been found. A correction can then be applied which will effectively extend the upper limit of the integral to infinity. In all cases the limit to which the integral was evaluated directly was about $3a$, varying slightly as between different models for the convenience of integration. At this distance the ratio ρ/ρ_0 has dropped to about 0·003. The behaviour of $\nu(r)$ will be shown both for corrected and uncorrected models. It turns out that cut-off at $r=3a$ which we arbitrarily imposed is much too near the centre, but the effect produced on $\nu(r)$ by making a cut at this distance permits us to predict the effect of terminating a model at a much greater radius.

The comparison of the projected densities of different models cannot be drawn until we fix a scale for the radius. This is most easily done by adjusting the constants of each system so that all models have the same central projected density ν_0 and so that at the same radius a' the projected density falls to $\nu_0/10$. The graph of $\nu(r)/\nu_0$ as a function of r/a' is given for *Pl*, *M.Pl* and *I* in Figs. 1, 2 and 3. It is not very convenient to represent all the curves on the same diagram, but it is not difficult to compare the different models, since in each figure the same twenty-four points (obtained from observations) are plotted. Since the projected density varies by a factor of 100, it is difficult to represent the ordinates on a uniform scale. It seems advisable therefore to multiply the scale of the ordinates by 10 for all radii r exceeding a'. In each diagram there are two curves; the continuous one is the graph of $\nu(r)/\nu_0$ for the model of infinite radius. The broken curve is the graph of the same function when the contribution both to $\nu(r)$ and to ν_0 of the material which lies outside a certain fixed sphere is completely neglected. Naturally, the effect of this cut-off depends very much on the space-density, and especially on its variation at great distances. In *Pl*, for instance, ρ behaves as r^{-5} for large values of r, and consequently the outer regions really contribute very little to the integral for $\nu(r)$. It follows that the two curves 10r this model are extremely close together until the radius approaches the limit of the finite model. On the small scale used for $r<a'$ the two curves are indistinguishable. In *M.Pl* and *I* the density behaves for large r as $r^{-2}(\ln r)^{-5/4}$ and

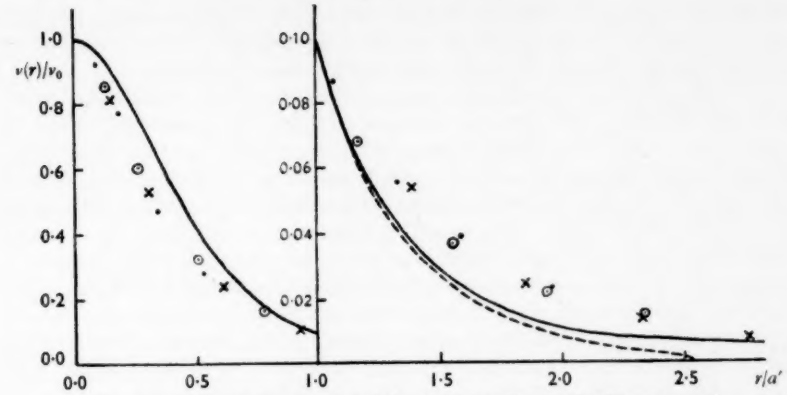

FIG. 1.—*The variation of projected density with radius for the Plummer model.*
• *NGC* 5904 ⊙ *NGC* 6341 × *NGC* 7078

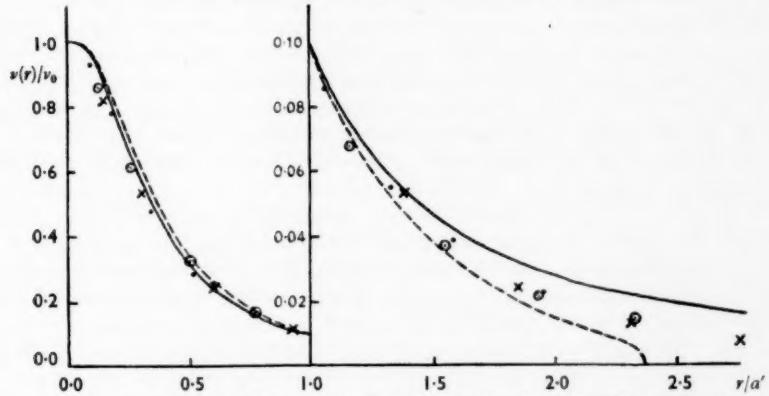

FIG. 2.—*The variation of projected density with radius for the modified Plummer model.*
• *NGC* 5904 ⊙ *NGC* 6341 × *NGC* 7078

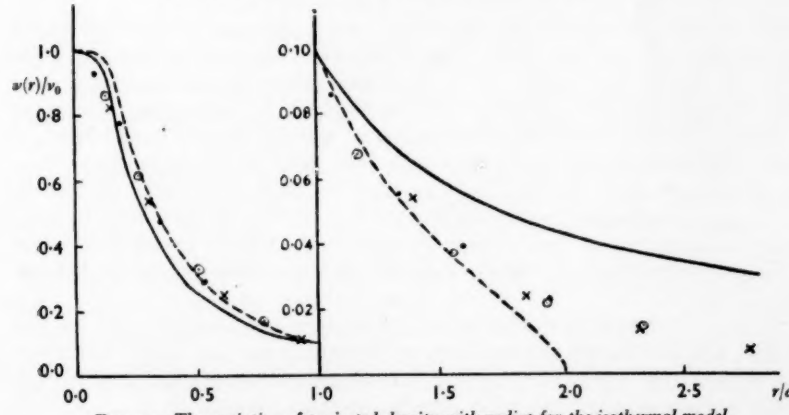

FIG. 3.—*The variation of projected density with radius for the isothermal model.*
• *NGC* 5904 ⊙ *NGC* 6341 × *NGC* 7078

r^{-2}, and in these two models the effect of the cut-off is more obvious. In both cases the finite model will appear to have a more extensive central core, but the projected density will fall off more rapidly in the outer regions.

9. *The comparison of these models with observation.*—The twenty-four points which are included in Figs. 1, 2 and 3 correspond to observations made by Lohmann (**17**) on three globular clusters, NGC 5904, NGC 6341 and NGC 7078. (These clusters are also known as M5, M92 and M15, but the symbol M is in such demand that this nomenclature will be avoided.) Lohmann has measured the luminosity emitted per unit area at a large number of points on the disks which these clusters present. Instead of giving his results in terms of apparent magnitudes, he estimates the number of stars of apparent magnitude 14^{m} which would be required in each area to produce the measured luminosity. If the fractional distribution of stellar masses is the same throughout a cluster, then the luminosity of any element of volume would be proportional to the total mass which the volume contains. In these circumstances Lohmann's figures for the luminosity (represented as a number of stars) would correspond to the projected density $\nu(r)$ which has been calculated for theoretical models. Lohmann has also made actual counts of the bright stars in these clusters, and so has found the distribution of these stars with radius. He finds that this does not correspond exactly with the distribution of luminosity, so it cannot be supposed that the proportion of stars of given mass is the same at all points. On the other hand, the differences in distribution which Lohmann finds are fairly small, and it seems likely that the distribution of mass differs very little indeed from the distribution of luminosity.

Taking Lohmann's figures as being proportional to $\nu(r)$, we find by interpolation the angular radius in each cluster at which $\nu(r)/\nu_0$ falls to $\frac{1}{10}$; this will be the standard radius a', now measured as an angle. The observations are then represented as points on Figs. 1, 2 and 3, in which $\nu(r)/\nu_0$ is plotted against r/a'. Three different symbols have been used, so as to distinguish between the three clusters. The same points occur in all three diagrams, and serve as a guide in comparing the theoretical curves. The remarkable feature of the observations, and a feature which was not pointed out by Lohmann, is that within the limits of observational accuracy the points obtained from all three clusters appear to lie on the same curve. This uniformity is to some extent confirmed by Shapley's figures for the total angular diameters (**18**). From these and Lohmann's results we find that the boundaries of the clusters are at radii corresponding to $6{\cdot}7a'$, $5{\cdot}5a'$ and $8{\cdot}4a'$. Apart from the observational uncertainty of measuring these radii, it is scarcely to be expected that they would be in much closer agreement. It has already been pointed out that a model which is theoretically infinite in extent will be modified in practice by the gravitational field of the galaxy. Thus the position of the finite boundary of a cluster will be determined not merely by the mass distribution in the cluster itself but also by the past motion of the cluster as a part of the galaxy. Shapley's values of the angular diameters therefore seem to be quite consistent with the suggestion that the three clusters are dynamically similar.

The comparison between Lohmann's observations and the theoretical curves we have obtained brings out a number of interesting points. In the first place it is obvious that the finite boundary, whose arbitrary imposition leads to the broken curves, is in all cases too near the centre. The point is stressed by

Shapley's measurements, which put the finite boundary at about three times the radius imposed on the theoretical models. The finite models serve only to indicate the general effect of cutting off an infinite model at some finite distance.

Of the three infinite models it is evident from Fig. 1 that Plummer's model, *Pl*, does not fit these observations. The density does not fall off sufficiently rapidly near the centre, but it becomes too small in the outer regions.

The isothermal model, *I*, shows in Fig. 3 much better agreement near the centre, but the density still does not decrease sufficiently rapidly in this area. Beyond $r=a'$ the projected density falls off much too slowly, and the curve in no way fits the observations. This part of the curve can, of course, be modified considerably if we assume a finite boundary. (Chandrasekhar (**15**) gives values for $\nu(r)$ for an isothermal model with a finite boundary, but his bounding radius is little more than half the one chosen here, and this in turn is probably only about a third of the value required to fit Shapley's estimates of the bounding radii.) The effect of cutting off the extreme outer layers is to reduce the projected density for $r>a'$, though the difference between theory and observation near the centre will be slightly increased. It seems rather unlikely that a boundary of radius $7a'$ will so modify the infinite model as to bring about a real agreement between theory and observation.

The model *M.Pl* which is derived by introducing angular momentum terms into Plummer's model, the polytrope $n=5$, seems to fit the observations very closely in Fig. 2, except for the usual discrepancy in the central area. For $r>a'$ there is a general tendency for the curve to be above the points. This would be corrected to some extent by the exclusion of the mass beyond $r=7a'$, and it seems that the curve would then fit the observations remarkably well. It will be recalled that this model is derived from equation (19) in which there are two parameters. The index $\mu=\frac{7}{2}$, $(n=5)$ clearly fixes the main properties of the model, but the initial value of ψ at $x=0$ is also at our disposal. (This quantity ψ_0 is related to α, which is the constant controlling the extent to which the angular momentum terms are involved.) For convenience of integration ψ_0 was first taken to be 1; then to investigate the effect of changing this constant, a second solution was obtained with $\psi_0=0{\cdot}9$. This agreed even more closely with the observations than did the first solution, and it is this model which has been used in Table II and in Fig. 2. Evidently we might expect to improve on this solution by changing the starting constant ψ_0, but it is doubtful whether the observations are sufficiently accurate to justify the extra labour.

This comparison with observation, revealing a good agreement with *M.Pl* but not so good in the case of the others, might be checked in another way. If we take the case of the cluster NGC 5904, for example, we can find the total mass inside a cylinder of radius $2{\cdot}0a'$ from the integral

$$2\pi \int_0^{2\cdot 0a'} r\nu(r)\,dr.$$

This quantity can be estimated for all three models; it corresponds, as it were, to the moment of the area under the curves in Figs. 1, 2 and 3 about the line $r=0$. The curves are sufficiently alike for all to give about the same value. This is the mass inside the cylinder examined by Lohmann, and he associates with it an integrated apparent magnitude of $6^{m}{\cdot}8$. In the same way we can obtain three estimates of the mass inside a cylinder of radius $6{\cdot}7a'$, the estimated radius

of NGC 5904. Since the three curves of $\nu(r)$ are very different beyond $r = 2{\cdot}0a'$, these values are very different. Since we know the integrated magnitude of the part we can now calculate three values for the integrated magnitude of the whole, and this can be compared with Shapley's observed value (**18**). Here the check breaks down, for Shapley's value is 7^{m}, suggesting that the whole is fainter than the part! There must be some discrepancy in the measurements of integrated magnitude, and this obviously prevents us from making this check. It should be added that Lohmann's estimates of the integrated magnitudes of the regions he has observed are in reasonable agreement with the values given by Vyssotsky and Williams (**19**). These are slightly brighter than Lohmann's, but they refer to a slightly larger region.

It is to be hoped that this discrepancy can soon be resolved, for these observations of integrated magnitudes provide a valuable test. The three models give entirely different results, as can be seen from Table III. In this is given, for each cluster, the fraction of the total mass which lies in the cylinder examined by Lohmann. This fraction can, of course, be evaluated according to each of the three models.

TABLE III

The fraction of the total mass which is observed by Lohmann, as calculated for each model

Model Cluster	*Pl*	*M.Pl*	*I*
NGC 5904	0·901	0·582	0·323
NGC 6341	0·937	0·694	0·459
NGC 7078	0·950	0·634	0·346

From these ratios it is clear that if the clusters have a density distribution like the *M.Pl* model, then the integrated magnitude of the part observed by Lohmann should be in each case about half a magnitude fainter than that of the whole cluster. For the isothermal model the difference is about one magnitude.

10. *The velocity-dispersion in the clusters.*—In several dynamical theories of globular clusters it is possible to obtain a formula connecting either the total mass or the central density with the velocity-dispersion. Unfortunately we have no direct knowledge of the central densities, and though there are estimates of the total masses and of the velocity-dispersion, they are still very uncertain. To obtain the mass of a cluster by a method which does not involve dynamics it seems clear that we must use absolute luminosities. The masses of NGC 5272 (M3) and NGC 6205 (M13) have been determined in this way by Lohmann (**20**). The absolute photovisual magnitude of each is obtained by correcting Shapley's absolute photographic magnitude for colour. For both clusters the quantity comes out to be $-8^{M}{\cdot}8$. Some of the luminosity is directly attributable to the bright stars visible in the cluster. Thus the number of stars in each of the brighter magnitude classes is known. Lohmann assumes that the rest of the luminosity is due to a distribution of faint stars comparable with the distribution of absolute magnitudes in the neighbourhood of the Sun, as found by Kuiper (**21, 22**). In this way Lohmann deduces the distribution of absolute magnitudes in each cluster, and hence the distribution of stellar masses. Actually Kuiper gives two different distribution functions, and Lohmann uses each in turn. In this way he derives for NGC 5272 a total mass of $6{\cdot}4 \times 10^{4}\odot$ or $7{\cdot}7 \times 10^{4}\odot$;

and for NGC 6205, $9{\cdot}7 \times 10^4 \odot$ or $11{\cdot}8 \times 10^4 \odot$. The difference between the two clusters arises from the fact that NGC 5272 has more intrinsically bright stars, and NGC 6205 must therefore have many more faint stars to reach the same total absolute luminosity.

On this evidence it is reasonable to assume that a cluster of absolute magnitude $-8^M{\cdot}8$ has a total mass of $9 \times 10^4 \odot$. There may easily be an error of 30 per cent in either direction, but only a cluster with exceptionally few bright stars will have the same absolute magnitude and a mass exceeding $12 \times 10^4 \odot$. This rough approximation can be applied to NGC 5904, NGC 6341 and NGC 7078, the three clusters considered in Lohmann's earlier paper. For each the absolute photographic magnitude has been given by Shapley (**18**), and the colour index by Becker (**23**). Thus we can obtain the absolute photovisual magnitudes. It is assumed further that the distribution of stars of different brightness is the same in all clusters. It therefore follows that the mass of a cluster of absolute photovisual magnitude M is N solar masses, where N is given by the formula

$$N = 9 \times 10^4 \times 10^{-0{\cdot}4(M+8{\cdot}8)}.$$

The masses of the three clusters determined in this way are given in the first line of Table IV. For NGC 6341 Hachenberg (**24**) has obtained a mass of $25 \times 10^4 \odot$, over three times the value given here. It is difficult to see how this mass could have such a faint absolute magnitude.

TABLE IV

Above the line are constants adopted from observational data on the three clusters. The quantities below the line are calculated from them on the assumption that the clusters are of M.Pl type

Cluster	NGC 5904	NGC 6341	NGC 7078
Total mass	$7{\cdot}2 \times 10^4 \odot$	$7{\cdot}2 \times 10^4 \odot$	$9{\cdot}5 \times 10^4 \odot$
Distance	10·1 kpc	10·3 kpc	11·5 kpc
Radius	36·7 pc	21·0 pc	30·3 pc
Radius at which the projected density is $\nu_0/10$	5·52 pc	3·84 pc	3·59 pc
Acceleration due to gravity at boundary	$7{\cdot}5 \times 10^{-10}$ cm/s^2	$2{\cdot}28 \times 10^{-9}$ cm/s^2	$1{\cdot}45 \times 10^{-9}$ cm/s^2
Central density	330 $\odot$/pc^3	1070 $\odot$/pc^3	1460 $\odot$/pc^3
h	4·4 km/s	5·5 km/s	6·0 km/s
$h(0)$	4·2 km/s	5·3 km/s	5·8 km/s
$h(a')$	2·2 km/s	2·7 km/s	3·0 km/s
T_E, time of relaxation	$1{\cdot}08 \times 10^9$ yr.	$7{\cdot}6 \times 10^8$ yr.	$6{\cdot}2 \times 10^8$ yr.

The distances and the angular diameters have been given by Shapley, and so the linear radius of each cluster is readily found. The angular radius at which the projected density falls to a tenth of its central value is interpolated from Lohmann's results, and converted to linear measure. This determines the scale of the model considered. On the assumption that the clusters have the properties of the particular *M.Pl* model we have examined, the central density and the velocity-dispersion can now be calculated.

To obtain the central density we make use of the total mass. The mass inside a sphere of radius R is given by the expression $R^2G^{-1}(-d\Omega/dr)_{r=R}$. On changing

the variables in the way which transforms (18) to (19), we find that this expression can also be written as

$$4\pi\rho_0 c^3\psi_0^{-5}(-x^2\,d\psi/dx)_{x=R/c}.$$

We also have for this particular solution $\psi_0=0{\cdot}9$, $a'/c=2{\cdot}696$. Hence ρ_0 can be found for each of the clusters. It is very noticeable that for NGC 5904 the central density is only about a quarter of the value obtained for the other two clusters. This is seen to be a consequence of the large value of a'. The density of this cluster falls off much more slowly than in either of the others, and consequently the same total mass can be attained with a much lower central density.

The root-mean-square velocity at the centre, denoted by h, is now found from the formula

$$h^2=0{\cdot}439G\rho_0 a'^2.$$

Unfortunately the quantity h cannot be observed directly. What we hope will ultimately be determined is the root-mean-square velocity in the line of sight for a cylindrical column of material passing through the centre. If this quantity be denoted by $h(0)$, then we have

$$h^2(0)=h^2\int_0^\infty \rho(x)\Omega(x)\,dx\Big/\Omega(0)\int_0^\infty \rho(x)\,dx.$$

Similarly the root-mean-square velocity in the line of sight may also be found for a cylindrical column with its axis at a distance r from the centre. Denoting this quantity by $h(r)$, we have the relation

$$h^2(r)=h^2\int_r^\infty \rho(x)\Omega(x)\left(1-\frac{r^2}{1+\alpha x^2}\right)\frac{x\,dx}{(x^2-r^2)^{1/2}}\Big/\Omega(0)\int_r^\infty \rho(x)\,\frac{x\,dx}{(x^2-r^2)^{1/2}}.$$

In this case the velocity in the line of sight in the region of greatest density is not radial to the cluster but is tangential. We have already stressed that the dispersion falls off much more rapidly for the tangential components than for the radial one. It follows that $h(r)$ decreases quite rapidly with increasing r. The quantities $h(0)$ and $h(a')$ have been evaluated for the three clusters, and appear in Table IV.

The only observational material on velocity-dispersion in clusters is given by Joy (**25**). He gives the radial velocities of a number of variable stars in several globular clusters. There is no indication of the part of the clusters in which the stars are found, but it seems that the dispersion in the velocity measurements is likely to correspond more nearly with the theoretical quantity $h^2(a')$, the dispersion in a cylinder at a distance a' from the centre, than with $h^2(0)$. For NGC 5904 Kurth estimates from Joy's results that the root-mean-square velocity is 2·00 km/s. This agrees quite satisfactorily with the theoretical figure of 2·2 km/s. For NGC 6341 no results are available. For NGC 7078 the value deduced by Kurth is 15·5 km/s. This is far away from the theoretical value of 3·0. However, it should be mentioned that whereas in the case of NGC 5904 the dispersion is calculated from 22 variables, 14 of which could be given full weight, the dispersion in NGC 7078 is obtained from two variables only, neither of which could be given full weight. The disagreement between theory and observation in this case need not therefore be taken very seriously. Indeed, Joy writes: "The velocities

for individual stars are clearly of insufficient precision to justify any conclusions as to peculiar motions or rotation effects." It therefore seems that the observations on velocity-dispersion should be introduced only at the end of the calculations; it would be dangerous to work backwards from these observed dispersions and so obtain the total masses. Such a method has been adopted by Kurth, who is thus led to the conclusion that the mass of NGC 7078 is a hundred times that of NGC 5904. If this is so, it is very difficult to account for the absolute magnitudes, which differ by no more than $0^{M}.3$.

Two further points need to be made. Whatever the dynamical model of the clusters may be, we can calculate directly from the mass and the radius the acceleration due to gravity at the boundary. (This is also given in Table IV.) This is only a fraction of the acceleration due to the galaxy in the direction normal to its plane. From the density variation near the plane a value of $6{\cdot}75 \times 10^{-9}$ cm/s^2 has been found (**1**), and the work of Oort and van Woerkom (**26**) leads to a value $8{\cdot}4 \times 10^{-9}$ cm/s^2 up to 10 000 parsecs from the galactic plane. Although the three clusters considered are in high galactic latitudes, it seems quite certain that at the boundaries of the clusters the attraction of the galaxy is the dominant force.

Lastly it is both interesting and important to calculate the time of relaxation of these models, the time which will elapse before close encounters cause a major redistribution of kinetic energy. Chandrasekhar's formula for this time T_E (**16**) is based on the assumption that the distribution of velocities is Maxwellian, whereas this is not so in the model we have used. However, it seems likely that the formula will still give the right order of magnitude. In using the formula we have taken the average mass of a star to be $0{\cdot}5\odot$, as was obtained by Lohmann. It should also be noted that Chandrasekhar's quantity $\overline{v^2}$ is the mean-square speed, so that its value in our notation is $3h^2$ at the centre of a cluster. The actual values of T_E, given in the last line of Table IV, are not quite large enough for us to infer at once that close encounters play a negligible part in the dynamics of clusters, but it must also be remembered that only a small part of the material within a sphere of radius $a'/10$, say, is permanently within that sphere. Chandrasekhar's formula is based on the cumulative effects of close encounters, but in the model considered these will not be frequent. The small energy changes will diffuse fairly rapidly through the system, but will not be sufficiently frequent in the history of any one star to alter its energy really drastically. This is the real justification for the dynamical methods here used, ignoring, as they do, the effects of close encounters.

We therefore conclude that the modification of Plummer's model by the introduction of angular momentum terms leads to a model which is dynamically self-consistent, in the sense that the gravitational field which it produces is such as will maintain the velocity-distribution exactly. This model appears to fit the variation of brightness of the observed disk, as measured by Lohmann for three globular clusters. It also provides a relation between the total mass and the velocity-dispersion which is in general agreement with the estimates which we have for these quantities.

The University,
Manchester, 13:
1951 *November* 30.

References

(1) G. L. Camm, *M.N.*, **110,** 305, 1950.
(2) Erik Martens, *On the spherical dynamical equilibrium-distribution of stars of unequal masses,* Göteborg, 1928.
(3) P. ten Bruggencate, *Die Sternhaufen*, Berlin, 1927.
(4) S. W. Shiveshwarkar, *M.N.*, **96,** 751, 1936.
(5) E. Finlay-Freundlich, *M.N.*, **105,** 237, 1945.
(6) E. Finlay-Freundlich, *M.N.*, **107,** 268, 1947.
(7) R. Kurth, *Zeits. f. Astrophys.*, **28,** 1, 1950.
(8) R. Kurth, *Zeits. f. Astrophys.*, **29,** 26, 1951.
(9) R. Kurth, *Zeits. f. Astrophys.*, **29,** 33, 1951.
(10) H. C. Plummer, *M.N.*, **71,** 460, 1911.
(11) A. S. Eddington, *M.N.*, **75,** 366, 1915.
(12) J. H. Jeans, *M.N.*, **76,** 70, 1915.
(13) H. von Zeipel, *K. svenska Vetensk Akad. Handl.*, **51,** No. 5, 1913.
(14) R. Emden, *Gaskugeln*, Leipzig, 1907.
(15) S. Chandrasekhar, *Principles of Stellar Dynamics*, p. 231, Chicago, 1942.
(16) S. Chandrasekhar, *loc. cit.*, p. 67.
(17) W. Lohmann, *Zeits. f. Astrophys.*, **12,** 1, 1936.
(18) H. Shapley, *Proc. Nat. Acad. Sci.*, **30,** 61, 1944; also *P.A.*, **57,** 211, 1949.
(19) A. N. Vyssotsky and E. T. R. Williams, *Ap. J.*, **77,** 301, 1933.
(20) W. Lohmann, *Zeits. f. Naturforschung*, **2a,** 477, 1947.
(21) G. P. Kuiper, *Ap. J.*, **95,** 201, 1942.
(22) G. P. Kuiper, *Ap. J.*, **96,** 315, 1942.
(23) W. Becker, *Sterne und Sternsysteme*, p. 55, Leipzig, 1942.
(24) O. Hachenberg, *Zeits. f. Astrophys.*, **18,** 49, 1939.
(25) A. H. Joy, *Ap. J.*, **110,** 105, 1949.
(26) J. H. Oort and A. J. van Woerkom, *B.A.N.*, **9,** No. 338, 1941.

THE OXFORD SOLAR SPECTROSCOPE

H. H. Plaskett

(Received 1952 January 4)

Summary

The prismatic spectroscope, used with the Oxford solar telescope, has a clear aperture of 15·2 cm and a focal length of 8·96 m. The linear dispersion varies from 2·8 mm A^{-1} at λ 4000 to 0·5 mm A^{-1} at λ 6500. The horizontal apparatus function, determined from the Kr line λ 4319·6, has a half-width of 0·048 A with a marked asymmetry to the red. The practical resolving power at this wave-length is 93 900, less than one-third of that predicted by diffraction theory. Because of the asymmetry in the apparatus function the centres of intensity of solar absorption lines are displaced to the red by amounts which vary as their equivalent widths; precautions must therefore be adopted in the measurement of Doppler displacements. The vertical apparatus function (up and down the slit) has a half-width of 0·167 mm. This tends to wash out the spectra of fine details on the solar surface, but theory and practical experience show that spectra of solar granules can be obtained. For unanalysed white light, incident on a slit with a height of 19 mm, the general scattered light in the focal plane is 1·6 per cent.

The solar equipment of the University Observatory, Oxford, consists of a solar telescope of 32 cm aperture and 19·8 m focal length (**13**), and a large prismatic spectroscope. This latter instrument is described, its performance determined and its limitations noted in the three succeeding sections of this paper.

1. *Description*

This auto-collimating spectroscope has a clear aperture of 15·2 cm (6 in.) and a focal length of 8·96 m (29·4 ft.). Dispersion is provided by three prisms, two of 60° and one, silvered on its back face, of 30°. These prisms have a height of 15·2 cm (6 in.) and a base of 24·8 cm (9·8 in.). The dispersion varies from approximately 2·8 mm A^{-1} at λ 4000 to 0·5 mm A^{-1} at λ 6500. When allowance is made for absorption in the prisms the theoretical resolving power at λ 4320 is 303 000.

The spectroscope is mounted horizontally in a brick tunnel in the basement of the Observatory. The beam from the solar telescope is turned horizontally to the west by a small flat C (Fig. 1) and the solar image is focused in the plane of the slit. The slit and plate-holder unit is mounted on the T-shaped pier, B. The beam, emerging from the slit, passes into the tunnel and falls on the objective and prisms mounted on pier A. Reflected off the silvered face of the 30°-prism the beam retraces its course and the focused spectrum is photographed on the same level as, and very nearly in the plane of the slit.

1.1. *Mechanical parts.*—The slit and the plate holder are mounted in a massive, hollow, cast-iron box some 45 cm wide by 28 cm high by 33 cm deep (17·5 × 11 × 13 in.^{3}). This heavy box rests on a casting D (Plate 2, 1) which is bolted through spring washers and a cork pad to the cross-bar of the T-shaped pier; for collimation in the horizontal plane the box may be moved north or

south on its base D, and finally locked in position, by four push-screws. The box, open on the side towards the objective and prisms, is connected by a light-tight flexible bellows to a corresponding opening in the east wall of the tunnel.

The slit, E, has jaws 5 cm high, one of which may be moved by a half millimetre pitch screw against a spring to give an opening of any required width. The height of slit exposed is determined by one of a number of slots in a diaphragm which slides in ways almost in contact with the front face of the slit-jaws. The slit is carried by a tube some 6 cm in diameter and 33 cm long, in which it is rotatable through a small angle. This tube passes through the front face of the metal box to which it is rigidly attached by a heavy metal flange. The other end of this tube, well inside the metal box, is closed by a rectangular aperture which passes the beam, here some 5 mm wide, on its way from the slit to the objective. Normally this aperture, and consequently the beam from the slit, are completely unobstructed, but by operating a lever on the front face of the metal box a mask may be swung into the beam so as to shadow either one or other half of the distant objective. This provides a simple means of applying the Hartmann test for focal setting.

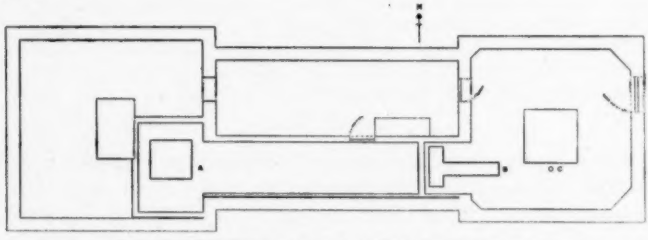

FIG. 1.—*Spectroscope tunnel.* (*Scale* 1 *cm*=2·3 *m.*)

A gun-metal plate, F, some 33×33 cm^2 is pivoted at G and H to the cast-iron box. A carrier for the plate holder, I, may be moved in ways up and down this gun-metal plate by means of a handle, J. Rectangular openings, on the same horizontal level as the slit, in both the cast-iron box and the gun-metal plate allow the spectrum to fall on the photographic plate; the passage between the iron box and the gun-metal plate is rendered light-tight by a short length of bellows. The gun-metal plate may be rotated on its pivots through $\pm 5^\circ$ so as to set the photographic plate tangential to the focal surface of the objective. Three gun-metal plate holders are provided; each takes a plate $25{\cdot}4 \times 10$ cm^2 (10×4 in.^{2}), inserted by removing the back, and has carrying handles and lugs for clipping it into the carrier, as well as the usual dark slide.

The objective and the prisms are mounted on a heavy ribbed casting, K (Plate 2, 2)*, of surface area $1{\cdot}10 \times 1{\cdot}17$ m^2 (43×46 in.^{2}). Four massive screws at the corner of this casting provide collimation in the vertical plane; these screws are seated in four metal bosses, spigoted into a 5-cm thick cork pad which covers the whole top of the pier, A (Fig. 1). To the casting, K (Plate 2, 2), motionless on the pier by virtue of its weight, is pivoted a sub-base. This latter, adjustable for angle in the horizontal plane, carries the slides for the prism cells, L, M, N and the objective cell, O. The three triangular slides, to which the prism cells

* Reproduced from *Engineering*, p. 335, 1939 March 24, where further details on the mechanical design will be found.

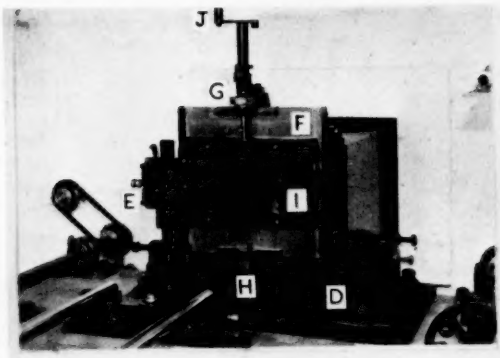

1

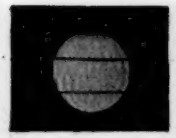

3

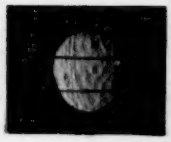

4

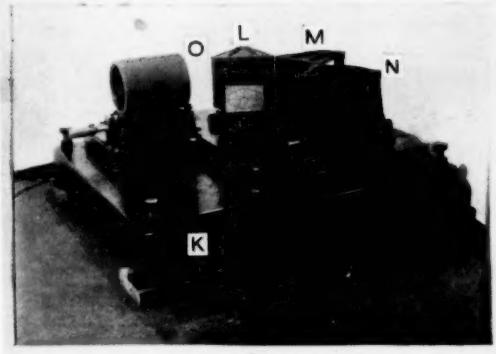

2

5

6

7

1. *Slit and plate-holder unit.*
2. *Objective and prism-carrying unit.*
3. *Foucault test of 30°-prism and O.G.* } *knife edge to right.*
4. *Foucault test of 3 prisms and O.G.* }
5. *Typical scattered light plate.*
6. *Mg b region* × 1·67 *with full aperture.*
7. *Mg b region* × 1·67 *with diaphragm in position.*

H. H. Plaskett, The Oxford solar spectroscope.

may be interchangeably screwed, are carried on a Browning–Proctor minimum deviation link work (**8**) operated by a screw and carriage (not in position when the photograph was taken). The objective cell, O, slightly adjustable for angle on its slide, may be moved for focusing through 15 cm by a screw and nut; its setting is read off a scale.

A metal-lined three-ply box, itself lined with cork to a depth of 5 cm, sits on the cork pad on the top of the pier, and completely encloses, but does not touch, the objective- and prism-carrying unit. This box, of which the back and a part of the top are removable to give access to the optical parts, has a base of $1{\cdot}47 \times 1{\cdot}40\ m^2$ ($58 \times 55\ in.^2$) and a height of 0·79 m (31 in.). A circular hole in the east wall of this box allows the beam from the slit to enter the objective and to return to the photographic plate; a bellows connects the front of the lens cell with the inside of this box, thus making the front component of the lens a window into the enclosure. The spindles of the screws for focusing and changing the position of minimum deviation are carried through seals in the east wall of the box. Sprocket wheels on these spindles engage corresponding sprocket wheels on two shafts which run in self-aligning ball bearings along the north and south walls of the tunnel. These shafts, again through sprocket wheels, can be rotated by hand wheels on the cross-bar of the T-shaped pier (B, Fig. 1). Engagement of the sprocket wheels is provided by loose, flexible chains to minimize any transmission of vibration. The focal setting of the objective, read by a small telescope just above pier B, and the wave-length of minimum deviation can thus be altered at will from this pier without entering the tunnel.

Other features, for example an optical bench on the stem of the T-shaped pier, are included in the mechanical design. The details of this design, as well as the actual construction, are due to C. F. Casella & Co.; the proved stability of the instrument and its convenience and flexibility in use are a tribute to their skill and the excellence of their workmanship.

1.2. *Optical parts.*—The prisms and the objective (with their cells), and the spectroscope slit, are due to Adam Hilger & Co. The prisms, cut from a large block of optical glass (just as it came from the fire-clay pot) and annealed after cutting, are of dense flint with refractive index, dispersion and transmission almost identical with the Jena Glass (Schott & Gen.) of type F3. To minimize the effects of internal inhomogeneity the faces of the prisms are locally figured. The achromatic objective of 15·2 cm aperture is a special design of J. W. Perry, Head of the Applied Optics Department at Hilger's. It consists of two single components, separated by 22 cm, to reduce the chromatic difference of spherical aberration. The minimum focal length of 895·8 cm occurs at λ 5100 with an increase for single transmission of 1·5 cm at λ 8000 and of 2·8 cm at λ 4000. The radius of curvature of the focal surface is estimated from the design to lie between two and three metres. Three of the four surfaces of the lens are concave to the slit so that the real, white-light images of the slit can be masked off to reduce the general scattered light.

The spectroscope was first assembled as a unit under good conditions of temperature control (see next sub-section) in 1938 September. It was immediately evident that the definition was poor. The top and the bottom halves of the optical train gave spectra which did not superpose and which focused in planes differing by 0·7 cm. Even when one-half of the train was masked off the definition was not good, and Hilger's willingly agreed to take the prisms

back for further examination and possible re-figuring. On examination with a large aperture interferometer, not available when the prisms were originally figured, Hilger's found that the 30°-prism was satisfactory, but that further work could usefully be done on the two 60°-prisms. On the completion of this work the prisms and the objective were bloomed and returned to Oxford in 1946. On re-examination in the spectroscope a marked improvement in definition was found; in particular the difference between the top and bottom halves of the optical train had disappeared. Dr Adam used the spectroscope in this form to obtain interferometric spectra (**1**) in the autumn of 1946.

It seemed probable, however, that some further improvement in definition could be secured by masking off part of the optical train. Knife-edge tests in the focal plane, using the Na D_1 line from a Philips Lamp as a source (Plate 2, 3—30°-prism alone, Plate 2, 4—all three prisms in train) fully confirmed Hilger's conclusion that the 30°-prism was satisfactory, and that the remaining trouble arose from abrupt changes of refractive index in the two 60°-prisms. Under these circumstances almost any masking seemed bound to effect some improvement, but the best results were obtained early in 1948 with a diametral rectangular aperture of the full width of the prisms (15·2 cm) and of vertical height 3·1 cm. The lower edge of this mask also casts a shadow on the photographic plate for the virtual image of the slit produced by the one convex lens surface. The effect of this mask on the definition of the solar spectrum can be judged from Plate 2, 6, 7. The upper of these two spectra was taken with the full aperture, and the lower with the diaphragm in position. It can be seen, though unfortunately not in the reproduction, that the Mg–Fe doublet at λ 5167 (separation 0·18 A) and the Fe–Fe^+ pair at λ 5169 (separation 0·14 A) are both more clearly resolved in the spectrum taken with the diaphragm in position.

In spite of the reduction in aperture to nearly one-quarter, the diaphragmed spectroscope used in conjunction with the solar telescope remains moderately fast. Spectra sufficiently dense for the measurement of sight-line velocities are obtained with a normal slit-width of 0·04 mm on Ilford Rapid Process Panchromatic plates in the following exposure times:—

Region λ 5900	Dispersion 0·71 mm A^{-1}	Exposure 1 second
4227	2·23	8 seconds
4010	2·80	64 seconds

It is the performance and limitations of the spectroscope, masked as described above, which are discussed in the remaining two sections of the paper.

1.3. *Temperature control.*—Because of the change of refractive index with temperature, it is essential that the temperature of the prisms be controlled within narrow limits. For the glass of these prisms a change of 1 deg. C gives a wavelength displacement of 0·6 A; thus if between the top and the bottom of the prisms there were a temperature difference of 0·023 deg. C a line widening would be produced comparable with the minimum distance, 0·014 A, which is theoretically resolvable at λ 4320. The only possibility of realizing so high a degree of uniformity within the prisms is to maintain them at a temperature constant within about these limits ($\pm$ 0·023 deg. C), and to trust that the relatively high conductivity of their cast-iron cells will smooth out any small residual temperature gradients.

On the advice of the Building Research Station no heating elements are placed inside the cork-lined enclosure which contains the prisms, the objective

and their base. Instead the temperature of the air outside the enclosure, that is in the tunnel, is maintained constant within 0·1 deg. C by means of two heating circuits, each dissipating one kilowatt and each controlled by its own thermostat. The thermostats are moderately sensitive mercury thermometers with sealed-in, adjustable platinum contacts. Each carries a current of 10 micro-amp; this current controls the potential of a grid, and the latter in turn the anode current of the valve which operates the on-off switch of the power supply to the heating circuits. The thermostats and valve relays are supplied by Baily, Grundy and Barrett of Cambridge, and give continuous, trouble-free service.

The thermostats control the temperature in their immediate vicinity to better than 0·1 deg. C. To ensure that the whole of the tunnel is also at this temperature, it is essential to keep the air vigorously stirred. On the floor of the chamber containing pier A (Fig. 1) and at diagonally opposite corners are two powerful fans which run continuously; these keep the air outside the cork-lined enclosure in rapid turbulent motion. In addition three fans on the roof of the tunnel are switched on for a few hours each day to help maintain uniformity of temperature between the chamber and the tunnel proper. It is of course essential that the moving currents of air should not actually cross the optical path and produce "bad seeing". The optical path from the slit to the front component of the objective is therefore completely enclosed by a metal-lined three-ply tube of rectangular cross-section, fixed to the walls of the tunnel but flexibly connected by a bellows to the opening in the cork-lined enclosure. This metal tube helps to maintain uniformity of temperature across the beam, but in addition, and before an exposure is made, air may be blown through the tube to eliminate temperature gradients.

The prisms, the objective and their base in the cork-lined enclosure are thermally insulated from the air of the tunnel and from the pier on which they stand. By a slow process of conduction the inside walls of the cork-lined enclosure assume the temperature imposed on the air outside, but with the temperature ripple greatly reduced in amplitude. To prevent stratification within the enclosure, the air is stirred for a few hours each day (though not when an exposure is in progress) by a fan blade driven by a belt from a small motor on the floor of the tunnel. The temperature of the air inside the enclosure can be read from a sensitive Beckmann thermometer to an estimated 0·001 deg. C, and is found to remain reasonably constant. Thus in the 1951 observing season from April 5 to November 10, when the temperature of the tunnel was continuously maintained at 24·0 deg. C $\pm$ 0·1 deg. C, the temperature inside the enclosure was read 135 times at more or less regular intervals. The root mean square deviation of a single reading from the mean was $\pm$ 0·027 deg. C—a constancy close to the stipulated requirement.

2. *Characteristics*

2.1. *Collimator illumination.*—The Cassegrain mirror of the solar telescope (**13**) forms a central stop, the diameter of which is 0·6 that of the main mirror. Each point in the solar image is thus at the vertex of a hollow cone of rays, and from the geometrical–optical point of view this hollow cone would be expected to propagate itself beyond the slit to give an annular illumination of the spectroscope objective. Examination of the collimator illumination for a normal slit-width of 0·04 mm, and a height of 3 mm (effectively a pin-hole for the 9 m distant

objective), shows, however, very nearly uniform illumination with no trace of a central shadow. To get a well-developed central shadow the slit-width has in fact to be increased to 0·16 mm. This result is in agreement with experience with stellar spectroscopes used in conjunction with the large Cassegrain reflectors, though these latter have, of course, much smaller obscuration ratios than the Oxford telescope. The absence of the central shadow for a normal slit-width is due to diffraction.

A simple, and correspondingly artificial, picture of what is occurring can be obtained by regarding the mirrors of the solar telescope as self-luminous sources, a pin-hole image of which is being formed by the slit on the spectroscope objective. If s be the slit width (0·04 mm), b the distance of the objective from the slit (taken as 8·74 m) and λ be the wave-length, then according to Rayleigh (**15**) the diameter of the image on the collimator of a luminous point on the telescope mirror will be

$$D = 2b\lambda/s = 26{\cdot}2 \text{ cm for } \lambda 6000,$$

that is, nearly twice the diameter of the collimator itself. The actual distribution of intensity in this image, given by the ordinary two-dimensional Fresnel theory, is

$$A(x) = \text{const.}[\{C(v_2) - C(v_1)\}^2 + \{S(v_2) - S(v_1)\}^2], \tag{1}$$

where

$$C(v) = \int_0^v \cos\frac{\pi}{2}v^2\,dv \simeq \frac{1}{2} + \frac{1}{\pi v}\sin\frac{\pi}{2}v^2,$$

$$S(v) = \int_0^v \sin\frac{\pi}{2}v^2\,dv \simeq \frac{1}{2} - \frac{1}{\pi v}\cos\frac{\pi}{2}v^2,$$

and the approximate expressions are accurate (**14**) to better than a tenth of 1 per cent for $v \geqslant 6$. In eqn. (1) v_1 and v_2 are defined by

$$v_1 = \left(\frac{a}{a+b}x - \frac{s}{2}\right)\sqrt{\frac{2(a+b)}{ab\lambda}}; \quad v_2 = \left(\frac{a}{a+b}x + \frac{s}{2}\right)\sqrt{\frac{2(a+b)}{ab\lambda}},$$

where x is the distance measured along the arc (in the image plane) from the centre of the geometrical image of the slit, a is the distance from the luminous object to the slit (in our case taken to be 8·83 m), and $b(=8{\cdot}74$ m), s and λ have the meanings already assigned.

Using eqn. (1), $A(x)$ has been calculated for a wave-length of $\lambda 6000$ for slit-widths 0·04 and 0·16 mm, and normalized. Then if $T(x)$ be the intensity distribution on the collimator as given by geometrical optics, the actual intensity distribution will be given by

$$O(x) = \int_{-\infty}^{\infty} T(\xi)A(x-\xi)\,d\xi. \tag{2}$$

The result of this calculation is shown in Fig. 2. In so far as this simple treatment may be regarded as valid, the figure makes it clear why the shadow visible for a slit-width of 0·16 mm disappears for a normal slit-width of 0·04 mm.

2.2. *Focal surface.*—Focal settings of the objective as a function of position on the photographic plate are shown in Fig. 3. The abscissae are distances, measured in centimetres, from the left-hand edge of the plate; for this origin the slit is at $x = -3$ cm. The ordinates are the focal settings, determined by the Hartmann method, measured in centimetres and with an arbitrary origin; the larger the setting the farther the objective is from the photographic plate. Curve I is obtained by backing the objective, in position in the spectroscope, with a plane mirror and determining the focal setting for the slit illuminated by the *D* lines

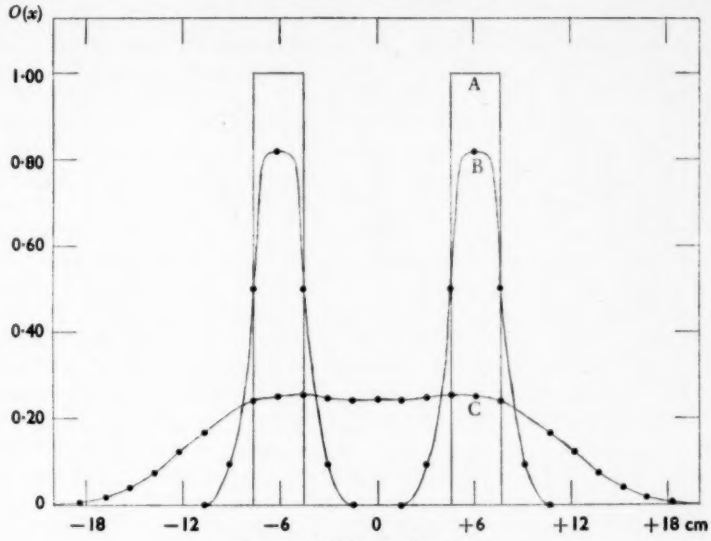

FIG. 2.—*Collimator illumination.*

Abscissae : Distances x in centimetres from centre of collimator.
Ordinates : Illumination in arbitrary units.
Curve A : Illumination according to geometrical optics.
Curve B : Illumination from Fresnel theory for slit-width 0·16 mm.
Curve C : Illumination from Fresnel theory for slit-width 0·04 mm.
Filled circles are points computed from eqn. (1).

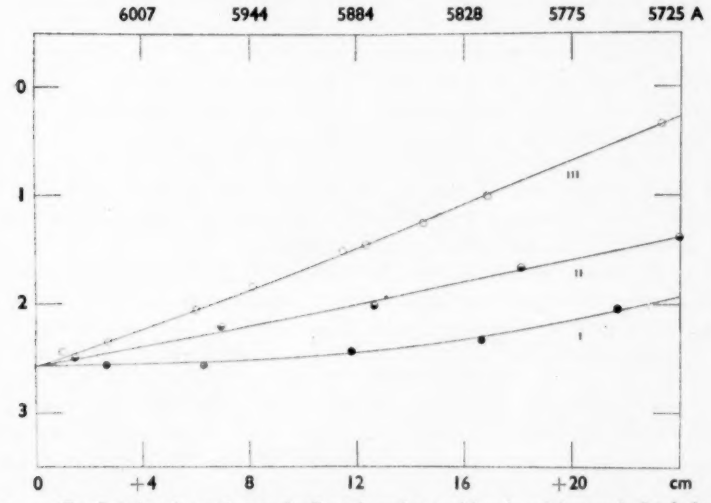

FIG. 3.—*Focal settings in centimetres (ordinates) against positions in centimetres in focal plane (abscissae). Slit at x = −3 cm.*

Curves I and II are monochromatic (λ 5900) focal settings for double transmission through objective backed by plane mirror (I), and backed by prisms (II). Curve III gives focal settings as functions of wave-length.

of Na; the slit image is moved from point to point across the plate by slightly rotating the mirror and the focal setting determined for each point. Curve I thus shows the curvature of field for double transmission through the objective; its radius of curvature is 4·4 m, a satisfactorily large amount. Curve II shows the focal settings for the *D* lines after double transmission through the objective and prisms; the *D* lines are moved across the plate by changing the position of minimum deviation of the prisms. The difference between the monochromatic curves I and II clearly indicates that the prisms are having some effect on the focal properties of the system. Finally curve III gives the focal settings as normally found in taking a spectrum; λ5900 is roughly central, and the plate covers a range from λ6073 at the left to λ5725 at the right-hand edge. The only wave-length in minimum deviation in this spectrum is that returned back on to the slit itself, that is, λ6125 approximately. Curves II and III differ because of the chromatic properties of the objective, the minimum focus of which occurs at λ5100. The three curves, it should be noted, have been brought into agreement at $x=0$ by the addition of a small arbitrary constant to the focal settings.

The unexpected feature of these focal settings is the difference between monochromatic curves I (objective backed by mirror) and II (objective backed by prisms). Its interpretation I owe to Mr J. W. Perry. The slit is some 6 cm farther away from the objective than is the photographic plate, so that the beam, as it emerges after its first transmission through the objective, is slightly convergent. For rays reflected off a plane mirror (curve I), or passing through a system of prisms in minimum deviation (extreme left of II) this convergence is unaltered, but for rays passing through prisms away from their position of minimum deviation (as happens at right of II) the convergence, as Herman (**4**) at least suggests, must be increased. A trigonometrical ray-trace through the system for the *D* lines on the left of the plate (that is, 45 A away from the position of minimum deviation), and on the right of the plate (470 A away from position of minimum deviation), predicts a difference in focal setting of 1·07 cm. The actual difference, as compared with curve I, is 0·53 cm. The predicted increase of convergence is thus of the right order of magnitude, but it appears probable that the prisms are having some additional effect on the focal properties of the objective. This may arise because, out of minimum deviation, the objective is vignetted (noticeably so if the collimator illumination be examined from the right-hand side of the plate), and this vignetting may affect the field curvature which is determined by the Petzval sum and the extra axial astigmatism.

2.3. *Horizontal apparatus function.*—Following Redman (**16**) the horizontal apparatus function has been found from the measured profile of the Kr line, λ4319·6. This line, examined under high resolution by a number of workers (**7**), is apparently without structure and has a half-width of the order of 0·008 A. Since this is less than the half-width of 0·0126 A of the theoretical apparatus function (predicted by diffraction theory), it is reasonable to suppose that the profile of this line, measured with the spectroscope, will give a good determination of the actual apparatus function. It should, however, be emphasized that van Cittert (**2**) has shown that the apparatus function depends upon the mode of slit illumination (coherent, non-coherent, or some combination of the two). Consequently, while the apparatus function about to be found may be regarded as typical of what the spectroscope can do, it is not necessarily applicable to spectra obtained under different experimental conditions.

The Kr line λ 4319·6 was produced in a G.E.C. discharge tube run at 300 V d.c. A field lens, a few centimetres in front of the slit, formed an image of the small region of discharge on the collimator; the magnification was such that this image was slightly larger than the aperture over the collimator. The extra-focal patch from the field lens gave a very nearly uniform illumination over the height of the slit. The slit was set at the normal or van Cittert width for this wave-length region, of 0·025 mm. Over the slit was placed the neutral-tint wedge (W. iv) used in previous investigations, and one spectrum of Kr λ 4319·6 was taken through this wedge; the wedge was then removed and through a neutral-tint filter an exposure of identical duration was made. The first of these spectra was thus photometrically self-calibrated under simultaneous and identical conditions, a considerable photometric gain; the second gave a measure of the flux incident on the wedge as a function of height, as well as another determination of line profile. Three backed Ilford Special Rapid plates were taken, with two or more spectra per plate, and with exposure times of 4, 5½ and 6½ hours per spectrum. After a lapse of at least two weeks the plates were brush-developed in Parkhurst developer.

The neutral-tint wedge, W. iv, was re-calibrated in position on the slit of the spectroscope. The line λ 4358, given by a G.E.C. "Osira" mercury lamp, was used as a source with the same mode of collimator and slit illumination described above. This lamp can scarcely be regarded as a photometrically steady source, but by varying the order in which exposures were made it was possible to convert any possible secular change of flux with time into an accidental error. To change the flux incident on the slit by a known amount, one or more of four neutral filters could be inserted before the field lens. The transmission of these filters had been measured at the National Physical Laboratory at six different wave-lengths; from measures made there it was also known that the greatest angular deviation produced by any filter was 22 seconds of arc, corresponding to a displacement on the collimator of under a millimetre. Any error produced by this slight displacement was made accidental by changing the orientation of the filters in different exposures. The calibration was based on 36 wedge and 48 filter exposures, wedge and filter exposures on any one plate being of exactly identical duration (from 20 to 80 seconds depending upon the plate). From microphotometric measures of these spectra the transmission of the wedge as a function of height could be found in the usual way; as in previous investigations of this particular wedge (**10, 11**) a strictly linear variation of the logarithm of the transmission with height was found with a wedge constant of

$$\sigma_\lambda = 0{\cdot}275 \pm 0{\cdot}001 \text{ mm}^{-1}.$$

This may be compared with the values of $0{\cdot}268 \pm 0{\cdot}003$ found in 1922 and $0{\cdot}278 \pm 0{\cdot}003$ found in 1936 at the same wave-length but under very different experimental and spectroscopic conditions. Adopting 0·275 for λ 4358, the value at the Kr line λ 4319·6 may, from the previously found variation of wedge constant with wave-length, be taken as 0·278.

From this calibration of the wedge and from the spectra of the Kr line taken under the conditions already described, it was readily possible to derive profiles for the line. The spectra were marked at intervals of 0·4 mm of height on the line, and microphotometer tracings were made in the wave-length direction at these heights with an effective slit width of 0·03 mm, a height of 0·14 mm and a

recording magnification of 48·2. From these cross-sections at different heights in the wedge spectrum a provisional characteristic curve was constructed, and this in turn was corrected in the usual way (**12**) for non-uniformity of incident illumination. From the true characteristic curve thus derived and from the microphotometer deflections as a function of linear position on the plate it was possible to derive a profile for each measured spectrum. All the relative intensities (arbitrarily made 100 for the line centre) were plotted as a function of wave-length, the latter found from the dispersion, and a smooth curve was drawn through them. From five well-exposed spectra on the three plates five such curves were thus available. The values of intensity at a number of specified wave-lengths were then read off these curves, and the arithmetic mean taken of the five intensities at each wave-length. The root mean square residual from this mean was found to average 6·3 per cent—a satisfactorily small quantity when it is noted how exceedingly sensitive the intensity is to wave-length.

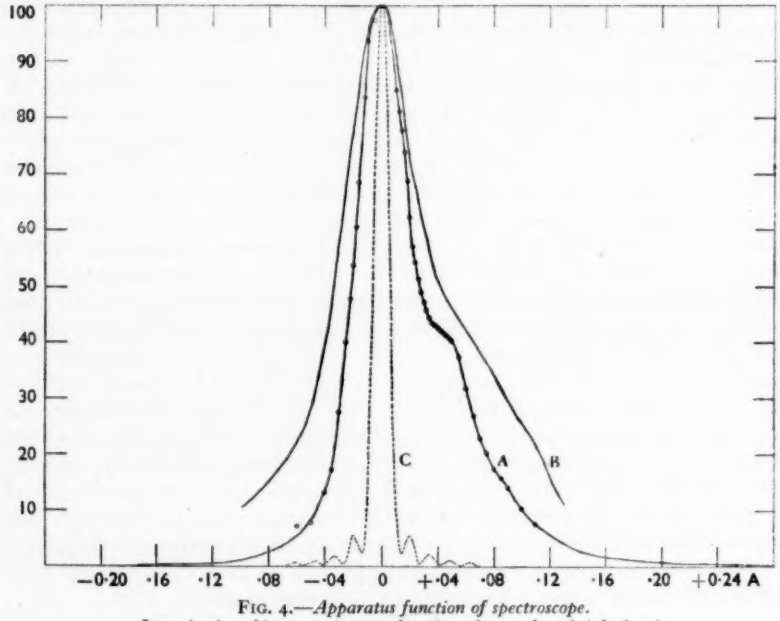

FIG. 4.—*Apparatus function of spectroscope.*
Intensity in arbitrary units as a function of wave-length (abscissae).
Curve A: for masked spectroscope.
Curve B: with no mask.
Curve C: diffraction theory.

The resulting mean profile is shown in Fig. 4 as a function of wave-length (continuous line with observed points). It is well determined except in the wings, which are a pure extrapolation, guided to some extent by the wings which have been found for the vertical apparatus function. This weakness in the wings is the price which has to be paid for self-calibration by exposure through the wedge. In accordance with our initial assumption we take this line profile of Kr λ4319·6 to be the horizontal apparatus function of the spectroscope at this wave-length. In so far as the Kr line has a definite width and the photographic plate a finite

resolving power this apparatus function errs in the sense of exaggerating the width of the core. Its characteristic features are the large half-width of 0·048 A and the presence of a very strong satellite on the long wave-length side. For comparison there is included in Fig. 4 the profile of the Kr line obtained from four spectra made in the same way with the undiaphragmed spectroscope. Since the half-width of this profile is 0·076 A, nearly 60 per cent greater than that with the spectroscope diaphragmed, it is evident how much is gained by always using the spectroscope in the latter form. Also for comparison is given the ideal diffraction pattern with a half-width of 0·0126 A for an infinitely narrow slit, assuming the absorption in the prisms to be that given by Eppenstein (**3**). The practical and theoretical resolving powers, corresponding to these patterns, are 93 900 and 303 000 respectively.

The difference between the actual and the predicted apparatus functions is thus considerable. It is due to aberrations in the spectroscope, largely produced by the sharp changes of refractive index which, from the Foucault test, are present in the glass of the prisms. All solar spectroscopes, whether grating or prismatic, show similar, though on the whole less marked, departures from theoretical expectations. In this respect they contrast unfavourably with the small laboratory spectroscope. It is, however, perhaps worth recalling Redman's remark (**16**) that it is only in instruments of large focal ratio, such as solar spectroscopes, that the approximate half-width of the diffraction image (focal ratio times wave-length) exceeds the minimum sized image (diameter = 0·02 mm) given by the ordinary photographic plate. Hence photographic laboratory instruments with focal ratios smaller than 20 could depart nearly as widely from theoretical performance as the average solar spectroscope without the user being aware of it.

2.4. *Vertical apparatus function.*—The vertical apparatus function gives the intensity as a function of y (that is, perpendicular to the dispersion) of a point source on the spectroscope slit. To find this function, a fine wire of known diameter was stretched across and very nearly in contact with the slit. Spectra of the Sun, taken at λ4320, then showed the shadow of the wire, the intensity distribution in which could be found from wedge spectra exposed on the same plate with identical exposure time. The spectrophotometric details of the work were carried out as described in the preceding sub-section, except that the plates were not brush-developed and that a microphotometer magnification of 6·89 was used. Five plates were available for determining the intensity distribution in the shadow of the wire, and from these the mean intensity as a function of y was found precisely as described above. The root mean square residual for a single determination was 2 per cent, a satisfactorily small error. Systematic errors arising on the one hand from imperfect contact of the wire with the slit and finite resolving power of the emulsion, which tend to wash out the profile, and on the other hand from Eberhard effect which tends to deepen it, have not been estimated, but from the shallow, broad shape of the profile should not be large.

The observed intensity distribution, $O(y)$, in the profile of the shadow is given by

$$O(y)=\int_{-\infty}^{\infty} T(\eta)A(y-\eta)d\eta = 1-\int_{y-a/2}^{y+a/2} A(u)\,du. \qquad (3)$$

Here $T(y)$ is the shape of the shadow in the focal plane in the absence of smearing, that is a rectangular profile of width a ($=0{\cdot}057$ mm) and zero intensity, and $A(y)$ is the normalized vertical apparatus function. $A(y)$, thus found from the

observed profile of the shadow, is plotted (filled circles) as a function of y in Fig. 5; the abscissae are millimetres in the focal plane, counted positive in the direction towards the bottom of the focal plane. The half-width is 0·167 mm. For comparison the diffraction-theory apparatus function, corresponding to the masked objective with rectangular aperture of vertical height 3·1 cm, is shown in the same figure as a dotted curve. This diffraction pattern in the vertical direction has a half-width of 0·098 mm as contrasted with the 0·025 mm in the horizontal direction, but in spite of this great theoretical width the observed vertical apparatus function is still wider. This is a consequence, presumably, of non-homogeneity of refractive index in the prisms together with astigmatism due to the spectrum not being in exact minimum deviation.

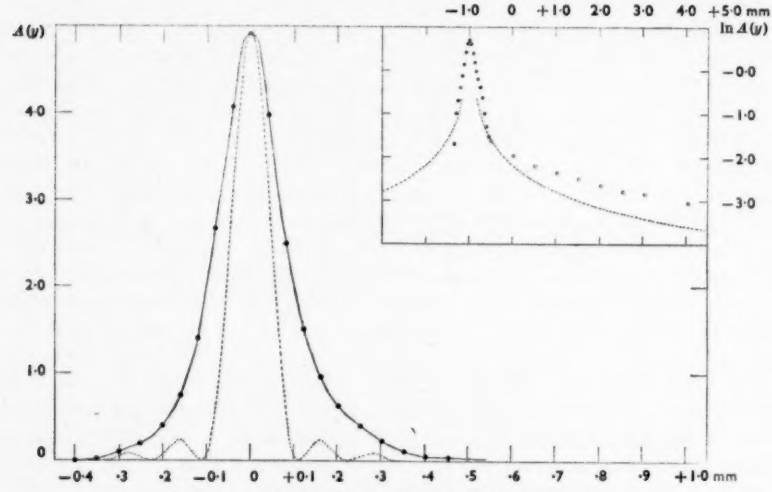

FIG. 5.—*Vertical apparatus function (normalized).*
Abscissae are millimetres in focal plane, positive values downwards. Inset is ln $A(y)$.

2.5. *General scattered light.*—Superposed on the spectrum there is a flux of general scattered light. This originates from that white light, admitted by the slit but lost to the image-forming beam by reflection and scattering on the various optical surfaces, which either directly or after further reflection and scattering arrives in the focal plane to produce there a more or less uniform illumination. The ratio per unit area in the focal plane of scattered-light flux to flux in the spectrum thus increases approximately linearly with the height of the slit and with the dispersion (mm A^{-1}) of the spectrum. The ratio also increases towards the short wave-lengths where the true absorption of the image-forming beam increases.

The ratio per unit area of scattered to spectral light at λ4320 is found from five backed plates. A small range from one of these plates is shown in Plate 2, 5. The four exposures on each plate are spectra of the centre of the solar image made with a wide slit (0·075 mm) and with precisely identical exposure times (of the order of 3 min). The spectrum at the top, with radiation unanalysed for colour before entering the slit, is made with a slit height of 19 mm and exposed through a diaphragm in the focal plane 33 mm high. The image of the illuminated height of the slit is heavily over-exposed; on either side of it, but limited by the

height of the diaphragm in the focal plane, can be seen a more or less uniform fog. This fog is produced by the general scattered light. The spectrum at the bottom, also with radiation unanalysed for colour before entering the slit, is of the same part of the solar image, but with the flux per unit area incident on the slit reduced by a factor of 0·0137. This is achieved by interposing three of the neutral-tint filters, calibrated by the National Physical Laboratory, in front of the slit. For this spectrum the slit height is 3·2 mm, and the height of the diaphragm in the focal plane 9 mm. From the roughly comparable densities in this spectrum and in the fog on either side of the top spectrum it is evident that the scattered light for a slit height of 19 mm is only some 2 per cent of the light in the spectrum. The two remaining spectra on the plate are a wedge and non-wedge spectrum to give the characteristic curve, corrected for any non-uniformity of flux incident on the wedge. They are taken through a diaphragm in the focal plane 9 mm high. To keep the superposed scattered light to a minimum in these two spectra the radiation from the Sun, before entering the slit, passes through a Wratten No. 39 filter.

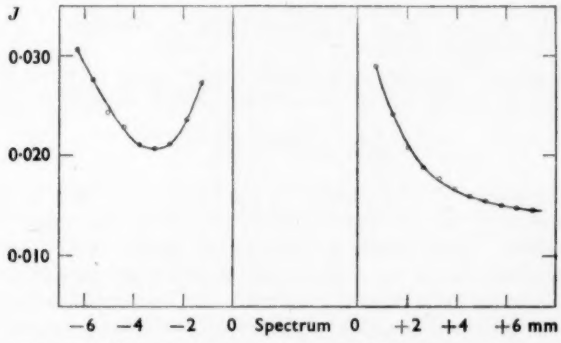

FIG. 6.—*Values of J for a typical scattered-light spectrum* (*Plate* 2, 5).

With magnification 6·89, microphotometer tracings are made across the plate in the *y*-direction, that is, perpendicular to the dispersion. From the measured deflections and the characteristic curve obtained from the wedge spectrum (corrected for non-uniformity and assumed free from scattered light) the intensity J (in units of flux per unit area in the solar spectrum) is found as a function of y from the fog on either side of the top spectrum made with the 19-mm high slit. The values of J thus found for a typical plate (that illustrated in Plate 2, 5) are shown in Fig. 6. If $S(h)$ is the general scattered-light flux per unit area for a slit h mm high, and I the flux per unit area in the adjacent spectrum (found from the spectrum taken with a slit 3·2 mm high), then

$$J=\frac{S(19)}{I+S(3{\cdot}2)}\simeq\frac{S(19)}{I+\frac{1}{6}S(19)},\quad\text{or}\quad\frac{S(19)}{I}\simeq J(1+\tfrac{1}{6}J),$$

on the assumption that the general scattered light varies linearly with slit height. Taking J to be of the order of 0·02, then the J-curve represents the required $S(19)/I$ with an accuracy of 0·3 per cent—an accuracy greater than that of the spectrophotometry, where a characteristic curve for λ4320 has been necessarily used for the white-light flux J.

Taking the J-curve then as the required ratio of scattered-light flux to flux in the spectrum, its variation with y has to be explained. As can be seen from Fig. 6, J decreases rapidly with increasing distance from the spectrum, but at the top of the plate (neg. y) commences to increase again beyond $y=-3$ mm. This increase arises because we are leaving the umbra of the shadow cast by the diaphragm for the virtual image of the 19-mm high slit, and are entering the penumbra; in fact, if the eye is placed in the focal plane beyond $y=-10$ mm the virtual image can be seen escaping beyond the edge of the diaphragm. For positive values of y, that is, towards the bottom of the focal plane, we are always in the umbra and are getting the true scattered light which must be incident on the spectrum.

The increase of J towards the spectrum is due to the wings of the vertical apparatus function. That this is so can be seen from Plate 2, 5, where it will be observed that the Fraunhofer lines extend well beyond the limits of the spectrum fixed by the height of the slit. The flux ratio originating in this way towards the bottom of the plate is

$$\frac{O(y)}{I}=\int_{-\infty}^{\infty} i(\eta)A(y-\eta)\,d\eta=\int_{y}^{\infty} A(u)\,du,$$

where $i(y)$ is the flux ratio per unit area in the spectrum ($i(y)=1$ for $y<0$, and $=0$ for $y\geqslant 0$), and $A(y)$ is the normalized vertical apparatus function. We then have

$$J(y)=\frac{O(y)}{I}+\frac{S(19)}{I},$$

and if we assume that $S(19)/I$ is given by the asymptotic value to which J tends for large values of y, we can find $O(y)/I$ and therefore the wings of the vertical apparatus function. The results for $\ln A(y)$ are shown as an insert in Fig. 5, where the open circles are the mean values found from the five scattered-light plates and the filled circles are the values found in the preceding sub-section. Though the two sets of values do not overlap they do at least fit at their junction; since both determinations give normalized values of $A(y)$, that is, absolute values, this fit is quite unforced and may be regarded as satisfactory. The dotted curve is tangent to the maxima of the theoretical diffraction pattern. For positive y the wing of $A(y)$ is nearly 30 per cent greater than that given by theory; for negative y, where the wing cannot be determined because of the penumbra of the shadow of the diaphragm, there is at least an indication that $A(y)$ is approaching theory.

The asymptotic values of $J(y)$ for y large, that is, the required ratio of general scattered-light flux to flux in the spectrum, are given in Table I for each plate. It will be noted that the mean ratio of scattered light for the two panchromatic plates is 1·54 per cent, and for the two ordinary plates 1·15 per cent. This is the anticipated result. The general scattered light is made up of all wave-lengths which enter the slit (in our case the whole spectrum of the Sun as transmitted by the Earth's atmosphere), but the photographic plate can only record that part of this wave-length range to which the emulsion is sensitive. Hence a greater scattered-light ratio will be given by the panchromatic than by the ordinary emulsion. In view of the great height of the slit, the dispersion of nearly 2 mm A^{-1} and the short wave-length of λ4320 where the determination is made, a scattered-light ratio of 1·54 per cent may be regarded as satisfactory for an auto-collimating spectroscope. By a preliminary analysis with an ordinary colour filter of the radiation entering the slit and by using a slit only a few

millimetres high, it is clear that even at λ 4320 the general scattered light can be reduced to negligible proportions.

3. *Limitations*

The technical problems of solar spectroscopy may be classed into profile determination, measurement of line displacements and discrimination of spectra from different parts of the solar image. Given the mechanical and thermal stability, and the freedom from scattered light of the Oxford spectroscope, the limits within which reliable results can be obtained in these problems are fixed by the horizontal and vertical apparatus functions.

TABLE I

Flux Ratio of Scattered Light/Spectrum at λ 4320

Date 1948	Slit Height mm	Slit Width mm	Exp. m s	$S(19)/I$	Emulsion
June 17	19	0·075	3 03	0·0146	Ilf. R. Proc. Pan.
June 26	19	0·075	3 00	0·0163	Ilf. R. Proc. Pan.
July 3	19	0·075	3 00	0·0121	Ilf. Sp. Rapid
July 5	19	0·075	3 00	0·0120	Ilf. Sp. Rapid
July 5	19	0·075	3 00	0·0104	Ilf. Sp. Rapid

3.1. *Profile determination.*—The observed intensity at nominal wave-length λ in a line profile is

$$O(\lambda) = \int_0^\infty T(\lambda')A(\lambda - \lambda')\,d\lambda', \qquad (4)$$

where $T(\lambda)$ is the true shape of the profile and $A(\lambda)$ is the normalized horizontal apparatus function. The value of the required $T(\lambda)$ derived from this equation is very sensitive to errors in $O(\lambda)$ and $A(\lambda)$, and becomes the more sensitive the more nearly $T(\lambda)$ approaches in half-width the horizontal apparatus function; compare van de Hulst (**6**). The horizontal apparatus function therefore fixes a lower limit to the width of the Fraunhofer line for which the profile can be found. Thus Redman (**16**), with an apparatus function of half-width approximately 0·145 A, has confined his determination of central intensities to lines of Rowland number 8 and greater, and Houtgast (**5**), with the Potsdam spectroscope with a remarkably sharp apparatus function of half-width 0·029 A, to lines of 7 and greater. To Redman's rule (**17**) that "existing instruments are inadequate to deal with lines fainter than about Rowland number 5" the Oxford spectroscope with an apparatus function of half-width 0·048 A is no exception.

If the spectroscope be used as a monochromator for an interferometer, then it is the apparatus function of the latter which appears in the integral equation (4). Since the resolving power of the interferometer can be very high and the width of its apparatus function correspondingly small, it might be thought that no limit exists to the practical determination of absorption line profiles with an interferometer combined with a spectroscope. Treanor (**18**), however, has shown that, owing to the periodicity of the apparatus function of the interferometer, increasing amounts of false light are superposed on the fringe system as the resolving power of the interferometer is increased and with it the range is decreased. Thus using Treanor's exact equation (9) we find for the Oxford spectroscope false light of 0·24 per cent for a Fabry–Perot interferometer of range 0·36 A and resolving power 500 000, and false light of 1·50 per cent for a range of 0·18 A and resolving power of 10^6. These are small amounts and since they are accurately calculable, provided the apparatus function is known for the circumstances under

which the spectroscope is being used (wave-length, slit-width and nature of its illumination), there is reason for hope that profile determination below Redman's limit may be possible.

3.2. *Line displacement.*—Because of the marked asymmetry in the horizontal apparatus function the observed profiles of solar absorption lines will also necessarily be asymmetrical. To show this effect "true" profiles for Fraunhofer lines have been computed for a purely scattering atmosphere (above a bounded photosphere) at a temperature of 6000 deg. K and with ten times the classical damping constant, and from these the observed profiles have been computed by eqn. (4). Calculations have been carried out for four lines with equivalent widths of 30, 69, 125 and 327 mA, corresponding roughly to Rowland numbers 0_+, 2, 4 and 9. Fig. 7 shows the "true" and observed profiles for the first and second of these lines; the asymmetry of the observed profile is easily visible. The centres of intensity and the centroids, the latter found from numerical integration, are given in Table II. The centres of intensity of the observed lines are displaced to the red with respect to the "true" lines by an amount which varies nearly linearly as the logarithm of the equivalent width of the line. The centroids of the lines, on the other hand, all show the same displacement within the errors of computation; this displacement, as is mathematically obvious from eqn. (4), for a symmetrical, true profile, is simply the displacement of the centroid of the apparatus function from its centre of intensity.

TABLE II

Displacements of Observed Lines

W	Centre Int.	Centroid
0·030 A	0·003 A	0·018 ± 0·001 A
0·069	0·010	0·019 ± 0·002
0·125	0·015	0·018 ± 0·005
0·327	0·022	0·029 ± 0·028

If the measurer of a spectrum were always presented with intensity profiles of the observed lines, and if he set his cross-wire on the centroid of a line, then the asymmetry of the apparatus function would only lead to a change of origin in wave-length. This would have no effect on the determination of sight-line velocities, or on the measurement of any other displacement where true, symmetrical profiles are bodily displaced. Measurement, however, is never so simple a matter. Quite apart from the transformation of the observed intensity profile by the photographic emulsion and of its appearance by Fechner's law, it is unknown where in this transformed profile the experienced measurer sets his cross-wire. The art of measurement is learned by finding a method of setting which leads to the greatest consistency, and the setting which gives this result may well be different for lines of different equivalent width and indeed for different measurers. It is therefore almost certain that the setting on the asymmetrical profiles produced by the Oxford spectroscope will be displaced by an amount which is a function of the equivalent width. This would for example be the case if the setting were always made on the centre of intensity of the observed profile.

The only way to overcome this difficulty is to make differential measures, that is, the position of a particular line must always be measured from an origin given by the same line photographed under standard conditions where its wave-length is known. Thus no matter how the setting is made, the measured displacement is correct and is independent of the equivalent width of the line. Standard

conditions are provided by a spectrum of the centre of the Sun, and the differential measurement is most conveniently made by using a Hartmann spectrocomparator or Evershed's positive-on-negative method.

3.3. *Discrimination of spectra.*—Fine details on the solar surface, more or less imperfectly imaged on the slit (as a result of seeing and the telescope) give spectra still further obliterated by the vertical apparatus function. A convenient test object of this phenomenon is provided by solar granulation. According to Keenan (**9**), granules have a diameter of approximately 1·1 seconds of arc, a brightness ratio to intergranular regions of 1·15, and occupy about 26 per cent of the area of the solar surface. Assuming the granules to be evenly spaced, a slit 0·41 seconds of arc in width (corresponding to a normal Oxford slit-width of 0·04 mm) will cut centrally through a granule once every 8·9 seconds of arc, and

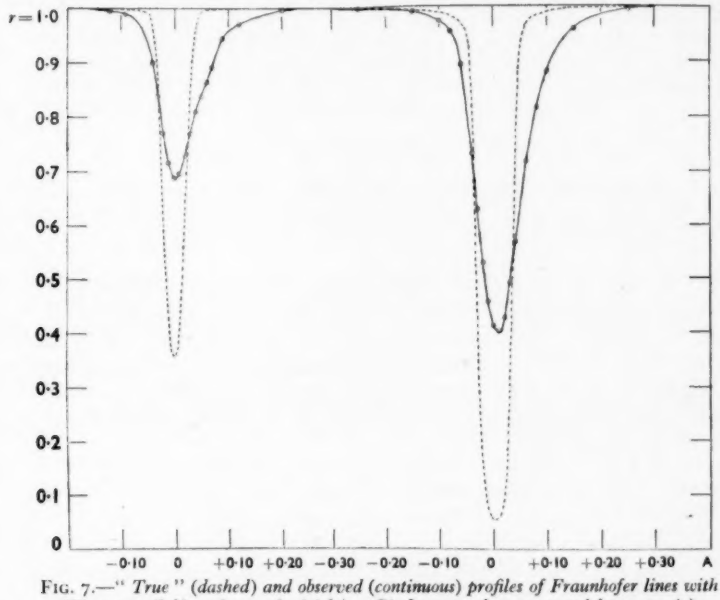

FIG. 7.—" *True* " *(dashed) and observed (continuous) profiles of Fraunhofer lines with* $W=0{\cdot}030$ *(left) and* $=0{\cdot}069$ *(right). Circles are values computed from eqn.* (4).

in the same interval will cut off-centre through a number of others. The illumination, observable just behind the slit, produced by a somewhat simplified form of granulation of this kind and imaged in perfect seeing by a perfect telescope is shown in Fig. 8. The variation in the heights (proportional to the flux per unit length through the slit) of the granules is due in part to the slit not cutting the granules centrally and in part to an assumed variation of brightness due to the finite life of the granules.

The spectra of these idealized granules tends to be obliterated by the vertical apparatus function. The resulting intensity distribution, computed from the vertical apparatus function and an equation similar to (4), is shown as a smooth curve in Fig. 8; this is simply the intensity distribution of the streaks produced in the spectrum by the granules. The amount of obliteration is considerable, but it seems reasonable to suppose that spectroscopic details of granules, affected in a known way by the intergranular regions, could be obtained for the three or

four brightest granules shown in the 4-mm height of slit in Fig. 8. Observations of granular spectra during the last four years show indeed much the same intensity distribution as has been theoretically calculated. Solar detail, very much finer than granulation, even if it were adequately imaged on the slit, would however be so obliterated by the vertical apparatus function as to be nearly invisible.

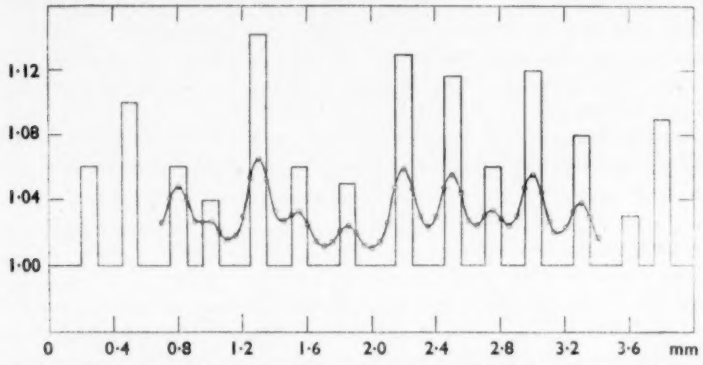

FIG. 8.—*Ideal granulation (rectangular profiles) as reproduced by spectroscope (continuous curve). The circles are intensities computed from integral equation. Ordinates are intensities, and abscissae are millimetres in focal plane perpendicular to direction of dispersion.*

Help has been received at all stages in the design and construction of the spectroscope. I wish to mention specifically that received from the late Mr R. M. Abraham of Casella's, to whom is largely due the success of the mechanical parts, from Mr J. W. Perry of Hilger's, who designed the objective and suggested the interpretation of its focal properties and finally from Mr G. H. Neale, who supervised the construction of the tunnel, did all the joinery and assisted in the erection of the instrument.

University Observatory,
Oxford:
1952 *January* 3.

References

(1) M. G. Adam, *M.N.*, **108**, 446, 1948; *Comm. Univ. Obs., Oxford*, No. 26, 1948.
(2) P. H. van Cittert, *Zeits. f. Phys.*, **65**, 547, 1930.
(3) O. Eppenstein, *Handbuch der Physik*, **18**, 204, 1928.
(4) R. A. Herman, *Geometrical Optics*, p. 25, Cambridge, 1900.
(5) J. Houtgast, *Variations in Profiles etc.* Dissertation, Utrecht, 1942.
(6) H. C. van de Hulst, *B.A.N.*, **10**, 75, 1946.
(7) C. V. Jackson, *Phil. Trans.* A, **236**, 1, 1936.
(8) H. Kayser, *Handbuch der Spektroscopie*, Leipzig, **1**, 501, 1900.
(9) P. C. Keenan, *Ap. J.*, **89**, 604, 1939.
(10) T. L. Page, *M.N.*, **96**, 604, 1936; *Comm. Univ. Obs., Oxford*, No. 7, 1936.
(11) H. H. Plaskett, *M.N.*, **91**, 870, 1931.
(12) H. H. Plaskett, *M.N.*, **96**, 402, 1936; *Comm. Univ. Obs., Oxford*, No. 6, 1936.
(13) H. H. Plaskett, *M.N.*, **99**, 219, 1939; *Comm. Univ. Obs., Oxford*, No. 14, 1939.
(14) Lord Rayleigh, *Scientific Papers*, III, p. 129, Cambridge, 1888.
(15) Lord Rayleigh, *Scientific Papers*, III, p. 429, Cambridge, 1899.
(16) R. O. Redman, *M.N.*, **97**, 552, 1937.
(17) R. O. Redman, *M.N.*, **98**, 325, 1938.
(18) P. J. Treanor, *M.N.*, **109**, 389, 1949; *Comm. Univ. Obs., Oxford*, No. 28, 1949.

ON SPHERICALLY SYMMETRICAL ACCRETION

H. Bondi

(Received 1951 October 3)

Summary

The special accretion problem is investigated in which the motion is steady and spherically symmetrical, the gas being at rest at infinity. The pressure is taken to be proportional to a power of the density. It is found that the accretion rate is proportional to the square of the mass of the star and to the density of the gas at infinity, and varies inversely with the cube of the velocity of sound in the gas at infinity. The factor of proportionality is not determined by the steady-state equations, though it is confined within certain limits. Arguments are given suggesting that the case physically most likely to occur is that with the maximum rate of accretion.

---

1. The importance of the accretion of interstellar gas by stars has been recognized since the work of Hoyle and Lyttleton (**1, 2, 3**). In their work the problem, later investigated in detail by Bondi and Hoyle (**4**), was that in which the rate of accretion was limited principally by the relative motion of the star and the gas cloud, the effects of pressure being considered negligible in comparison with the dynamical effects. The result derived in these papers was that

$$dM/dt = 2\pi\alpha(GM)^2V^{-3}\rho_\infty, \tag{1}$$

where M is the mass of the star, dM/dt is the rate of accretion, ρ_∞ the density of the gas cloud far from the star, V is the relative velocity of the star and the distant (undisturbed) parts of the cloud, G is the constant of gravitation, and α is a numerical constant which was first estimated to be equal to 2. Later work (**4**) showed that the steady-state equations did not determine α, although it seemed likely that it should always be between 1 and 2. It was also shown that if the star entered a cloud of uniform density with a plane boundary, α settled down to a value near 1·25.

In all this work pressure effects were neglected, the argument being that any heat generated would be radiated away rapidly, so that the temperature of the gas was always very low. Considerable mathematical simplification is introduced by this assumption, and it was shown that it was likely to be satisfied in most cases of astrophysical interest (**3**). The mathematical difficulties of the more general problem, in which both dynamical and pressure effects are considered, seem insuperable at present. However, the extreme case of negligible dynamical effects is again far simpler, and will be discussed in this paper. It may reasonably be expected that the case discussed here together with the case discussed previously bracket the complete problem.

2. The problem to be discussed may be defined as follows:

A star of mass M is at rest in an infinite cloud of gas, which at infinity is also at rest and of uniform density ρ_∞ and pressure p_∞. The motion of the gas is spherically symmetrical and steady, the increase in mass of the star being ignored

so that the field of force is unchanging. The pressure p and density ρ are related everywhere by

$$p/p_\infty = (\rho/\rho_\infty)^\gamma, \tag{2}$$

where γ is a constant satisfying $1 \leqslant \gamma \leqslant \frac{5}{3}$.

With a suitable choice of γ, equation (2) is equivalent to the physical condition that no heat is radiated or conducted away. Hence the solution should provide the most complete contrast possible with the problem previously investigated. The equations governing the problem are easily set up. If we take r to be the radial coordinate and v the *inward* velocity of the gas, the equation of continuity is

$$4\pi r^2 \rho v = \text{constant} = A \text{ (say)}, \tag{3}$$

where A is the accretion rate.

Bernoulli's equation is

$$\frac{v^2}{2} + \int_{p_\infty}^{p} \frac{dp}{\rho} - \frac{GM}{r} = \text{constant } (=0). \tag{4}$$

The constant is readily seen to vanish by virtue of the boundary conditions at infinity. Combining (2) and (4) we have

$$\frac{v^2}{2} + \frac{\gamma}{\gamma-1}\frac{p_\infty}{\rho_\infty}\left[\left(\frac{\rho}{\rho_\infty}\right)^{\gamma-1} - 1\right] = \frac{GM}{r}. \tag{5}$$

Equations (3) and (5) are two equations for the two variables v and ρ in terms of r, the distance from the centre of the star.

The equations may be made non-dimensional by the appropriate use of the velocity of sound in the gas at infinity, which as usual we denote by c. By the well-known formula

$$c^2 = \gamma p_\infty/\rho_\infty. \tag{6}$$

Let us introduce non-dimensional variables, x, y, z, to replace r, v, ρ, respectively, as follows:

$$\begin{aligned} r &= xGM/c^2, \\ v &= yc, \\ \rho &= z\rho_\infty. \end{aligned} \tag{7}$$

Then (3) and (5) take the non-dimensional form

$$x^2 yz = \lambda, \tag{8}$$

$$\tfrac{1}{2}y^2 + (z^{\gamma-1} - 1)/(\gamma - 1) = 1/x, \tag{9}$$

where λ is given by

$$A = 4\pi\lambda(GM)^2 c^{-3}\rho_\infty. \tag{10}$$

Accordingly λ is the non-dimensional parameter determining the accretion rate. It plays the same role as α in equation (1). It will also be observed that the relative velocity V of equation (1) has been replaced by c in (10).

3. The explicit solution of equations (8) and (9) for general γ is possible not in terms of the variables y and z but only if an auxiliary variable depending only on $y^2/z^{\gamma-1}$ is introduced. It is particularly interesting that mathematical requirements lead to the introduction of this variable, since

$$u = yz^{-(\gamma-1)/2} \tag{11}$$

has immediate physical significance as the ratio of the local bulk velocity v of the gas to the local velocity of sound $(\gamma p/\rho)^{1/2}$. Substituting (11) into (8) and solving for y and z we have

$$y = u^{2(\gamma-1)}(\lambda/x^2)^{(\gamma-1)(\gamma+1)}, \tag{12}$$

$$z = (\lambda/x^2 u)^{2(\gamma-1)}. \tag{13}$$

Then (9) becomes

$$\tfrac{1}{2}u^{4(\gamma+1)}\left(\frac{\lambda}{x^2}\right)^{2(\gamma-1)/(\gamma+1)} + \frac{1}{\gamma-1}\left(\frac{\lambda}{x^2 u}\right)^{2(\gamma-1)(\gamma+1)} = \frac{1}{x} + \frac{1}{\gamma-1}. \tag{14}$$

Rearranging the terms and multiplying by $(x^2/\lambda)^{2(\gamma-1)/(\gamma+1)}$ we find that (14) takes the form

$$f(u) = \lambda^{-2(\gamma-1)/(\gamma+1)} g(x), \tag{15}$$

where

$$f(u) = \tfrac{1}{2}u^{4/(\gamma+1)} + \frac{1}{\gamma-1}u^{-2(\gamma-1)/(\gamma+1)} = u^{4/(\gamma+1)}\left(\frac{1}{2} + \frac{1}{\gamma-1}\frac{1}{u^2}\right), \tag{16}$$

$$g(x) = x^{4(\gamma-1)/(\gamma+1)}\left[\frac{1}{x} + \frac{1}{\gamma-1}\right] = \frac{x^{4(\gamma-1)/(\gamma+1)}}{\gamma-1} + x^{-(5-3\gamma)/(\gamma+1)}. \tag{17}$$

A study of the functions f and g serves to determine u as a function of λ and x. The variables y and z are then readily found by (12) and (13).

4. We shall first assume that $1 < \gamma < \frac{5}{3}$. The two limiting cases $\gamma = 1$, $\gamma = \frac{5}{3}$ will be examined later. With this assumption both f and g are each the sum of a positive and negative power of the respective variables and hence each of them has a minimum. The minimum of $f(u)$ occurs for $u = u_m = 1$ and is of value

$$f = \tfrac{1}{2}(\gamma+1)/(\gamma-1) = f_m \text{ (say)}.$$

The minimum of $g(x)$ occurs for $x = x_m = \frac{1}{4}(5-3\gamma)$ and is of value

$$g = \frac{1}{4}\frac{\gamma+1}{\gamma-1}[\tfrac{1}{4}(5-3\gamma)]^{-(5-3\gamma)/(\gamma+1)} = g_m \text{ (say)}.$$

In our problem x varies between infinity and the value corresponding to the surface of the star. This last value is very small indeed. As an example, if the star is taken to be the Sun, and $c = 1$ km/s corresponding to a gas temperature at infinity of nearly 3 000 deg. K, the surface value of x is only 5×10^{-6}. Even for a red giant the surface value of x would be less than 10^{-2} unless the temperature of the gas at infinity were quite improbably high (more than, say, 5×10^4 deg. K). Accordingly x will attain the value x_m in the physically significant interval. Hence, somewhere in that interval, the right-hand side of (15) will reach a value as low as $\lambda^{-2(\gamma-1)/(\gamma+1)} g_m$. But the lowest value f can reach is f_m. Hence λ cannot exceed λ_c, where

$$\lambda_c = \left(\frac{g_m}{f_m}\right)^{(\gamma+1)/2(\gamma-1)} = \left(\frac{1}{2}\right)^{(\gamma+1)/2(\gamma-1)}\left(\frac{5-3\gamma}{4}\right)^{-(5-3\gamma)/2(\gamma-1)}. \tag{18}$$

Our first result is therefore that the accretion rate A cannot exceed the value

$$4\pi\lambda_c (GM)^2 c^{-3}\rho_\infty. \tag{19}$$

Table I gives the value of λ_c for a few values of γ.

TABLE I

γ	1	1·2	1·4 $= \frac{7}{5}$	1·5	$\frac{5}{3}$
λ_c	$\frac{1}{4}e^{3/2} \doteqdot 1{\cdot}12\ldots$	$\frac{1}{4}(0{\cdot}7)^{-3{\cdot}5} \doteqdot 0{\cdot}872\ldots$	0·625	0·500	0·250

5. In order to obtain a more detailed picture it is necessary to discuss $f(u)$ and $g(x)$ more fully, and to take account of the boundary conditions of the problem. Since, at infinity, v vanishes but p and ρ tend to finite limits, it follows that u tends to zero there.

It is now easy to consider the problem graphically. Fig. 1 shows f and g drawn for the typical case $\gamma = \frac{7}{5}$. The resulting variation of u as a function of x is shown in Fig. 2 for the cases (i) $\lambda = \frac{1}{4}\lambda_c$, (ii) $\lambda = \lambda_c$ and (iii) $\lambda = 4\lambda_c$. It will be seen that the boundary condition at infinity implies that u is very small near infinity (points beyond A on the graphs). For $\lambda < \lambda_c$, as x diminishes, u rises gradually to a maximum (B) and diminishes to zero (C) as x tends to zero. The closer λ approaches λ_c from below, the sharper the maximum B. No part of the curve A′B′C′ (on which u is very large both at infinity and near $x = 0$) is of physical significance, since u given by this curve does not satisfy the boundary condition at infinity. No jump from the curve ABC to A′B′C′ is possible, since this would imply an infinite acceleration. Along ABC the variable u is always less than unity, so that the motion is subsonic. Along A′B′C′ the value of u exceeds unity.

The case $\lambda = \lambda_c$ is quite different. For in this the curves have contact at B = B′. Coming from A, the physically significant curve can continue either to C or to C′. In the first alternative, the curve is the limiting form of the curves for $\lambda < \lambda_c$. The curve has a discontinuous tangent at B and there is hence a finite jump in the acceleration. Although this is perhaps physically not very plausible, there does not seem to be any argument disallowing this motion altogether. It may be significant that at B the value of u is unity, so that the bulk velocity equals the velocity of sound.

The curve ABC′ is perfectly smooth and monotonic. For $x > x_B$ the motion is subsonic, while for $x < x_B$ the motion is supersonic. The system is in a state quite different from any state possible for $\lambda < \lambda_c$.

If λ exceeds λ_c then the pattern of the curves changes as indicated, and no solution is possible.

We see hence that there are two quite different types of motion. Type I exists for $\lambda \leqslant \lambda_c$. The motion is everywhere subsonic (except at $x = x_m$ if $\lambda = \lambda_c$), and u has a single maximum which is less than or equal to unity. The bulk velocity v has a maximum if $\gamma < \frac{3}{2}$ but not if $\gamma \geqslant \frac{3}{2}$. (This follows from a simple consideration of y' in terms of u.) For $\gamma < \frac{3}{2}$ the velocity v tends to zero as r tends to zero, for $\gamma = \frac{3}{2}$ it tends to a limit (equal to $\frac{1}{4}c\lambda$), and for $\gamma > \frac{3}{2}$ it tends to infinity. The density is always a monotonic function of the radius. Type II exists only if $\lambda = \lambda_c$. In this case u, v, ρ are all monotonic functions of the radius.

The special case $\lambda = 0$ may be briefly referred to here. In this case the gas is at rest, forming a tenuous continuation of the star. Since $y = 0$ we have by (9)

$$z^{\gamma-1} = 1 + (\gamma - 1)/x. \tag{20}$$

Figs. 3, 4 and 5 show y and z as functions of x for $\gamma = 1$, $\frac{7}{5}$ and $\frac{5}{3}$ respectively. Three values of λ are taken in each case, namely $\lambda = \lambda_c$, $\lambda = \frac{1}{4}\lambda_c$ and the case $\lambda = 0$ just referred to. It will be seen from the figures that z does not depend very critically on λ, varying only slightly between the extreme cases $\lambda = 0$ and $\lambda = \lambda_c$, especially in the case of the higher γ values.

6. It remains to discuss the two limiting cases $\gamma = 1$ and $\gamma = \frac{5}{3}$ respectively.

If $\gamma = 1$ equation (9) becomes

$$\tfrac{1}{2}y^2 + \ln z = 1/x. \tag{9′}$$

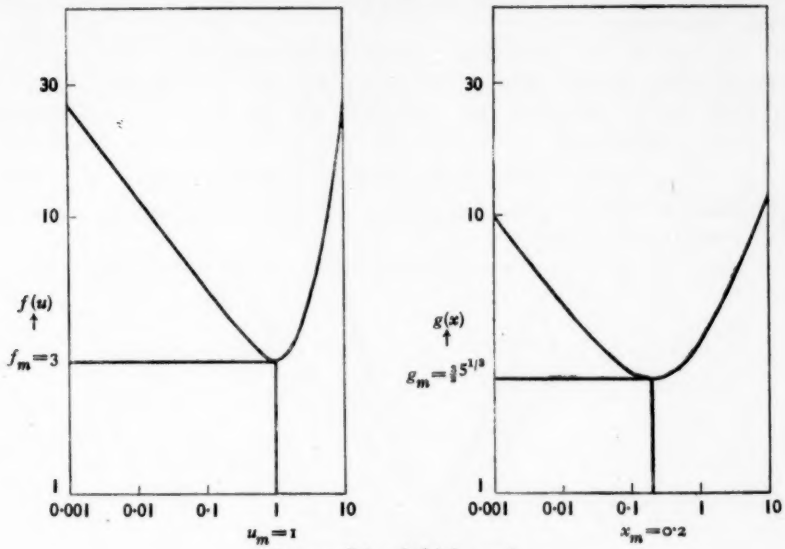

FIG. 1.—*f(u) and g(x) for* $\gamma=\frac{7}{5}$.

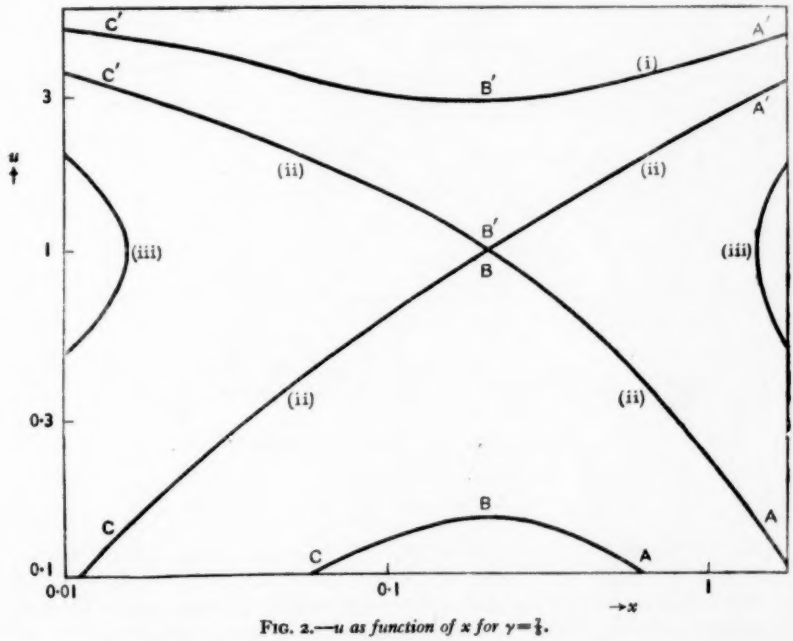

FIG. 2.—*u as function of x for* $\gamma=\frac{7}{5}$.
(i) $\lambda=\frac{1}{4}\lambda_c$;
(ii) $\lambda=\lambda_c$;
(iii) $\lambda=4\lambda_c$.

It is easy to eliminate z between (8) and (9′) since, by (11), $y=u$ in the present case. Accordingly

$$\tfrac{1}{2}y^2-\ln y=-\ln\lambda+(1/x+2\ln x). \qquad (14')$$

The minimum of the left-hand side occurs for $y=1$ and equals $\frac{1}{2}$, while the minimum of the bracket on the right-hand side occurs for $x=\frac{1}{2}$ and equals $2-2\ln 2$. Accordingly

$$\lambda_c=\tfrac{1}{4}e^{3/2}=1{\cdot}120\ldots, \quad \ln\lambda_c=0{\cdot}1138\ldots. \qquad (18')$$

This is also the limit of expression (18) as $\gamma\to 1$, so that λ_c is continuous at $\gamma=1$. Fig. 4 represents this case.

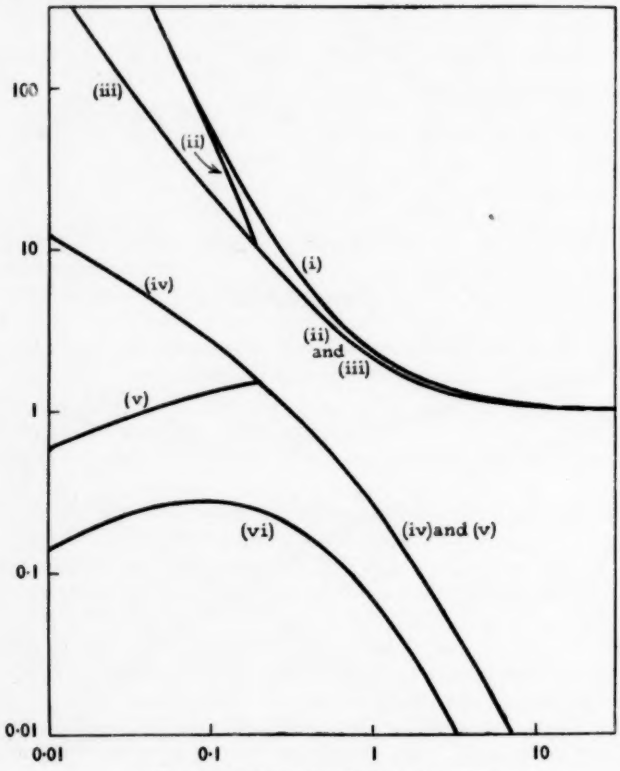

FIG. 3.—*y and z as functions of x for* $\gamma=\frac{7}{5}$.
(i) z ($\lambda=0$);
(ii) z ($\lambda=\lambda_c$, Type I);
(iii) z ($\lambda=\lambda_c$, Type II);
(iv) y ($\lambda=\lambda_c$, Type II);
(v) y ($\lambda=\lambda_c$, Type I);
(vi) y ($\lambda=\frac{1}{4}\lambda_c$).

The case $\gamma=\frac{5}{3}$ is an even simpler extension of the ordinary case. The only real change is that x_m (which decreases monotonically as γ increases) now equals zero. Accordingly there is now no difference between Type I and Type II motions for $\lambda=\lambda_c=\frac{1}{4}$ (Fig. 5).

It can be seen that u, y and z, considered as functions of x and γ, are continuous in $1 \leqslant \gamma \leqslant \frac{5}{3}$.

7. The final question that must be considered is what determines the value of λ in any actual case. It has been seen that the steady-state equations possess a solution whenever $0 \leqslant \lambda \leqslant \lambda_c$. The particular value of λ actually occurring must therefore be determined by other considerations. This is analogous to the

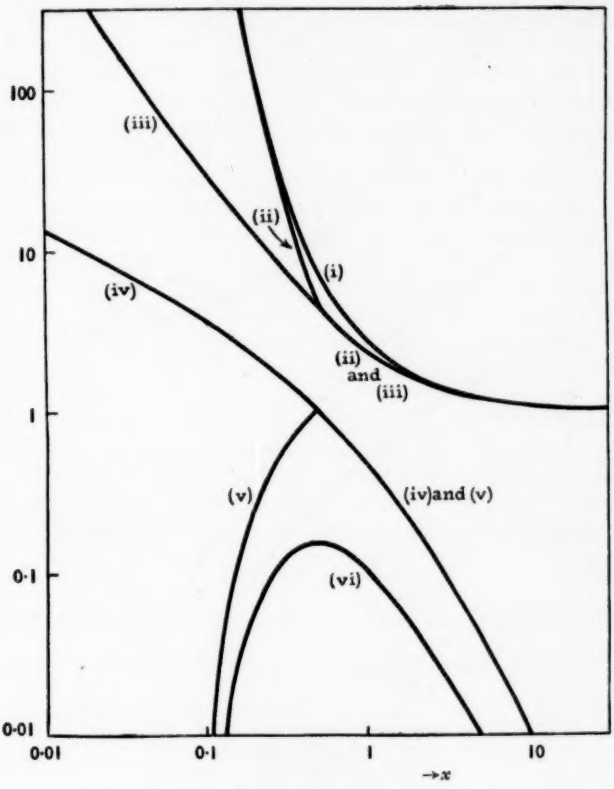

FIG. 4.—y and z *as functions of* x *for* $\gamma = 1$.
(i) z ($\lambda = 0$);
(ii) z ($\lambda = \lambda_c$, Type I);
(iii) z ($\lambda = \lambda_c$, Type II);
(iv) y ($\lambda = \lambda_c$, Type II);
(v) y ($\lambda = \lambda_c$, Type I);
(vi) y ($\lambda = \frac{1}{4}\lambda_c$).

velocity-limited case of accretion where α is not determined by the steady-state equations (4). The method used there to determine a specific value of α was to consider the case in which the star entered a cloud of gas with a plane boundary. The use of such a model would lead to very great mathematical difficulties in the present case, since the conditions of time-independence and spherical symmetry would have to be dropped simultaneously.

The boundary conditions at the surface of the star do not seem to be of help in the problem, since the star will swallow up any material falling into it without imposing any real conditions on the velocity, density, or pressure of the incoming materials.

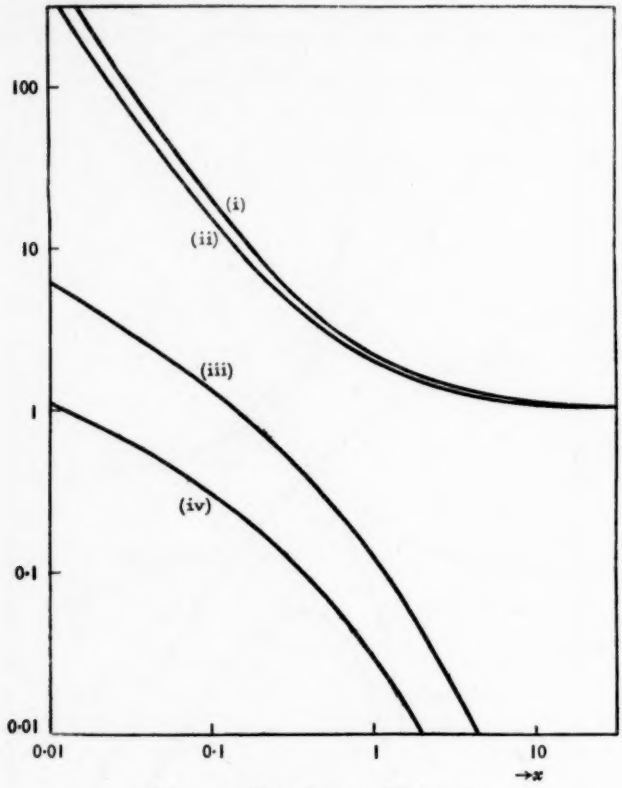

FIG. 5.—*y and z as functions of x for* $\gamma=\frac{5}{3}$.
(i) z ($\lambda=0$);
(ii) z ($\lambda=\lambda_c$);
(iii) y ($\lambda=\lambda_c$);
(iv) y ($\lambda=\frac{1}{4}\lambda_c$).

There remains the possibility of investigating the stability of the system with respect to small disturbances. Even if only spherically symmetrical perturbations are admitted, a partial differential equation of considerable complexity results. It is easily seen from it that disturbances are in part propagated with the velocity of sound relatively to the material, but the nature of the part that remains behind is not easily found. However, this may be a possible method of approach to the problem.

There is yet another possibility of investigating the stability of the system, and that is by comparing the energy of the system in its various states. The state with the lowest energy would then be expected to be the only stable state. Owing to the fact that our system is not isolated (the star itself not being considered part

of the system) the validity of this approach is not quite assured, and similarly doubts may arise owing to the infinite extent of the system. Nevertheless, since the comparison of the energy of the system in every spherical shell leads to the same result, it seems very likely that the method gives the correct answer.

The energy of the gas per unit mass is constant by virtue of our assumptions (*cf.* equation (4)). Accordingly a comparison of the densities is all that is involved. Consider now z as function of λ for fixed x. Then it may be seen from equations (13), (15) and (16) that for u less than unity z decreases as λ increases. Accordingly the energy of the system in every spherical shell is lower for the Type I state with $\lambda=\lambda_c$ than for any other Type I state. Comparing now, for $\lambda=\lambda_c$, the Type I and the Type II states, it is immediately seen that, for $x\geqslant x_m$, the densities are the same, but that for $x<x_m$ the density (and hence the energy) is lower in the Type II state.

Accordingly the system has, in the sense described, the lowest energy in the Type II state, and we may expect to find a natural system in this state with $\lambda=\lambda_c$. If $\gamma=\frac{5}{3}$, the difference between the Type II state and the Type I state with $\lambda=\lambda_c$ disappears, and we would expect to find the system in this joint state. The result that the Type II state is the one most likely to be realized is very satisfactory, since the behaviour of all the functions is most uniform and smooth in this state. The result is also in agreement with the intuitive idea that, since there is nothing to stop the process of accretion, it takes place at the greatest possible rate, i.e. with $\lambda=\lambda_c$.

8. The two cases of accretion that have been examined so far may be called velocity-limited and temperature-limited respectively. The intermediate range of cases presents far greater difficulties. However, it may be possible to conjecture what the result is in the following way.

In the velocity-limited case of accretion the accretion rate A is given (**4**) by

$$A\doteqdot 2\cdot 5\pi(GM)^2V^{-3}\rho_\infty, \tag{21}$$

while for, say, $\gamma=\frac{3}{2}$ in the temperature-limited case the result is

$$A=2\pi(GM)^2c^{-3}\rho_\infty. \tag{22}$$

If we therefore write down the formula

$$A\doteqdot 2\pi(GM)^2(V^2+c^2)^{-3/2}\rho_\infty,$$

it seems likely that it represents the order of magnitude of the accretion rate in the intermediate case, in which a star of mass M moves with relative velocity V in a uniform cloud of gas, in which the undisturbed density and the velocity of sound have the values ρ_∞ and c respectively. This formula, in agreement with intuitive ideas, suggests that if c exceeds V, temperature (pressure) imposes the chief limitation on the rate of accretion; whereas if V exceeds c, dynamical limitations are of greater importance.

The limitations due to pressure have probably been somewhat overestimated in this work. For if the cloud is able to radiate away some of the heat of compression then the adiabatic law will not apply, the pressure near the star will be diminished, and the accretion rate somewhat increased. How large this effect will be depends on the composition of the cloud. If there is a high proportion of constituents (such as hydrogen molecules (**2**)) that easily radiate at

moderate temperatures, then the effect will be appreciable. In this case the effective value of γ will be closer to unity than to the standard value for the gas in question. If γ equals unity the process is isothermal.

The work of the present paper, together with previous work, is likely to give a fair estimate of the order of magnitude of accretion in all cases of physical interest. Further progress in this field will probably require the consideration of non-steady states.

Trinity College,
Cambridge :
1951 *October* 2.

References

(1) F. Hoyle and R. A. Lyttleton, *Proc. Camb. Phil. Soc.*, **35**, 405, 1939.
(2) F. Hoyle and R. A. Lyttleton, *Proc. Camb. Phil. Soc.*, **36**, 325, 1940.
(3) F. Hoyle and R. A. Lyttleton, *Proc. Camb. Phil. Soc.*, **36**, 424, 1940.
(4) H. Bondi and F. Hoyle, *M.N.*, **104**, 273, 1944.

ON THE EFFECT OF INTERSTELLAR MATTER ON THE MOTION OF A STAR

K. N. Dodd and W. H. McCrea

(Received 1951 November 5)

Summary

It is shown that the retarding force upon a star exerted by interstellar matter through which it moves is effectively the same as that previously evaluated by Bondi and Hoyle, whether or not accretion takes place in the way they consider, so long as the interstellar matter has the general properties they assume. It is, however, suggested that the actual accretion may occur in the way considered without the operation of the rest of the mechanism envisaged by Bondi and Hoyle. If there is a density-gradient transverse to the path of the star, there is a transverse force, and this is evaluated. In this case any accreted or captured material must possess angular momentum about the centre of the star, and this also is evaluated. Some of the calculations illustrate the power of the vector methods in dynamics that were expounded by the late Professor E. A. Milne.

---

1. *Introduction.*—The theory of accretion by stars according to the mechanism originally investigated by Hoyle and Lyttleton* has been elaborated by Bondi and Hoyle.† The possible importance of this process in regard to problems of stellar evolution is now widely appreciated. Actually there are two fairly distinct fields in which its application is important, though naturally the two effects of the mechanism are or may be produced simultaneously. The first application is to the evolution of an individual star: here all that is relevant about the mechanism is the possibility it affords of supplying the star with fresh material. The second application is to stellar dynamics and so to the evolution of stellar systems, the relevant factor here being the retarding force produced by the mechanism upon the star (with its possibly increasing mass).

The latter application was briefly discussed by Bondi and Hoyle in the paper quoted, where they evaluate the retarding force and solve the resulting equation of motion.

In the present paper we show that the force is effectively the same as that evaluated by Bondi and Hoyle whether or not actual accretion takes place in the way they consider. We evaluate the force when the density of the interstellar material is non-uniform, in which case the force has a component transverse to the path of the star. If accretion occurs in this case, we show that there is also an effect upon the angular momentum of the star, though its astrophysical significance requires further investigation.

2. *Particle-orbits.*—We require certain properties of a hyperbolic orbit of a particle P moving under an inverse square law of force acting towards a centre O. Some of them could be quoted from other sources. However, it probably takes no more space to derive these, together with the other formulae required, by the

* F. Hoyle and R. A. Lyttleton, *Proc. Camb. Phil. Soc.*, **35**, 405, 1939; **36**, 424, 1940.
† H. Bondi and F. Hoyle, *M.N.*, **104**, 273, 1944.

methods expounded by the late Professor E. A. Milne.* It is an opportunity to illustrate the way in which these vector methods lead directly from the equation of motion to results expressed in terms of the desired parameters. They avoid any necessity for introducing auxiliary parameters, such as the eccentricity, which are not needed in the final results.

We write $\overrightarrow{OP}=\mathbf{r}$ and $r=|\mathbf{r}|$, with a similar use of the italic letter for the modulus in the case of other vectors. The force of attraction is taken to be μ/r^2 per unit mass. Then we have as first integrals of the equation of motion (Milne, *op. cit.*, Section 269(2), (3), (4))

$$\mathbf{r}\times\dot{\mathbf{r}}=\mathbf{h}, \tag{2.1}$$

$$\tfrac{1}{2}\dot{r}^2-\mu/r=W, \tag{2.2}$$

$$\mathbf{h}\times\dot{\mathbf{r}}=-\mu\mathbf{r}/r+\mathbf{B}, \tag{2.3}$$

where $\mathbf{h}$, $\mathbf{B}$, W are constants of integration.

Particle projected from infinity.—We require to consider the case in which P is projected "from infinity" with velocity $\mathbf{U}$, the perpendicular from O to the line of projection being $\mathbf{s}$. We write

$$\mathbf{U}=U\mathbf{i}, \qquad \mathbf{s}=s\mathbf{p}, \qquad \mathbf{q}=\mathbf{i}\times\mathbf{p}, \tag{2.4}$$

where $\mathbf{i}$, $\mathbf{p}$, $\mathbf{q}$ are fixed orthogonal unit vectors.

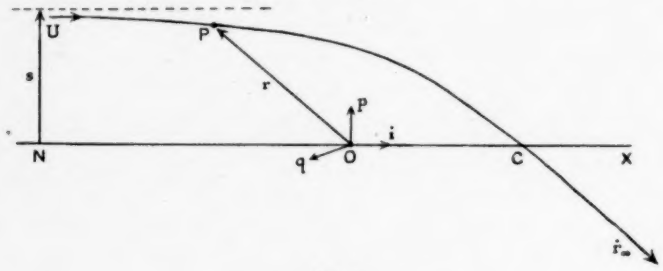

FIG. 1.

As initial conditions we have therefore

$$\dot{\mathbf{r}}=\mathbf{U}, \qquad \mathbf{r}/r=-\mathbf{i}, \qquad 1/r=0. \tag{2.5}$$

Using these in (2.1)–(2.3) we obtain

$$\mathbf{h}=\mathbf{s}\times\mathbf{U}=-sU\mathbf{q}, \tag{2.6}$$

$$W=\tfrac{1}{2}U^2, \tag{2.7}$$

$$\mathbf{B}=-\mu\mathbf{i}-sU^2\mathbf{p}. \tag{2.8}$$

Asymptotic velocity.—Now let $\dot{\mathbf{r}}_\infty=u_\infty\mathbf{i}+v_\infty\mathbf{p}$ be the final velocity when P is receding "to infinity". So $|\dot{\mathbf{r}}_\infty|=U$ and hence, when $\dot{\mathbf{r}}=\dot{\mathbf{r}}_\infty$, we have $\mathbf{r}/r=\dot{\mathbf{r}}_\infty/U$. Then (2.3) gives

$$\mathbf{h}\times\dot{\mathbf{r}}_\infty=-\mu\dot{\mathbf{r}}_\infty/U+\mathbf{B}.$$

This yields

$$\begin{aligned}\mathbf{h}\times(\mathbf{h}\times\dot{\mathbf{r}}_\infty)&=-\mu\mathbf{h}\times\dot{\mathbf{r}}_\infty/U+\mathbf{h}\times\mathbf{B}\\&=\frac{\mu^2}{U^2}\dot{\mathbf{r}}_\infty-\frac{\mu}{U}\mathbf{B}+\mathbf{h}\times\mathbf{B}.\end{aligned} \tag{2.9}$$

* E. A. Milne, *Vectorial Mechanics*, Sections 265–274, London, 1948.

Noting that the left-hand member reduces to $-h^2\dot{\mathbf{r}}_\infty$, (2.9) gives

$$\left(h^2+\frac{\mu^2}{U^2}\right)\dot{\mathbf{r}}_\infty=\frac{\mu}{U}\mathbf{B}-\mathbf{h}\times\mathbf{B}.$$

Using (2.6), (2.8) this leads to

$$u_\infty=U-\frac{2U}{1+s^2U^4/\mu^2}, \tag{2.10}$$

$$v_\infty=-\frac{2sU^3}{\mu(1+s^2U^4/\mu^2)}. \tag{2.11}$$

Point C.—We require to find the characteristics of the point C of the orbit such that $\overrightarrow{OC}$ is parallel to $\mathbf{U}$. At C let

$$\mathbf{r}=x\mathbf{i}, \qquad \dot{\mathbf{r}}=\dot{\mathbf{r}}_c=u\mathbf{i}+v\mathbf{p}. \tag{2.12}$$

Then from (2.1), (2.3)

$$x\mathbf{i}\times\dot{\mathbf{r}}_c=\mathbf{h}, \tag{2.13}$$

$$\mathbf{h}\times\dot{\mathbf{r}}_c=-\mu\mathbf{i}+\mathbf{B}. \tag{2.14}$$

If we multiply (2.14) by $\mathbf{i}$. and note, using (2.13),

$$\mathbf{h}\times\dot{\mathbf{r}}_c.\,\mathbf{i}=\mathbf{h}.\,\mathbf{r}_c\times\mathbf{i}=-h^2/x,$$

we find

$$x=s^2U^2/2\mu. \tag{2.15}$$

From (2.14), on multiplying by $\mathbf{i}\times$ and $\mathbf{p}\times$, respectively, we find further that

$$u=U, \tag{2.16}$$

$$v=-2\mu/sU. \tag{2.17}$$

Particle projected from general point—asymptotic velocity.—We shall require the asymptotic velocity $\dot{\mathbf{r}}_1$ of a particle projected with initial velocity $\dot{\mathbf{r}}_0$ from a general point $\mathbf{r}_0$. Let unit orthogonal vectors $\mathbf{i}$, $\mathbf{j}$, $\mathbf{k}$ be taken such that

$$\mathbf{r}_0=x\mathbf{i}, \qquad \dot{\mathbf{r}}_0=u_0\mathbf{i}+v_0\mathbf{j}, \tag{2.18}$$

and write

$$\dot{\mathbf{r}}_1=u_1\mathbf{i}+v_1\mathbf{j}, \qquad |\dot{\mathbf{r}}_1|=w. \tag{2.19}$$

Then from (2.1), (2.3), (2.18)

$$\mathbf{h}=xv_0\mathbf{k}, \tag{2.20}$$

$$\mathbf{B}=(\mu-xv_0^2)\mathbf{i}+xu_0v_0\mathbf{j}. \tag{2.21}$$

Since $\mathbf{r}/r=\dot{\mathbf{r}}_1/w$ for the asymptotic motion, (2.3) gives

$$\mathbf{h}\times\dot{\mathbf{r}}_1=-\mu\dot{\mathbf{r}}_1/w+\mathbf{B}.$$

This yields

$$\begin{aligned}\mathbf{h}\times(\mathbf{h}\times\dot{\mathbf{r}}_1)&=-(\mu/w)(\mathbf{h}\times\dot{\mathbf{r}}_1)+\mathbf{h}\times\mathbf{B}\\&=-(\mu/w)(-\mu\dot{\mathbf{r}}_1/w+\mathbf{B})+\mathbf{h}\times\mathbf{B}\end{aligned}$$

or

$$(h^2+\mu^2/w^2)\dot{\mathbf{r}}_1=(\mu/w)\mathbf{B}-\mathbf{h}\times\mathbf{B}. \tag{2.22}$$

Using (2.20), (2.21) we then find

$$u_1=(\mu^2-\mu xv_0^2+x^2u_0v_0^2w)w/(\mu^2+x^2v_0^2w^2), \tag{2.23}$$

$$v_1=(\mu xu_0v_0-\mu xv_0w+x^2v_0^3w)w/(\mu^2+x^2v_0^2w^2). \tag{2.24}$$

Also, from (2.2), $w^2=u_0^2+v_0^2-2\mu/x$. (2.25)

3. *Calculation of the retarding force.*—Following Bondi and Hoyle, we consider a star of mass M moving with velocity $-\mathbf{U}$ through a distribution of interstellar matter. This matter, which we shall call "the cloud", is taken to have the

general properties postulated by these authors. In particular, the thermal motions of its particles are assumed to be negligible. We take an origin O fixed at the centre of the star and consequently regard the particles as being projected at a large distance from O with velocity $\mathbf{U}$ relative to O. Here we contemplate only the conditions after a steady state is assumed to have been established.

We wish to calculate the force by which the cloud retards the motion of the star. The force we are about to determine is actually equal and opposite to that required to hold the star in a Newtonian frame of reference when the cloud streams steadily past, having velocity $\mathbf{U}$ at a large distance "up-stream". So long as the force so determined is sufficiently small it may be taken to be the force we wish to calculate.

If OX is the axis in the $\mathbf{i}$-direction, consider any plane Π normal to OX and meeting it at a point N a large distance up-stream from O. Let $\mathbf{s}$ be the position vector relative to N of any point of Π.

Let $\rho(\mathbf{s})$ be the density of the cloud at the point $\mathbf{s}$. It may be any function of $\mathbf{s}$. But ρ may not be supposed to vary in the direction of OX, if the conditions are taken to be strictly steady. For such a variation would result in a variation with time of the amount of material flowing past the star.

Case of no collisions.—If we entirely exclude the possibility of collisions between the particles of the cloud, even in the vicinity of the line OX, then every particle will describe a hyperbolic orbit about O of the sort studied in Section 2 with $\mu=\gamma M$, where γ is the constant of gravitation. We first evaluate the force in this case. As usual in such work, we neglect the effect of particles colliding directly with the surface of the star itself.

Let dS be an element of Π at position $\mathbf{s}$. Then the mass of the particles crossing dS per unit time is

$$\rho(\mathbf{s})U\,dS. \tag{3.1}$$

The change of momentum per unit mass of these particles is $\mathbf{U}-\dot{\mathbf{r}}_\infty$. Hence the force $\mathbf{F}$ upon the star exerted by particles which cross Π within a circle of centre N and radius s is

$$\mathbf{F}=\int\rho(\mathbf{s})(\mathbf{U}-\dot{\mathbf{r}}_\infty)U\,dS, \tag{3.2}$$

where the integral is over the area of this circle and $\mathbf{U}-\mathbf{r}_\infty$ is given by (2.10), (2.11).

If $\mathbf{F}$ has components $\mathbf{X}$, $\mathbf{P}$ along and perpendicular to OX, when we use the expressions (2.10), (2.11) in (3.2), we find

$$X=2U^2\int\frac{\rho(\mathbf{s})\,dS}{1+s^2U^4/\mu^2}, \tag{3.3}$$

$$\mathbf{P}=\frac{2U^4}{\mu}\int\frac{\rho(\mathbf{s})\mathbf{s}\,dS}{1+s^2U^4/\mu^2}. \tag{3.4}$$

This gives the general result required.

Case of linear variation of density.—For any applications of the results it is almost certainly adequate to use a linear approximation to the variation of the density. This case will certainly serve to illustrate the nature of the results. But we may also notice that the force $\mathbf{P}$ which arises from the variation of $\rho(\mathbf{s})$ is in fact unaffected by quadratic terms in this variation.

Let **j** be the direction in which the variation of $\rho(\mathbf{s})$ occurs. This is the direction of grad ρ, which must be perpendicular to **i** in the case of a strictly steady state, as already remarked.

We take then

$$\rho(\mathbf{s}) = (1 + bs\cos\phi)\rho_0, \tag{3.5}$$

where ρ_0, b are constants and ϕ is the azimuthal angle in Π measured from the **j**-direction.

Substituting in (3.3), (3.4) we then find, since $dS = s\,d\phi\,ds$ and

$$\mathbf{s} = s\cos\phi\mathbf{j} + s\sin\phi\mathbf{k},$$

$$X = 2\pi\rho_0 \frac{\mu^2}{U^2} \ln\left(1 + \frac{s^2U^4}{\mu^2}\right), \tag{3.6}$$

$$Y = \pi b\rho_0\mu\left[s^2 - \frac{\mu^2}{U^4} \ln\left(1 + \frac{s^2U^4}{\mu^2}\right)\right], \tag{3.7}$$

where $\mathbf{P} = Y\mathbf{j}$.

We shall now write

$$x_0 = \mu/U^2, \qquad x = \xi x_0, \tag{3.8}$$

and when s, x are related according to (2.15) we then have

$$s^2 = 2x_0^2\xi. \tag{3.9}$$

So (3.6), (3.7) may be written in terms of ξ instead of s as

$$X = 2\pi\rho_0(\mu^2/U^2)\ln(1 + 2\xi), \tag{3.10}$$

$$Y = \pi b\rho_0(\mu^3/U^4)[2\xi - \ln(1 + 2\xi)]. \tag{3.11}$$

We shall be interested in the case of ξ large compared with unity. In that case we may note that, approximately,

$$\frac{Y}{X} = bx_0 \frac{\xi}{\ln 2\xi} \qquad (\xi \text{ large}). \tag{3.12}$$

Recalling the derivation of (2.15) we have that X, Y in (3.10), (3.11) give *the force on the star exerted by particles of the cloud whose orbits in the gravitational field of the star meet the axis* OX *at all distances up to* $x = x_0\xi$.

Before discussing these results we have to obtain the corresponding ones in the next case.

[It should be noted that (3.10), (3.11) do *not* imply that the force tends to infinity when $U \to 0$. For in any application of (3.6), (3.7) the value of s is certainly bounded above by the presence of other stars. The value of X, Y must not exceed the value given by (3.6), (3.7) when s is replaced by its upper bound. But it is then seen that *the latter values tend to zero* when $U \to 0$.

This remark is intended mainly to remove any misapprehension of a mathematical sort. In most applications it seems that U is likely to be sufficiently large for the upper bound of the distance ξx_0 to be more significant than the upper bound of s. But if the formulae are to be applied to a range of values of U, including very small values, then it must be remembered that the approximations appropriate to large ξ will not be valid throughout the range.]

Case of collisions on the axis.—Under the conditions of the preceding case the orbit of every particle intersects the axis OX. We shall now calculate the consequences of supposing that *all the material simultaneously arriving along such orbits at any element* $(x, x + dx)$ *of the axis coalesces there* before continuing its motion in the gravitational field of the star. The purpose of considering this

case will be discussed below (Section 5), where the way in which it differs physically from the case considered by Bondi and Hoyle will be noted.

We shall continue to use the density law (3.5).

From (2.15) we have

$$s\,ds = x_0\,dx, \tag{3.13}$$

and so from (3.1) the mass of the particles reaching dx per unit time is $m\,dx$, where

$$m = \rho_0 x_0 U \int_0^{2\pi} (1 + bs\cos\phi)\,d\phi = 2\pi\rho_0 x_0 U. \tag{3.14}$$

Using (2.17) the total momentum of these particles in the negative **j**-direction is

$$2\rho_0 x_0 \mu\,dx \int_0^{2\pi} (1 + bs\cos\phi)\cos\phi\,d\phi/s = 2\pi b\rho_0 x_0 \mu\,dx. \tag{3.15}$$

Consequently the velocity in this direction immediately after coalescence is v_0 where, from (3.14), (3.15),

$$v_0 = b\mu/U. \tag{3.16}$$

Also it follows at once from (2.16) that the velocity u_0 in the **i**-direction is

$$u_0 = U. \tag{3.17}$$

It should be noted that m, u_0, v_0 are all independent of x.

The motion after coalescence is then given by (2.18)–(2.25) with u_0, v_0 having the values (3.16), (3.17).

We notice in the first place that (2.25) gives

$$w^2 = U^2 + b^2\mu^2/U^2 - 2\mu/x. \tag{3.18}$$

It follows that all the material reaching OX in $0 \leqslant x < ax_0$, where from (3.18)

$$a = 2/(1 + b^2 x_0^2), \tag{3.19}$$

must remain gravitationally bound to the star. We shall return to this feature in Section 5, noting in particular the way in which it differs from the corresponding result in the conditions envisaged by Bondi and Hoyle. Meantime we calculate the force on the star exerted by material reaching OX in $ax_0 < x \leqslant \xi x_0$.

Evaluating the rate of change of momentum of this material, the required force has components

$$X = m\int_{ax_0}^{\xi x_0} (U - u_1)\,dx, \qquad Y = m\int_{ax_0}^{\xi x_0} v_1\,dx, \tag{3.20}$$

where u_1, v_1 are given by substituting the present values of u_0, v_0, w in (2.23), (2.24).

The resulting expressions are highly complicated. However, for our purpose we need write down only the dominant terms when we take $bx_0 \ll 1$ and $\xi \gg 1$. These are easily found to give

$$X \sim 2\pi\rho_0 \frac{\mu^2}{U^2} \ln\xi, \qquad Y \sim 2\pi b\rho_0 \frac{\mu^3}{U^4}\xi. \tag{3.21}$$

The result to be noticed is that these are precisely the asymptotic forms of (3.10), (3.11) (remembering that $\ln(1 + 2\xi) \sim \ln 2\xi = \ln\xi + \ln 2 \sim \ln\xi$ for large ξ).

[In this case, as in the case of no collisions, further considerations have to be taken into account when U is small. The results will be given elsewhere in connection with certain applications of the work: they are not needed in the present paper.]

Case of accretion column.—The treatment in the preceding section will not apply to the particular case where the density of the undisturbed cloud is uniform, i.e. where $b=0$. In that case the coalesced material will proceed to move along the axis OX and will encounter other incoming material as it does so. It is in fact the case considered in detail by Bondi and Hoyle. It should be remarked that the term "coalesce" is not intended to have any special physical connotations. It is convenient merely as a general description of the state of affairs treated by the mathematics.

Bondi and Hoyle show in particular that there is a value $x=ax_0$ such that all the cloud-material reaching the axis in $0\leqslant x<ax_0$ proceeds to move towards O, so that it becomes "accreted" by the star, while all the material reaching the axis along $x>ax_0$ proceeds to stream away from the star. They point out that the parameter a cannot in this case be evaluated by steady-state considerations alone. But they give reasons for inferring that the value of a must be between 1 and 2.

The authors proceed to evaluate the force upon the star exerted by the material reaching the axis between ax_0 and ξx_0 when $\xi\gg a$ and obtain, in our notation,

$$X=2\pi\rho_0(\mu^2/U^2)\ln\xi. \tag{3.22}$$

This is the correct asymptotic form resulting from their equations, though their method actually yields $\ln\xi+A$ in place of $\ln\xi$, as a closer approximation, where A is a constant which the method does not serve to determine.

Bondi and Hoyle give reasons for using a "cut-off value" of ξ in applications of (3.22). Here it need only be recalled that the existence of such a value depends upon the presence of other stars in the vicinity. The same cut-off effect must be considered to operate in all the cases we have considered.

4. *Discussion.*—For present purposes we shall call the force denoted by **X** the *resistance* and that denoted by **P** the *deflecting force.*

The resistance (3.22) as calculated by Bondi and Hoyle appears to depend upon the existence of their outward-flowing stream along the accretion axis. This depends in the first place upon the density of the cloud ahead of the star being sufficiently uniform. For, if the density varies appreciably in a direction transverse to the motion of the star, i.e. if the coefficient b is appreciable, the stream will not form. In this case, even if collisions between cloud-particles along the axis have their maximum possible effectiveness, equation (3.16) shows explicitly that the material will drift to one side of the axis instead of accumulating along the axis.

In the second place, even when the density is uniform, the existence of the stream depends upon the attainment of a steady state. This in turn depends upon the particle-orbits passing through the accretion axis. But perturbations by other stars, though insufficient to change the general character of the orbits below the cut-off value of ξ, may nevertheless cause them to miss the axis by a small amount and so prevent the formation of the stream. Such effects will apply more to particles associated with the larger values of s concerned (which are those contributing the main part of the force) than to particles associated with the smaller values of s. Thus the latter particles may still produce an inward-flowing stream on the axis near the star in the manner of the Bondi–Hoyle–Lyttleton theory, even where the outward-moving stream is not established, or only partially established.

The main object of the present paper is to point out that *the value of the resistance does not depend upon the realization of the special conditions required to produce streaming along the accretion axis.* This statement applies only to the dominant term in the force **X**. Since, however, the problem is in any event somewhat idealized, only this term need be considered. The conclusion then rests upon the agreement between (3.10) and (3.22) in respect of this term.

The conclusion is what would probably be expected on general physical grounds. But in view of the complicated motion of the material on the axis in the case of Bondi and Hoyle, we would not feel justified in presenting a physical argument without the backing of the mathematical calculations.

The chief point to notice is that the resistance is, to the first order, the same whether or not collisions between the cloud-particles occur along the accretion axis. For in this regard the respective derivations of (3.10) and (3.22) may be considered to deal with the extreme cases. This being so, any intermediate case is expected to lead also to the same value. Indeed, (3.21) may be regarded as dealing with one such intermediate case.

Fundamentally the conclusion is that the force is the same whether the particles act cooperatively over part of their motion, in the special manner considered by Bondi and Hoyle, or independently as in the derivation of (3.10). This is important because the derivation of (3.10) does not depend physically upon the assumption of a steady state. The result will continue to hold for a non-steady state if ρ_0 is taken to be a suitable mean value of the density ahead of the star. It will also continue to hold if the path of the star is not rectilinear, owing to the deflecting force either of the cloud or of another star.

Turning now to the deflecting force, (3.12) may be interpreted as meaning that this may be significant for the motion of the star if the density of the cloud varies appreciably over distances comparable with interstellar distances. For the cut-off value of ξ is such as to make $x_0\xi$ in (3.12) a distance of this order.

The conditions which would make **P** significant are ones that would preclude the formation of an axial stream. Here the extreme conditions are those leading to (3.11), (3.21), respectively, and these results agree in their dominant terms as already noted.

The deflecting force may, in general, not be important itself. It is, however, not clear how large the transverse density-gradient must be in order to upset the mechanism of accretion considered by Bondi and Hoyle. This must remain a subject for future study, but it may be that the effect of a transverse gradient on the mechanism of accretion is important even when it is too small to make the transverse force important.

5. *Accretion.*—From the non-convergence of the expressions for the forces X, Y it follows that these forces are contributed principally by those cloud-particles which are most remote from the star concerned but whose orbits are yet determined primarily by the gravitational field of that star and not by the field of neighbouring stars. Accretion, on the other hand, if it does occur, is contributed by cloud-particles whose orbits lie much closer to the star. It follows that various perturbation effects may modify the motion of the particles mainly responsible for the forces, while the mechanism of accretion still operates in the manner envisaged by Bondi and Hoyle. That is why it was important to see that the value of the forces does not in fact depend upon the Bondi–Hoyle–Lyttleton mechanism.

There is, however, some interest in seeing how a variation in cloud-density may tend to affect the accretion process. Some consideration of the problem has recently been given also by Gething.*

In the first place we have to recall that when an accretion column has been established in accordance with the Bondi–Hoyle–Lyttleton theory, the incoming cloud-particles collide with material already in the column and not directly with each other. Now the consequence of a transverse density-gradient in the cloud is to give the incoming material a resultant transverse momentum. In that case there cannot therefore be an accretion column lying symmetrically along the accretion axis. If the resultant transverse momentum is sufficiently large, there can in fact be no accumulation of material along the axis for the incoming particles to collide with; the only collisions to be considered would be collisions along the axis between the incoming particles themselves. If also the cloud-density were sufficiently small, such collisions would be rare and there would be no accretion.

However, for any given cloud-density ρ_0, there must be a range of values of the density-gradient as measured by b which leads to a situation intermediate between that of the Bondi–Hoyle–Lyttleton theory ($b=0$) and the extreme case of no accretion. Such an intermediate case must have the general character of that treated in (3.13)–(3.19).

In this case all the material arriving at the axis OX in $0 \leqslant x < ax_0$, where a is given by (3.19), is captured by the star. Also, since we are now dealing with the case where b is small, this equation gives $a \doteqdot 2$. Thus the amount of material "captured" is approximately the same as that "accreted" in the Bondi–Hoyle–Lyttleton theory. In the present case, however, the captured material may not all fall on to the star but some may go to form a distribution revolving in the vicinity of the star. The latter possibility can be shown, however, to require a somewhat large value of b.

We notice that, whereas the parameter a is indeterminate on steady-state considerations in the case $b=0$, it becomes determinate in the case of $b \neq 0$ here considered.

It is important to appreciate how this case differs from that considered by Bondi and Hoyle. In the present case the incoming particles are assumed to "coalesce" on the accretion axis, in the sense considered in Section 3. This means merely that, owing to collisions in the vicinity of the axis, the particles arriving there at any instant acquire a common velocity. Owing to the assumption that b is not zero (though it may be very small) this velocity at any point of the axis has a non-zero component perpendicular to the axis. It is part of the assumption that on account of this lateral drift the material concerned is not involved in further collisions with subsequently arriving incoming particles. In the case considered by Bondi and Hoyle, on the other hand, the material proceeds to move along the axis where it does encounter further incoming particles. Thus, although the present case is intermediate between that of Bondi and Hoyle and that of no collisions, it does not yield either of these cases as limits. In particular, it is not possible to infer that a must be determinate in Bondi and Hoyle's case by attempting to treat this as the limit of our case. We do not question that in Bondi and Hoyle's case a is not determined by the steady-state conditions but depends upon the way in which the state is established.

* P. J. D. Gething, *M.N.*, **111**, 468, 1951.

In fact one of us (K. N. D.) hopes shortly to publish some new calculations of this effect.

The more interesting point is that the *angular momentum* about O per unit mass of the captured material is, from (3.14), (3.16),

$$\frac{1}{ax_0}\int_0^{ax_0}\frac{b\mu}{U}\,x\,dx = b\,\frac{\mu^2}{U^3}, \tag{5.1}$$

taking $a=2$ as before. If we take μ to correspond to the mass of the Sun and take $U=5$ km/sec as a typical value (being that also used by Bondi and Hoyle), this gives about $1{\cdot}4\times10^{35}\,b\,\mathrm{cm^2\,sec^{-1}}$.

We may compare this with the angular momentum per unit mass of the Sun itself. According to values given by Chapman*, this is about $5\times10^{14}\,\mathrm{cm^2\,sec^{-1}}$. Thus the value given by (5.1) is greater than or equal to this if b^{-1} is less than about 100 parsecs. Now b^{-1} is the distance over which the cloud-density changes by 100 per cent according to (3.5), and 100 parsecs would be a large value for the radius of a cloud.†

It is then tempting to conclude that any significant accretion of mass is likely to be accompanied by a significant change in the star's angular momentum. Nevertheless it has to be noted that, although the density-gradient required to produce this result is so small, its component transverse to the star's path would have to be in the same direction over a great length of this path. Without much further investigation it is therefore impossible to say whether the effect has any general significance in regard to the phenomenon of stellar rotation. It may serve merely to endow separate portions of accreted material with varying amounts of angular momentum about the star in the manner suggested by Gething in relation to Lyttleton's theory of comets.

Royal Holloway College:
1951 *October* 22.

* S. Chapman, *M.N.*, **108**, 236, 1948. (See p. 251.)
† W. H. McCrea, *The Observatory*, **70**, 100, 1950.

THE ALIGNMENT OF GALACTIC DUST

T. Gold

(Received 1951 December 5)

Summary

It is shown that the dynamical interaction between galactic gas and those dust particles which are elongated will, in certain circumstances, lead to a partial alignment of those particles. The direction which is preferred by the long dimension of the particles is that of the relative velocity between gas and dust.

The possible relation between this effect and the observed polarization of starlight is discussed.

---

1. *Statement of the problem.*—We aim to find the probability distribution of the orientation of elongated solid particles which results from their collisional interaction with a tenuous gas. The conditions we shall assume are those which are presumed to exist within the Galaxy. The essential simplifications are then as follows.

(*a*) Impacts between the solid particles and the gas molecules are discrete events; the problem is one of dynamics of collisions rather than fluid dynamics.

(*b*) Impacts of the solid particles with each other are too rare to be taken into consideration.

(*c*) Photon interactions result only in a negligible transfer of angular momentum to the particles compared with that resulting from molecular collisions. (This may be untrue in the close vicinity of bright stars.)

(*d*) Both gas and dust are sufficiently tenuous for interpenetration to occur. (For a dust particle as small as 5×10^{-5} cm and density 3, the distance travelled in gas of density 10^{-24} until the relative velocity is halved, is of the order of 10^{20} cm.)

(*e*) Thermal velocities of the gas molecules are small compared with the relative velocity of the bulk motions.

Owing to the different penetrating power of gas and dust, we expect the two media to pursue substantially different courses within the Galaxy; processes of collision and interpenetration of dust clouds with gas clouds must then be common. We shall consider the effect of such interpenetration on the orientation of elongated particles.

In the following discussion we are unable to use precise data for the shapes of dust particles; it is also uncertain how small the thermal velocities are compared with the bulk velocities. We shall therefore discuss at each stage the ideal condition, in which we consider needle-shaped particles of negligible thickness and ignore thermal agitation, and we shall then mention the effects of departures from these ideal conditions.

For the description of the orientation of a particle we shall use spherical polar coordinates (θ, ϕ), the direction $\theta = 0$ being that of the relative bulk velocity between gas and dust.

2. *Dynamics of an elongated dust particle.* (*a*) *The direction of the angular momentum vector.*—Collisions between dust and gas are assumed to be inelastic.* The angular momentum given to the dust particle at such a collision is then $\boldsymbol{P}' = \boldsymbol{r} \times m\boldsymbol{v}$, where $\boldsymbol{r}$ is the position vector from the centre of mass of the particle to the point of impact, m the mass of the molecule, and $\boldsymbol{v}$ the relative velocity. (If $\boldsymbol{\omega}$ is the angular velocity of the particle, we ignore $\boldsymbol{\omega} \times \boldsymbol{r}$ in comparison with $\boldsymbol{v}$.)

In the idealized case $\boldsymbol{v}$ is entirely in the direction $\theta = 0$; all contributions like $\boldsymbol{P}'$ are thus confined to the plane $\theta = \pi/2$, and thus the total angular momentum $\boldsymbol{P}$ remains always in that plane.

In the actual case the total angular momentum after n collisions is

$$\boldsymbol{P} = \boldsymbol{P}_0 + \sum_n \boldsymbol{P}_k' \quad \text{or} \quad \boldsymbol{P}_0 + \sum_n \boldsymbol{r}_k \times m_k \boldsymbol{v}_k,$$

where $\boldsymbol{P}_0$ is the initial angular momentum. The departure of $\boldsymbol{P}$ from the plane $\theta = \pi/2$ now arises from $\boldsymbol{P}_0$, which we take to be of thermal origin, and from the thermal variability of the direction of the $\boldsymbol{v}_k$. In the case when the original temperature of the dust equals that of the gas, the variability of the $\boldsymbol{v}_k$ does not add to the spread of direction of $\boldsymbol{P}$, which is already fully accounted for by the term $\boldsymbol{P}_0$. $\boldsymbol{P}$ is thus brought close to the plane $\theta = \pi/2$ when $\sum_n \boldsymbol{r}_k \times m_k \boldsymbol{v}$ is large compared with a term like $\boldsymbol{P}_0$, which may be taken to represent the initial thermal angular momentum of the particle, or that appropriate to the temperature of the gas, whichever is the greater. This condition can be satisfied only if the velocity of interpenetration is supersonic.

(*b*) *The relation between the angular momentum vector and the orientation of the particle.*—We denote the principal moments of inertia of the particles by I_x, I_y, I_z, the x direction being taken to coincide with the long dimension. In the idealized case the vector $\boldsymbol{r}$ must lie entirely in the x direction, since the particle is assumed to have negligible y and z dimensions. All contributions to the angular momentum $\boldsymbol{P}_k'$ are in the y–z plane; and in the simple case when $\boldsymbol{P}$ is confined to the plane $\theta = \pi/2$, the x direction of a particle remains in a plane of constant ϕ; each particle has, therefore, to move through the polar direction $\theta = 0$, whilst there is no such preferred direction in the equatorial plane.

In a real case where the particle has certain dimensions in the y and z directions, two new considerations arise. Firstly $\boldsymbol{r}$ is not entirely confined to the x direction, and the angular momentum imparted at an impact is thus not entirely confined to the y–z plane. Secondly I_x is different from zero, and as the particle performs free nutations between collisions, its x-axis is then not completely constrained to move in a plane. We now aim to show that these two effects do not completely destroy the previous argument, but that a restriction on the y and z dimensions of the particle in comparison with the x dimension will imply a restriction of the angle by which the motion may carry the x direction out of a plane of constant ϕ.

* This will in fact be a close approximation for the conditions which are envisaged. The temperature T of the dust particle is low, being of the order of the radiation temperature of the space. Gas molecules with kinetic energies much in excess of $\frac{1}{2}kT$ will lose most of their energy to crystal lattice vibrations, and at higher energies also to lattice displacements and ionizations. This energy is subsequently lost by the dust particle through radiation, with a negligible momentum transfer. The gas molecule may then be embedded or stick, or move off with a small velocity; the momentum transferred to the dust is very nearly that of the incoming molecule. The value of the minimum velocity for collisions to be inelastic depends on the substance of the dust, but is unlikely to be more than one kilometre per second.

Most position vectors $\boldsymbol{r}_k$ (and all the large ones) will be still dominantly in the x direction, and most contributions $\boldsymbol{P}_k'$ (which are all in the fixed plane $\theta=\pi/2$) will therefore be close to the y–z plane of the particle; they will thus be associated with the two major axes of inertia I_y and I_z rather than with I_x.

To consider the free motion of a particle it is convenient to use Poinsot's theorem. The condition that the angular momenta $\boldsymbol{P}_k'$ are principally in the y–z plane then implies that the "ellipsoid of inertia" is rolling with its centre close to the "invariable plane". As the distance of the centre from the invariable plane cannot change for a free motion, the long axis of the ellipsoid (if it is much longer than the other two, i.e. if I_x is much smaller than I_y and I_z) cannot depart far from parallelism to the invariable plane. If, as before, the invariable plane is constrained to be a plane of constant ϕ, the x (long) axis of the ellipsoid, and hence of the particle, is constrained to remain nearly parallel to it.

3. *Probability distribution of orientation.*—We define an "alignment factor" for an assembly of particles by projecting each particle into one particular plane of constant ϕ (say $\phi=0$); in that plane we then sum all components in the direction $\theta=0$ and in the direction $\theta=\pi/2$, and we then take the ratio of the two sums. (This definition may be of value in considering the optical polarization effect on light travelling in or near the $\theta=\pi/2$ plane.)

In the idealized case all planes of constant ϕ are equally populated by spinning particles, and within each such plane all angles of θ are equally probable. The alignment factor is then simply given (for arbitrarily large numbers of particles) by

$$\int_0^{\pi/2} d\phi \int_0^{\pi/2} \cos\theta \, d\theta \Big/ \int_0^{\pi/2} d\phi \int_0^{\pi/2} \sin\theta \cos\phi \, d\theta = \pi/2.$$

We have not calculated the alignment factor for any other case; but we estimate, for example, that it will differ from $\pi/2$ by only a few per cent if the particles are more than ten times as long as they are thick.

4. *The polarization of starlight.*—It now seems probable that the polarization of starlight has to be explained by selective absorption in interstellar space. Hence, one enquires into agencies which will result in alignment of elongated dust particles, as no other suitable absorbing medium is known.

Previous explanations (**1, 2**) have used the hypothesis that sufficiently strong interstellar magnetic fields exist, and that a sufficient fraction of elongated particles have the required ferromagnetic or hysteresis properties. There has been no independent evidence for such strong magnetic fields, and certain theoretical considerations show the required strength to be improbable; and there has been no evidence for the otherwise implausible hypothesis that a major fraction of the dust possesses those particular physical properties.

The present effect must be expected to operate on all those particles which are elongated enough to have the desired optical property. The aligning process of double streaming is itself a necessary consequence of conditions which are generally believed to exist in the Galaxy.

Although there will be a diminution of the relative velocity in the course of an encounter between a gas and a dust cloud, such relative velocities cannot generally die out so long as there are encounters between clouds at all. For if we consider an encounter between two mixed clouds in which the dust possesses the same bulk motion as the surrounding gas, a separation would again occur, the motion of the gases being much more severely modified by the encounter

than that of the dust. A similar conclusion is reached if one considers any kind of turbulent motion of a mixture of gas and dust.

The finite thickness of the Galaxy implies that all the material above and below the central plane must at some stage penetrate through it; on dynamical grounds we must expect the maximum interpenetration of material to occur in the central plane, with the relative velocity directed normal to it. Double streaming within the central plane in other directions may also exist, but will be subject to much more rapid damping.

The observed polarization of starlight shows in most cases that the electric vector normal to the galactic plane is attenuated more than the vector in the plane (3). This sense of the effect, and its coherence over wide regions of the Galaxy, agree with the effect which must be expected from the process of double streaming. The maximum magnitude of the observed effect amounts to a variation of only 5 per cent in the extinction coefficient of the dust, depending on the orientation of the electric vector (2).

Trinity College,
Cambridge:
1951 *December* 3.

References

(1) L. Spitzer and J. W. Tukey, *Ap. J.*, **114**, 187, 1951.
(2) L. Davis and J. L. Greenstein, *Ap. J.*, **114**, 206, 1951.
(3) W. A. Hiltner, *Ap. J.*, **114**, 241, 1951.

RADIO ECHO OBSERVATIONS OF THE MAJOR NIGHT-TIME METEOR STREAMS

G. S. Hawkins and Mary Almond

(Communicated by Professor A. C. B. Lovell)

(Received 1952 February 15)*

Summary

This paper describes radio echo observations of the major night-time streams for the period 1946–1951. Radiant positions and velocities have been measured for the Perseids, Geminids and Quadrantids, and orbits have been computed for each stream. The characteristics of these streams are discussed, and evidence is presented for the existence of a core of larger meteors in the region of maximum density in the streams. A progressive movement of the radiant point has been detected for the Perseid and Geminid showers, which is in agreement with previous observations. The velocity distributions indicate that there may be a spread in heliocentric velocity within the streams of the order of 1–2 km/s. Radiant positions and hourly rates are also given for the Orionids, δ Aquarids, Lyrids and the night-time Taurids and Arietids.

1. *Introduction*

In the Northern Hemisphere the richest night-time meteor displays recurring annually are the Perseids, Geminids and Quadrantids, which, together with less active displays such as the Orionids and Lyrids, are classed as the major night-time meteor streams. Quetelet (**1**) first discovered the recurrent nature of the Perseid shower in 1836, and the regular displays of the Geminids (**6**) and Quadrantids were commented on by Herrick in 1838–39. These streams have since been exhaustively studied by visual methods (**1–13**) as far as moonlight, clouds and other adverse factors will allow. Early research was impeded by the inaccurate determinations of meteor velocities, but after Elkin (**14**) had initiated the technique of interrupted photography reliable results became possible, and Whipple and others have recently determined exact orbits for several bright Geminid (**15**) and Perseid (**16**) meteors. The development of radio echo methods has enabled measurements of velocity and radiant position of the fainter and more numerous meteors of a stream to be made independently of visual observing conditions. Studies by these radio techniques of the Geminid, Perseid, Quadrantid and other less active streams are described in this paper.

2. *Methods of observation*

(i) *Radiant co-ordinates.*—The apparatus used for radiant determination has been fully described elsewhere (**17**). By recording the range and time of appearance of radio echoes from meteor trails in two azimuthal directions it is

* Received in original form 1951 November 3.

possible to measure the radiant co-ordinates of a meteor stream with an accuracy of about $\pm 1°$. This accuracy represents the ideal limit obtained with a favourably placed point radiant supplying about 50 echoes an hour. For radiants of weaker activity the errors are greater, but seldom exceed 5°. It is also possible to detect a spread of meteor directions about the mean from the scatter of points on the range–time plots. This scatter of points gives a measure of the mean diameter of a radiant, although the precise shape of a radiating area cannot be found. In cases where a finite radiant diameter exists, the accuracy of position determination is again reduced and it is difficult to deduce the exact centre of maximum activity within the radiating area.

(ii) *Meteor velocities.*—Two equipments operating on wave-lengths of 4 m and 8 m were used for measuring velocities, as in previous experiments (**18, 19**), and it has been shown that these equipments are capable of an experimental accuracy of ± 5 per cent. The use of a narrow beam aerial reduces the number of sporadic meteors included in the records.

(iii) *Hourly rate of echoes.*—The most reliable measure of the activity of a stream was given by the radiant survey apparatus (**17**), where the transmitted power, receiver gain and other parameters were checked regularly in an attempt to obtain constant operating conditions. A further check on the stability of the operating conditions was provided by the observations of the rate of sporadic meteors. On the assumption that the mean rate of sporadic meteors remains constant at any particular position in the Earth's orbit, any variations in the observed radio echo rate can be used to calibrate the equipment from year to year. The sensitivity of the apparatus was set at a value which gave an hourly rate of echoes comparable to that obtained by a single observer under good visual conditions.

Additional hourly rate measurements have been obtained from the velocity equipments, and also from the records made with the apparatus used in the early experiments (**20, 21**).

(iv) *Long-duration echoes.*—In early experiments, durations were estimated by visual observation of a range–amplitude cathode ray tube display. In the more recent work, durations have been recorded by the continuously moving film of the radiant survey apparatus. As an example of the method, Fig. 1 (Plate 3) shows a record of echoes displayed on a range–intensity cathode ray tube, photographed on a film moving at 72 cm/h across the range axis. A short-duration echo appears as a bright dot*, whereas a long-duration echo is extended along the time axis so that its duration can be measured to within $\pm 1^s$. Additional information on long-duration echoes has been obtained from the photographic recorders (**18**) used in conjunction with other equipments. These recorders were triggered by a radio echo and photographed the variations in echo amplitude for a period of $0^s{\cdot}1$ at intervals of 1^s. By this means the lifetime of long-duration echoes may be measured to the nearest second.

3. *Observational data*

(i) *Radiant positions.*—Observations have been made of the radiant co-ordinates of the night-time streams over the period 1949 September to 1951 August, and the results for the Perseids, Geminids and Quadrantids are given in Table I.

* A single echo appears double on the display because twin transmitter pulses were used, separated by 50 km in range. This transmitter code facilitated the identification of echoes.

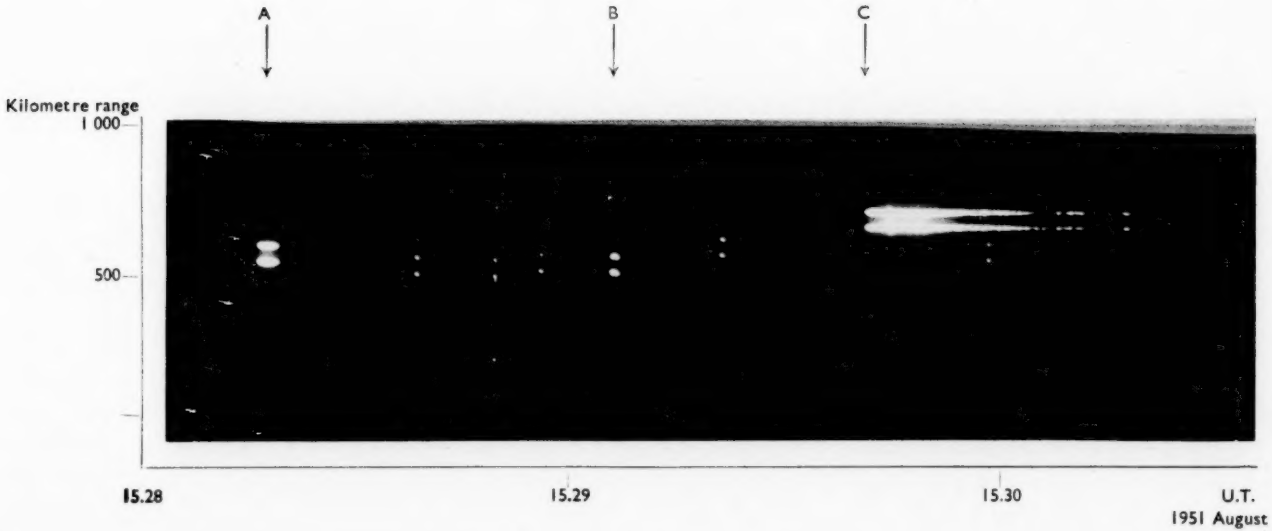

FIG. 1.—*Photographic record showing echoes at A, B and C.*

These measurements were made at the time of transit of the radiant and the change of date was made at 0^h U.T. From the characteristics of the range–time plots (**17**) the radiants have been divided into three classes, A, B and C, weighted in order of importance as 2:1:0. A weighted mean radiant position may then be deduced as in Table II. For the less active streams the observational errors are somewhat increased, so that day-to-day positions have not been given. In these cases the weighted mean position (W) has been given in Table I and the error in this value is about $\pm 3°$.

(ii) *Meteor velocities.*—Velocity observations have been made on the night-time streams during the period 1947 December to 1951 August. No significant variations were found in the velocities of each stream from day to day and the mean velocity for each year is given in Table I. Similarly the distributions of velocities obtained in each year did not justify separate treatment, and all velocities obtained for the Perseids, Geminids and Quadrantids have been combined into the histograms of Fig. 2. In the case of the Orionids, Leonids and other less active streams it was not possible to obtain enough velocity measurements to form a reliable distribution.

TABLE I

Date	Radiant R.A.	Radiant Dec.	Radiant Class	Radiant Diam.	Radiant No. of echoes used	☉	Echo H.R. Obs. at transit	Echo H.R. Red. to 1950	Mean vel. in atmos. km/s	No. of vels. measd.
	°	°		°		°				
Quadrantids										
1947 Jan. 3	...	...	...	...	...	282·6	34	...	...	...
1948 Jan. 4	...	...	...	...	...	283·0	76	...	37·1 ± 3·5	25
1949 Jan. 3	...	...	...	...	...	282·5	41	...	...	...
1950 Jan. 1	233	+52	A	10	33	280·6	14	21	...	...
Jan. 3	231	+47	A	12	140*	282·6	70*	103	...	...
Dec. 28	224	+52	B	5	23	275·9	10	10		
Dec. 30	228	+46	B	5	30	278·0	13	13		
1951 Jan. 1	231	+46	B	5	31	280·0	12	12		
Jan. 2	228	+51	B	8	47	281·0	19	19		
Jan. 3	233	+52	A	5	216	282·1	90	90	39·3 ± 3·4	37
Jan. 5	236	+51	B	4	28	284·1	28	28		
Jan. 6	236	+50	B	10	51	285·1	22	22		
Jan. 7	227	+49	B	6	34	286·2	15	15		
† Jan. 16	226	+61	A	11	74	295·3	26	26		
Lyrids										
1947 Apr. 22	...	...	...	...	...	31·3	7	...	...	...
1948 Apr. 22	...	...	...	...	...	32·0	20	...	...	...
1949 Apr. 22	...	...	...	...	...	31·7	10	...	...	...
1950 Apr. 21	...	...	...	...	...	31·4	6	...	...	...
1951 Apr. 22	273	+30	A	8	26	31·2	11	...	...	...

* Apparatus unstable and figures less reliable, so that the period 1950 December 28 to 1951 January 7 was taken as the reference epoch for sensitivity corrections.

† In 1951 a subsidiary burst of meteor activity was noticed near the Quadrantid radiant and has been included in the Quadrantid sequence. However, no velocity measurements were made, so that it is impossible to ascertain the exact relationship of this later radiant with the main Quadrantid stream.

TABLE I (*contd.*)

Date	Radiant R.A.	Radiant Dec.	Class	Diam.	No. of echoes used	⊙	Echo H.R. Obs. at transit	Echo H.R. Red. to 1950	Mean vel. in atmos. km/s	No. of vels. measd.
	°	°		°		°				
δ Aquarids										
1949 July 29	...	...	...	...	...	125·8	24	...	...	...
1950 July 28	339	−14	W	3	115	124·5	38	...	...	...
1951 July 27	336	+ 0	B	6	87	123·4	41	...	...	...
Perseids										
1946 Aug. 12	...	...	...	...	...	139·2	23	...	...	...
1947 Aug. 12	...	...	...	...	...	138·8	26	...	...	...
1948 Aug. 12	...	...	...	...	...	139·4	57	...	60·7 ± 4·7	27
1949 Aug. 12	...	...	...	...	...	139·2	57	...	60·3 ± 2·9	14
1950 July 29	28	+52	B	7	32	125·5	13	13		
July 30	31	+56	C	7	56	126·5	20	20		
July 31	40	+58	A	9	82	127·5	30	30		
Aug. 2	38	+56	B	8	56	129·4	20	20		
Aug. 3	42	+55	C	...	27	130·4	10	10		
Aug. 5	...	...	C	5	30	132·2	11	11		
Aug. 6	33	+52	A	4	47	133·2	20	20		
Aug. 7	39	+59	B	9	53	134·1	19	19		
Aug. 8	42	+57	A	10	57	135·1	20	20		
Aug. 9	43	+56	A	8	89	136·1	32	32	61·0 ± 5·0	41
Aug. 10	44	+57	A	9	66	137·0	24	24		
Aug. 11	45	+61	A	4	51	138·0	21	21		
Aug. 12	46	+57	A	3*	179	138·9	64	64		
Aug. 13	51	+59	A	<3*	165	139·9	59	59		
Aug. 14	52	+61	A	9	61	140·8	22	22		
Aug. 15	51	+62	A	10	57	141·8	20	20		
Aug. 16	49	+56	B	11	61	142·8	22	22		
Aug. 17	47	+52	B	9	49	143·8	21	21		
1951 Aug. 3	40	+60	C	5	22	130·1	16	13		
Aug. 4	42	+63	A	4	57	131·1	20	17		
Aug. 6	39	+50	A	9	88	133·0	37	30		
Aug. 7	45	+53	B	8	50	134·0	18	15		
Aug. 8	43	+57	A	10	75	135·0	27	22		
Aug. 9	43	+57	C	12	29	135·9	21	17		
Aug. 10	47	+59	C	12	38	136·8	38	31		
Aug. 11	49	+46	A	8	99	137·8	43	37	59·2 ± 5·3	83
Aug. 12	46	+57	A	8	108	138·8	39	32		
Aug. 13	44	+60	A	6	112	139·7	40	33		
Aug. 14	48	+58	A	10	101	140·7	36	30		
Aug. 15	37	+58	A	12	96	141·7	34	23		
Aug. 16	55	+59	A	7	51	142·7	18	15		
Aug. 17	43	+50	A	12	66	143·6	27	22		
Night-time Arietids										
1950 Oct. 14	37	+4	W	3	130	199·5	19	...	...	...

* On 1950 August 12 and August 13, 50 per cent of the echoes corresponded to a sharp sub-centre, the remainder were scattered in a circle of diameter 10°.

TABLE I (*contd.*)

Date	Radiant R.A.	Radiant Dec.	Class	Diam.	No. of echoes used	⊙	Echo H.R. Obs. at transit	Echo H.R. Red. to 1950	Mean vel. in atmos. km/s	No. of vels. measd.
	°	°		°		°				
Orionids										
1946 Oct. 18	...	...	...	...	...	204·3	18	...	...	...
1947 Oct. 20	...	...	...	...	...	206·0	14	...	...	...
1948 Oct. 22	...	...	...	...	...	208·8	20	...	...	...
1949 Oct. 23	95	+13	W	3	82	209·5	20	...	...	...
1950 Oct. 21	98	+ 9	W	3	70	207·2	17	...	...	...
Leonids										
1946 Nov. 17	...	...	...	...	...	234·3	24	...	...	...
1947 Nov. 16	...	...	...	...	...	233·0	3	...	...	...
1948 Nov. 14	...	...	...	...	...	231·8	11	...	...	...
1949 Nov. 16	...	...	...	...	...	233·5	7	...	...	...
1950 Nov. 16	...	...	...	...	...	233·1	11	...	...	...
Night-time Taurids										
1946 Nov. 9	...	...	...	...	...	226·0	18	...	...	...
1947 Nov. 6	...	...	...	...	...	222·7	9	...	...	...
1950 Nov. 9	55	+25	W	3	109	225·9	14	...	...	...
Geminids										
1946 Dec. 14	...	...	...	...	...	261·4	53	...	...	...
1947 Dec. 14	...	...	...	...	...	261·3	57	...	34·4 ± 1·2	10
1948 Dec. 13	...	...	...	...	...	261·1	56	...	...	...
1949 Dec. 8	108	+33	B	3	28	255·7	10	20		
Dec. 9	108	+36	B	3	36	256·7	14	29		
Dec. 10	110	+36	B	<3	39	257·7	15	30		
Dec. 11	110	+30	B	3	60	258·8	21	43		
Dec. 12	111	+32	B	<3	59	259·8	23	47	35·9 ± 4·6	122
Dec. 13	112	+30	A	3	113	260·8	40	81		
Dec. 14	115	+33	B	4	117	261·8	40	81		
Dec. 15	114	+34	B	7	32	262·8	10	20		
1950 Dec. 7	107	+37	B	3	52	254·4	19	19		
Dec. 8	101	+31	C	3	18	255·4	7	7		
Dec. 9	108	+30	B	<3	34	256·4	13	13		
Dec. 10	108	+32	A	4	88	257·4	27	27		
Dec. 11	111	+32	A	4	99	258·5	32	32	...	...
Dec. 12	112	+32	A	4	138	259·5	45	45		
Dec. 13	113	+30	A	3	217	260·5	79	79		
Dec. 14	115	+31	A	4	195	261·5	63	63		
Dec. 15	...	...	C	...	17	262·5	13	13		
Ursids										
1947 Dec. 22	195	+78	...	...	81	270·0	15	...	...	...
1948 Dec. 21	207	+82	...	...	...	269·4	15	...	...	...
1949 Dec. 22	207	+77	A	...	96	270·2	13	...	...	...
1950 Dec. 22	199	+77	A	...	105	269·8	20	...	...	...

(iii) *Hourly rate of echoes.*—The hourly rates of the various streams are given in Table I. For the three richest streams day-by-day rates are given as recorded by the radiant survey apparatus. This rate is a mean taken over the range–time envelopes of each aerial. The mean sporadic rates over the period of each shower were as follows:—

	Quadrantids	*Perseids*	*Geminids*
1949	...	...	2·8
1950	3·4	9·2	5·7
1951	5·0	11·1	5·5

Approximately 400 hours of observation have been used in evaluating each figure, and the statistical variation expected from purely random fluctuations is $\pm 0{\cdot}1$ meteors an hour. These figures have been assumed to give a measure of the relative sensitivity of the apparatus, and the observed hourly rates in each case have been reduced to the sensitivity of the corresponding period in 1950. Corrected rates for three streams are plotted against the Sun's longitude in Figs. 3(*a*), 4(*a*) and 5(*a*). The shape of these curves is confirmed by the mean hourly rates (Figs. 3(*b*), 4(*b*), 5(*b*)) deduced from the equipments referred to in Section 2(iii), between 1946–1951, but the standard deviation introduced by these inhomogeneous data is necessarily large.

The remaining streams, the Lyrids, δ Aquarids, night-time Arietids, Orionids and night-time Taurids are on the limits of observation by present radio echo techniques. However, the measured radiant positions, maximum hourly rate and date of maximum activity are given in Table I. The figures of maximum rate necessarily include a number of sporadic meteors and hence these figures must be taken as an upper limit to the activity of these streams.

4. *Determination of orbital elements*

The orbital elements given in Table II have been computed from the radio observations of the Perseids, Geminids and Quadrantids. The limits of error in the orbital elements have been derived from the estimated error of radiant determination, and the probable error of the velocity distributions.

Corrections for zenithal attraction and diurnal aberration have been applied to the mean radiant positions, and the mean velocities have been corrected for the attraction of the Earth and for atmospheric deceleration. An approximate value for the deceleration has been obtained from the equations proposed by Whipple and Öpik (**22**), which govern the dissolution of rapidly moving bodies in the upper atmosphere. For a meteor of mass m, moving with a velocity v, at a height h and incident at a zenith angle χ, the laws of conservation of momentum and energy give

$$m^{1/3}\,dv = \gamma A \rho_0 v e^{-h/H} \sec\chi\, dh, \tag{1}$$

$$l\,dm = \tfrac{1}{2}\lambda\gamma A m^{2/3}\rho_0 v^2 e^{-h/H} \sec\chi\, dh, \tag{2}$$

where H is the scale height and ρ_0 the air density at $h=0$. The constant A depends on the shape of the meteor particle, γ is the fraction of air molecules trapped in its surface, λ is the efficiency of the heating process and l is the energy required to evaporate unit mass of the particle.

Division and integration of these two equations gives

$$m = m_\infty \exp\left[\left(-\frac{\lambda}{4l}\right)(v_\infty^2 - v^2)\right], \tag{3}$$

TABLE II

Orbital Elements of the Perseids, Geminids and Quadrantids

	Ω	ω	i	e	q	a	Weighted Mean Radiant Position R.A. Dec.	Mean Velocity km/s
Perseids	139°.5±0°.5	153°±3°	114°±2°	0·91±0·04	0·96±0·15 A.U.	10·5±8 A.U.	45°.5+57°.0	60·5±4·6
Perseids corrected for deceleration	139·5±0·5	153	114	0·93	0·97	14·4		
Comet 1862 III	138·0	153	114	0·96	0·96	24·6		
Geminids	261·1±0·5	325±2	23±3	0·89±0·01	0·14±0·02	1·31±0·04	113·2+31·8	35·7±4·6
Geminids corrected for deceleration	261·1	325	23	0·89	0·14	1·4		
Quadrantids	282·5±0·5	166±3	67±2	0·44±0·03	0·97±0·04	1·7±0·1	231·2+49·0	38·5±3·4
Quadrantids corrected for deceleration	282·5	166	67	0·46	0·97	1·8		
Photographed Meteor (30)	282·1	168	74	0·72	0·93	3·4		

where m_∞ and v_∞ are the mass and velocity of the particle outside the Earth's atmosphere.

Substituting in (1) for m and integrating again yields

$$2\gamma AHm_\infty^{-1/3}\rho_a \sec\chi = e^{x_\infty}\int_x^{x_\infty} x^{-1}e^{-x}\,dx, \tag{4}$$

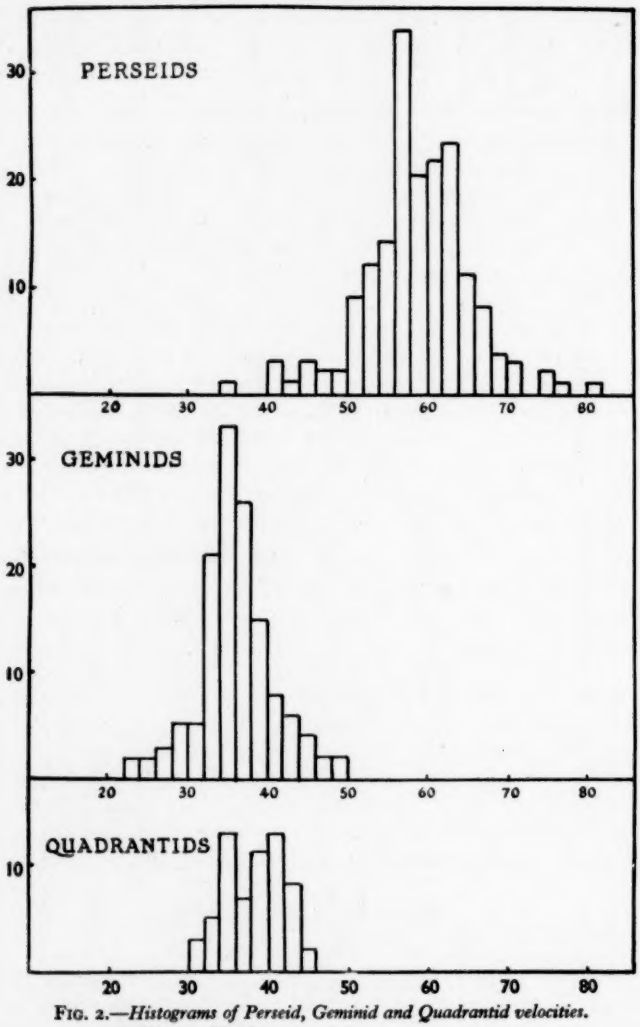

FIG. 2.—*Histograms of Perseid, Geminid and Quadrantid velocities.*
Ordinates: Number.
Abscissae: Observed velocity in atmosphere (km/s).

where $x = \lambda v^2/12l$ and ρ_a is the air density at the point where the deceleration is required.

Since the deceleration is small we may write

$$2\gamma AHm_\infty^{-1/3}\rho_a \sec\chi = \tfrac{1}{2}(x_\infty^{-1}e^{-x_\infty} + x^{-1}e^{-x})(x_\infty - x), \tag{5}$$

from which it is possible to deduce $(v_\infty - v)$, the change in velocity experienced by a meteor during its passage through the atmosphere.

The mass of the meteor outside the Earth's atmosphere, m_∞, has been derived from temperature measurements of the trails by assuming that the major part of the kinetic energy is converted into heat (**23**). For the meteors studied in

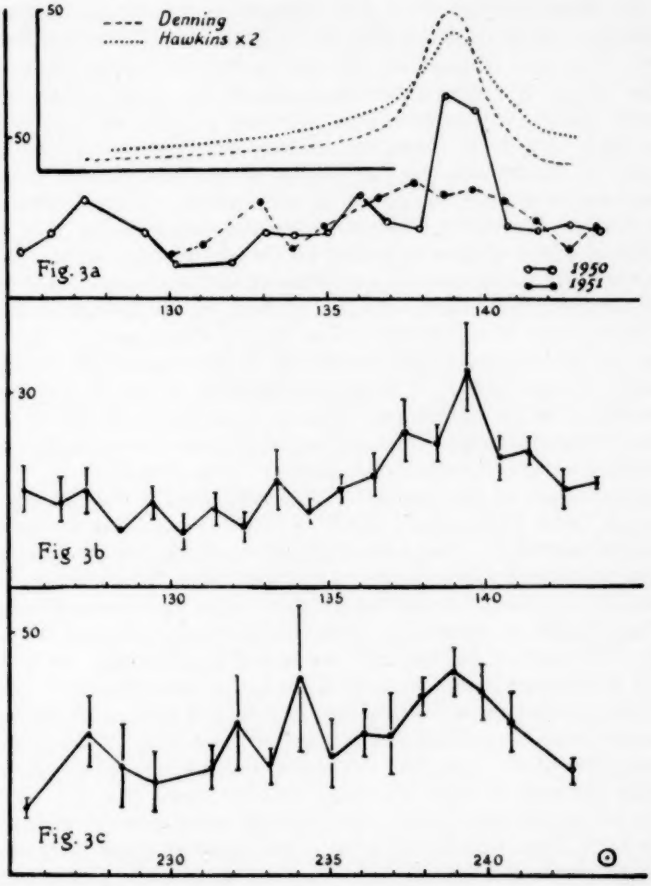

FIG. 3.—*(a) Hourly rate of Perseid stream, corrected for variations in sensitivity, plotted against Sun's longitude. (b) Mean hourly rate observed by all equipments plotted against Sun's longitude. The vertical lines indicate the probable error in the mean values. (c) Percentage of echoes with durations greater than one second plotted against the Sun's longitude. The vertical lines indicate the probable errors in the values.*

this work the masses were found to be of the order of 0·005 g. The constants $A(=0{\cdot}5)$, $l(=6\times10^{10}\,\text{erg/g})$ and $\lambda(=0{\cdot}5)$ have been adopted from the data of Whipple (**22**) and the upper-air data have been taken from Jacchia (**25**). The mean height, H, derived from radio echo data (**23, 24**) was taken as 95 km for Perseid meteors and 85 km for Geminid and Quadrantid meteors.

Substitution of these data in (5) gives the following corrections to be applied to the observed velocities:

Perseids 0·3 km/s, Geminids 0·4 km/s, Quadrantids 0·4 km/s.

The orbital elements corrected for this deceleration are given in Table II.

5. *Discussion*

(i) *The Perseid stream.*—The mean radiant position of this stream, and the large diameter of the radiating area, are in agreement with visual observations (**3, 4, 5**). The curve of corrected echo rate against Sun's longitude in Fig. 3(*a*) gives the density of matter across the stream in the cross-section traversed by the Earth. Early visual observations on stream density obtained by Denning (**9**), together with more recent observations, are plotted for comparison in Fig. 3(*a*). It can be seen that the position of maximum density of the stream has remained fixed over the period of observation. There is evidence of a change in mass distribution across the stream as shown in Fig. 3(*c*), where the percentage of echoes of duration greater than 1^s is plotted against Sun's longitude. Recent work (**26**) on the scattering of radio waves from meteor trails has shown that the duration of the radio echo is a measure of the ionization density and hence of the mass of the meteor. The results shown in Fig. 3(*c*) therefore indicate that the greatest proportion of large meteors is concentrated in regions of greatest stream density. A further characteristic of the core is disclosed by the contraction of the radiant area towards maximum, a feature of both radio and visual observations (**4**). This contraction indicates that meteors in the centre of the stream are less disturbed than meteors on the fringes.

The association of the Perseids with Comet 1862 III was demonstrated by Schiaparelli (**2**) in 1866. From Table II it can be seen that the radio results confirm this association. It has been suggested (**27, 28**) that the Perseid meteors could be produced by an ejection of material from the cometary nucleus at perihelion with subsequent secular perturbations by the planets, which, in time, would lead to a diffuse distribution of meteor orbits, with a spread in heliocentric velocity. The radiant area confirms the spread in orbits, and the evidence for a spread in heliocentric velocity is considered later (Section 5(v)).

(ii) *The Geminid stream.*—Radio echo, visual (**7, 8, 31**) and photographic (**15**) determinations of the radiant position and of the velocity of the stream are in agreement, but there is disagreement in the measurements of radiant diameter. The radio observations show that most meteors appear from a radiant area of diameter not greater than 4°, whereas the visual paths define a radiant diameter of about 12°. There is, however, a visual concentration conforming to the radio position, 50 per cent of the meteors delineating an area $4^\circ \times 3^\circ$ around the mean visual position (**29**). A comparison of the measurements of stream density is shown in Fig. 4(*a*) and it can be seen that both techniques show an asymmetrical distribution of material about the mean orbit, the Earth encountering less débris after maximum than before. The percentage of long-duration echoes shown in Fig. 4(*c*) also follows this asymmetry. Thus the Geminids possess a core of heavy meteors displaced to one side of the stream. In contrast to the Perseids, however, the radiant areas do not show any marked tendency for improved alignment of meteor paths as the core is traversed.

(iii) *The Quadrantid stream.*—Visual determinations (**4, 10–13**) of the radiant of the Quadrantids show a scatter of ±7° about a mean value of 232°, +52°.

The present radio determinations fall within these limits. The radiant area is found by both techniques to be large, and visually (**29**) there is evidence of perhaps three sub-centres of radiation. In 1951 the radio data suggested the possibility of two centres of equal intensity at 239°, +49° and 234°, +54°, but the radiants were on the limits of resolution and a mean position has been taken. The contraction of the radiant area at maximum is again pronounced, but the evidence for a core of large meteors is not conclusive. The similarity of the radio and visual data (**10**) regarding the duration of the stream is shown in Fig. 5 (*a*). Both results indicate that the stream is of short duration.

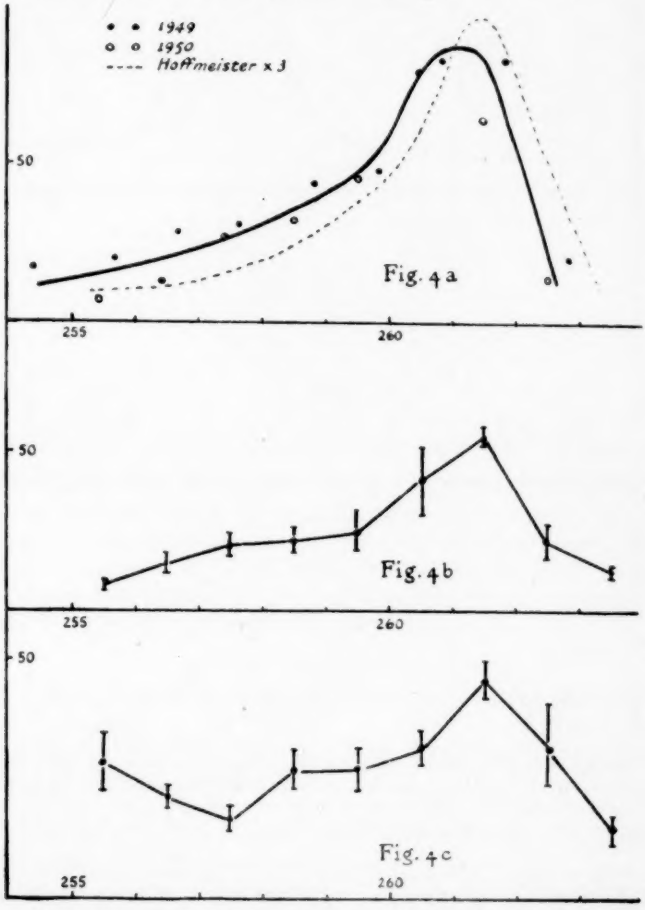

FIG. 4.—*(a) Hourly rate of Geminid stream, corrected for variations in sensitivity, plotted against Sun's longitude. (b) Mean hourly rate observed by all equipments plotted against Sun's longitude. (c) Percentage of echoes with duration greater than one second plotted against Sun's longitude.*

The orbit of this meteor stream is unique in that it exhibits both a short period and high inclination to the plane of the ecliptic, and is therefore markedly dissimilar from the orbit of any comet, minor planet or meteor stream at present

known. This exceptional orbit is confirmed by the radiant motion (**13**), and by photographic observations by Jacchia (**30**) of one Quadrantid meteor in 1951, the orbital elements of which are given in Table II. The mean radio echo orbit is drawn in Fig. 6.

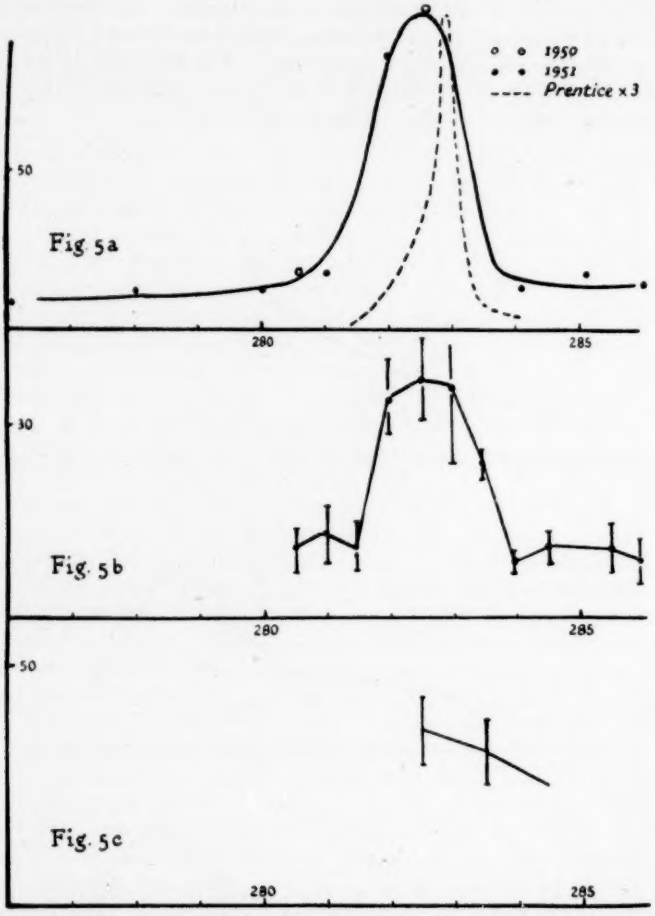

FIG. 5.—*(a) Hourly rate of Quadrantid stream, corrected for variations in sensitivity, plotted against Sun's longitude. (b) Mean hourly rate observed by all equipments plotted against Sun's longitude. (c) Percentage of echoes with duration greater than one second plotted against Sun's longitude.*

(iv) *Hourly rates.*—The hourly rates of the Geminid and Quadrantid streams when reduced to the sensitivity of 1950 are constant within the limits to be expected from statistical fluctuations. For these short-period streams this implies that the material is uniformly distributed around the length of the orbit. For the Perseids, the observations do not cover a long enough period for the presence or absence of a periodicity to be established. The absence of a marked peak in 1951 is conspicuous and outside the limits of statistical fluctuations. This may indicate local irregularities in the density of the Perseid stream.

Although the radio sensitivity was set to produce a rate comparable with the visual rate, there is some doubt as to whether the ratio of the rates remains constant throughout the various showers. So far it appears that the visual activity (**29**) of the Perseids, Geminids and Quadrantids are in the ratio 50:60:40, whereas the corresponding radio echo ratios are 60:80:90. Further observations are necessary to establish if any significance can be attached to these differences.

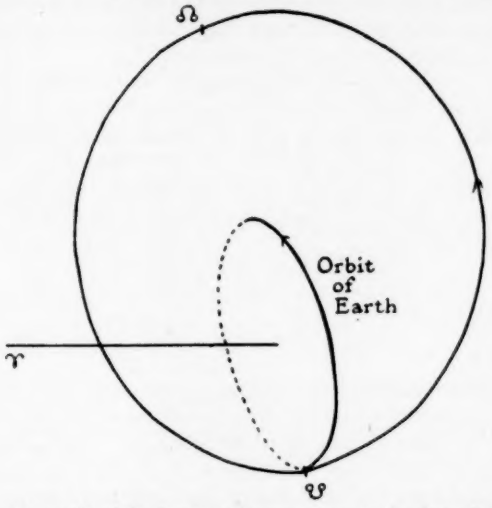

FIG. 6.—*Mean orbit of the Quadrantid stream drawn in the plane of the stream.*

(v) *Distribution of stream velocities.*—In dealing with the origin and subsequent perturbations of a stream, any spread in the heliocentric velocity of each stream is significant. The observed spread in geocentric velocity is caused in part by experimental errors in measurement, and in part by external factors, such as the inclusion of sporadic meteors in the sample. Thus the standard deviation σ_0 of the observed geocentric distribution is given by

$$\sigma_0^2 = \sigma_E^2 + \sigma_R^2 + \sigma_S^2 + \sigma_A^2 + \sigma_H^2,$$

where σ_E = standard deviation caused by random errors in the experimental technique,

σ_R = standard deviation which would result from the variation of apparent elongation of radiant points,

σ_S = standard deviation introduced by sporadic meteors,

σ_A = standard deviation caused by differential atmospheric deceleration, and

σ_H = standard deviation introduced by a real spread of heliocentric velocities in the stream.

Now σ_E may be found from the errors of individual velocities (**19**), σ_R from the observed radiant positions and diameters, σ_S from the measured background rate of sporadic meteors and σ_A may be estimated by using equation (5), assuming that two-thirds of the meteors observed were contained in a layer of the atmosphere of depth 15 km. It is therefore possible to estimate σ_H and hence the spread in

heliocentric velocity: this has been done in Table III. This indicates that there may be a velocity spread of 1 or 2 km/s in each stream, though the errors in σ_H are of the same order as σ_H and reduce the significance of the result. The spread in velocity found from the radio echo observations is considerably greater than the value found from photographic observations. In the case of the Geminids, Whipple (**15**) has published seven measurements of the velocity of individual meteors, and these velocities have a true spread of 0·23 km/s. This discrepancy may be due to the different range of mass groups observed with the two methods.

TABLE III

	Perseids	*Geminids*	*Quadrantids*
σ_E	1·7 km/s	1·2 km/s	1·0 km/s
σ_S	2·9	3·5	1·1
σ_R	2·1	1·5	1·7
σ_A	0·3	0·3	0·3
$\sqrt{\sigma_E^2+\sigma_S^2+\sigma_R^2+\sigma_A^2}$	4·0	4·0	2·3
σ_0	4·6	4·6	3·4
σ_H	2·3	2·3	2·5

(vi) *Motion of the radiant point.*—Applying the Gaussian method of weighted least squares it is possible to derive the mean daily motion of the radiant position, and this is given in Table IV for two of the radiants. The Geminid and Perseid radiants are found to have a diurnal change in R.A. of 1°·3 and 0°·6 respectively, which confirms the eastward drift found by visual and photographic methods (**3, 7, 8, 16**). No significant variations were found for the change in declination of these radiants.

TABLE IV

The Daily Motion of the Perseid and Geminid Radiants

	Perseids R.A.	Dec.		*Geminids* R.A.	Dec.
Jodrell Bank (Radio Echo)	$+0^\circ\cdot6\pm0^\circ\cdot1$	$+0^\circ\cdot1\pm0^\circ\cdot1$	Jodrell Bank (Radio Echo)	$+1^\circ\cdot3\pm0^\circ\cdot1$	$-0^\circ\cdot3\pm0^\circ\cdot1$
Whipple (**16**) (Photographic)	$+0^\circ\cdot7$	$+0^\circ\cdot1$	Whipple (**16**) (Photographic)	$+1^\circ\cdot1\pm0^\circ\cdot1$	$-0^\circ\cdot1\pm0^\circ\cdot1$
Denning (**3**) (Visual)	$+1^\circ\cdot3$	$+0^\circ\cdot3$	King (**8**) (Visual)	$+1^\circ\cdot2$	$-0^\circ\cdot1$
			Maltzev (**7**) (Visual)*	$+1^\circ\cdot0$	$+0^\circ\cdot1$

* The value given by Maltzev is based on a reinterpretation of King's original data.

A daily eastward motion of 1° parallel to the ecliptic maintains the radiant at a constant elongation from the apex of the Earth's way, and these results indicate that the meteors in the Perseid and Geminid stream move in orbits which show a progressive rotation in the line of apsides. In the case of the Quadrantids, more results are required before it will be possible to give a reliable value for the radiant motion.

6. *Acknowledgments*

This work was undertaken at the Jodrell Bank Experimental Station of the University of Manchester, to which the Department of Scientific and Industrial Research has contributed substantial financial assistance. The authors are also indebted individually to the Department for the award of maintenance grants. In a comprehensive survey of this nature all the available recording equipment has been used, and most of the personnel have participated in the work. In particular the authors are indebted to J. G. Davies, C. D. Ellyett and J. S. Greenhow for operating the equipment for measuring the meteor velocities, and to A. Aspinall for assisting in the operation of the radiant survey apparatus. Throughout the work Professor A. C. B. Lovell has been extremely helpful, both in participation in the observational programme and in giving guidance in writing the paper. Finally the authors wish to express their gratitude for advice given by Professor Z. Kopal and J. P. M. Prentice, for the cometary information supplied by Dr H. Wood and Dr J. G. Porter, and for helpful criticisms from Dr F. L. Whipple and Dr N. Herlofson.

University of Manchester,
Jodrell Bank Experimental Station,
Holmes Chapel, Cheshire:
1951 *November* 2.

References

(1) Quetelet, A., *Catalogue des Principales Apparitions d'Etoiles Filantes*, Brussels, 1839.
(2) Schiaparelli, G. V., *Note e Riflessioni intorno alla teoria astronomica delle stelle cadenti*, Firenze, 1867.
(3) Denning, W. F., *M.N.*, **62,** 161, 1902.
(4) Hoffmeister C., *Meteorströme*, Weimar, 1948.
(5) Olivier, C. P., *Meteors*, Baltimore, 1925.
(6) Herrick, E. C., *Silliman's J.*, Series I, **35,** 361, 1838.
(7) Maltzev, V. A., *Russ. Astr. J.*, **8,** 63, 1931.
(8) King, A., *M.N.*, **86,** 638, 1926.
(9) Denning, W. F., *Mem. R.A.S.*, **53,** 203, 1899.
(10) Prentice, J. P. M., *J.B.A.A.*, **51,** 19, 1941.
(11) Fisher, W. J., *H.C.*, **346,** 1930.
(12) Fisher, W. J., and Olmsted, Margaret, *H.C.*, **347,** 1930.
(13) Rigollet, R., *Ann. d'Astrophys.*, **14,** 181, 1951.
(14) Elkin, W. L., *Ap. J.*, **9,** 20, 1899; **10,** 25, 1899; **12,** 4, 1900.
(15) Whipple, F. L., *Proc. Am. Phil. Soc.*, **91,** (2), 189, 1947.
(16) Whipple, F. L., *Sky and Telescope*, **6** (70), 10, 1946–47.
(17) Aspinall, A., Clegg, J. A., and Hawkins, G. S., *Phil. Mag.*, **42,** 504, 1951.
(18) Davies, J. G., and Ellyett, C. D., *Phil. Mag.*, **40,** 614, 1949.
(19) Almond, Mary, Davies, J. G., and Lovell, A. C. B., *M.N.*, **111,** 585, 1951.
(20) Prentice, J. P. M., Lovell, A. C. B., and Banwell, C. J., *M.N.*, **107,** 155, 1947.
(21) Lovell, A. C. B., Banwell, C. J., and Clegg, J. A., *M.N.*, **107,** 164, 1947.
(22) Whipple, F. L., *Rev. Mod. Phys.*, **15,** 246, 1943.
(23) Davidson, I. A., and Hazzaa, I. B. (in preparation).
(24) Millman, P. M., and McKinley, D. W. R., *Sky and Telescope*, **8,** 114, 1949.
(25) Jacchia, L. G., *HCO–MIT Technical Reports* Nos. 2, 3 and 4, 1948–1949.
(26) Greenhow, J. S., *Proc. Phys. Soc.*, **65,** 169, 1952.
(27) Brédichin, T., *Bull. Imp. Nat. Moscow*, **1,** 1888.
(28) Hamid, S. E., Doctoral Thesis, Harvard University, 1950.
(29) Prentice, J. P. M. (private communication).
(30) Jacchia, L. G. (private communication).
(31) Hoffmeister, C. (private communication).

ON THE INTERNAL STRUCTURES OF JUPITER AND SATURN

B. Miles and W. H. Ramsey

(Received 1952 January 24)

Summary

One of the authors (*M.N.*, **111**, 427, 1951) has shown that the proportion of hydrogen in Jupiter is 76 per cent by mass and in Saturn 62 per cent by mass, assuming that the heavier elements are distributed uniformly throughout each planet. In the present calculations the heavier elements are assumed to be in part concentrated in a central core and in part distributed uniformly. This relaxation of the condition of chemical homogeneity has little influence on the estimated hydrogen contents, the extreme estimates for Jupiter being 76 and 84 per cent by mass and for Saturn 62 and 69 per cent by mass. The ellipticities of the planets due to their axial rotations suggest that each planet has a central concentration of heavy elements of the order of ten times the mass of the Earth; but the possibility of chemical homogeneity is not completely excluded by the present empirical data.

---

1. One of the authors has shown in a recent paper (**1**) that hydrogen is the predominant constituent of both Jupiter and Saturn. The ordinary molecular modification of solid hydrogen is stable only at the low pressures in the outer layers of the planets; in the deep interiors hydrogen will be metallic. Metallic hydrogen is the simplest of all solids from the point of view of atomic physics, and its pressure–density relationship can be computed accurately. The computed densities of solid molecular hydrogen, though less reliable than those of metallic hydrogen, are sufficiently accurate for calculations on the bulk characteristics of the planets. The theoretical pressure–density relationship refers to the absolute zero of temperature, but the temperatures in the interiors of the planets are too low to alter the densities appreciably; likewise, the presence of an atmosphere is of little importance, since its contributions to the mass and volume of the planet are negligible. Both Jupiter and Saturn are denser than hydrogen planets of the same mass, but by less than a factor of two. The relatively small proportions of heavier elements necessary to account for the observed mean densities were assumed in these calculations (**1**) to be distributed uniformly throughout each planet; in other words, the planets were assumed to be chemically homogeneous. The proportion of hydrogen in Jupiter was estimated to be 76 per cent by mass, and in Saturn 62 per cent by mass. The moments of inertia computed from the theoretical density distributions were close to, but definitely larger than, the values derived by means of the Radau–Darwin formula from the polar flattenings of the planets due to their axial rotations.

The principal weakness in the earlier calculations (**1**) is the assumption that the planets are chemically homogeneous. Each planet could contain a central concentration of heavy elements, as has been suggested by Jeffreys (**2**) and by Wildt (**3**). A central core of heavy elements is to be expected if the planets were formed by an aggregation process; only the heavier and less volatile materials would have been captured when the mass of the planet was small. Also, even if

a planet were initially chemically homogeneous, the heavier elements may have gravitated towards the centre. The discrepancies between the empirical and the computed moments of inertia indeed suggest central concentrations of heavy materials; but it will be shown later in the paper that the disagreement is partly due to the inadequacy of the Radau–Darwin treatment. In the present calculations the heavier elements will be assumed to be in part concentrated in a central core and in part distributed uniformly. It will be shown that this relaxation of the condition of chemical homogeneity has little influence on the estimated hydrogen contents of the planets. The central concentrations of mass influence primarily the computed moments of inertia of the planets and the ellipticities arising from their axial rotations. The extents of the central condensations will be estimated from the empirical data by a purely numerical method which is more accurate than the Radau–Darwin approximation.

2. If the density ρ of the material of a planet is known as a function of the pressure p, the bulk properties of the planet can be computed on the assumption of hydrostatic equilibrium. In the absence of rotation, the equation to be solved is

$$dp/dr = -\rho g(r), \tag{1}$$

where r is the distance from the centre of the planet and where $g(r)$ is the local acceleration due to gravity:

$$g(r) = (4\pi G/r^2)\int_0^r \rho(x)x^2\,dx, \tag{2}$$

G being the constant of gravitation. Equation (1) can be used for the Earth, since the centrifugal force is never more than 0·3 per cent of gravity. But on the surface of Jupiter the centrifugal force at the equator is 9 per cent of gravity, and on Saturn 16 per cent of gravity; it must therefore be taken into account in the hydrostatic equation (1). This can be done by the method adopted in the earlier paper (**1**). Any pressure p defines in the planet an oblate surface which is approximately a spheroid. Let r be the radius of the sphere which contains exactly the same volume as this surface. The pressure p is a function only of the parameter r, which will therefore be adopted as the independent variable. It can easily be shown that the equation for hydrostatic equilibrium is

$$dp/dr = -\rho\{g(r) - \tfrac{2}{3}\omega^2 r\}, \tag{3}$$

ω being the angular velocity of axial rotation; as before, $g(r)$ is defined by equation (2). This equation is to be solved as though the planet had spherical symmetry; the oblateness is allowed for in the definition of the parameter r. Equation (3) is not exact, fourth and higher powers of the angular velocity ω having been ignored; but it has been shown in reference (**1**) that it is adequate for the present purposes. This equation will be used throughout the paper; the angular velocity assumed for Jupiter corresponds to a rotational period of $9^h\,55^m$, and for Saturn to a period of $10^h\,38^m$.

Equation (3) will be integrated numerically on the assumption that the planet, apart from a central concentration of heavy elements, consists of a chemically homogeneous material whose pressure–density relationship is known. It is most convenient, as Bullen (**4**) found in analogous calculations on the terrestrial planets, to start the integration at the surface of the planet and to integrate inward to the core of heavy material. A single numerical integration is valid irrespective of the dimension of the central core. The mass of the central core depends on its

mean density, but it will be shown that the dependence is so slight that the density may be assumed to be infinite in these calculations. The only empirical data required in the integrations are the masses and radii of the planets. The mass and mean radius of Jupiter are

$$M = 1{\cdot}902 \times 10^{30}\,\text{g}, \qquad R = 69\,900\,\text{km}, \tag{4}$$

and of Saturn

$$M = 0{\cdot}569 \times 10^{30}\,\text{g}, \qquad R = 57\,550\,\text{km}. \tag{5}$$

The masses of the planets are known accurately, but the radii are uncertain by about 1 per cent. The mean density of Jupiter is $1{\cdot}33 \pm 0{\cdot}04\,\text{g/cm}^3$, and of Saturn $0{\cdot}71 \pm 0{\cdot}02\,\text{g/cm}^3$.

3. Planetary models have been constructed on the assumption that the planets consist entirely of hydrogen, apart from central concentrations of heavy materials; a numerical pressure–density relationship for hydrogen is contained in the earlier paper (1). The results of the calculations are presented in Tables I and II. In these tables r is the parameter introduced in equation (2), p and ρ are the corresponding pressure and density, and $M(r)$ is the mass contained within the surface defined by r:

$$M(r) = 4\pi \int_0^r \rho(x) x^2\,dx. \tag{6}$$

The hydrogen content of Jupiter is estimated to be about 80 per cent by mass and of Saturn about 65 per cent by mass, but the precise proportions depend on the densities of the central cores of heavy material. If the density of the heavy material is assumed to be $14\,\text{g/cm}^3$ at the pressures at the centres of the planets, the estimated hydrogen contents of Jupiter and Saturn are 76 and 63 per cent by mass respectively. The computed proportions of hydrogen are larger the denser the heavy material is assumed to be, and in the limit of infinite density the estimated hydrogen contents are 84 and 69 per cent by mass. At these enormous pressures the heavy material is unlikely to be less dense than $14\,\text{g/cm}^3$, which is only three times the corresponding density of hydrogen. Thus, irrespective of the dimensions of the central cores, the hydrogen contents compatible with the present planetary models are restricted to narrow limits, namely, 76 to 84 per cent by mass for Jupiter and 63 to 69 per cent by mass for Saturn. These small uncertainties in the compositions of the planets are not in themselves of especial interest in this paper. Moreover, the uncertainties have little influence on the computed moments of inertia and polar flattenings of the planets; the dimensions of the central cores are so small that the moments of inertia can be altered by only about 2 per cent. The dimensions of the central cores are of even less importance in the planetary models considered later in the paper. It will therefore be assumed that the central concentrations of heavy elements are so dense that they may be treated as mass points.

4. Planetary models have also been constructed on the assumption that each planet consists of a homogeneous mixture of hydrogen and helium, together with a dense central core of heavier elements. It has been shown in the earlier paper (1) that the density of a mixture containing n atoms of hydrogen to each atom of helium is

$$\rho = \{(n+4)/(n+4\alpha^{-1})\}\rho_{\text{H}}, \tag{7}$$

where ρ_{H} is the density of hydrogen at the pressure concerned and where α is the ratio of the densities of helium and hydrogen. The value of α is 4 in the

non-metallic outer layers of the planets, and it is 2·5 in the deep interiors where hydrogen is metallic. Equation (7) gives the pressure–density relationship of any mixture of hydrogen and helium in terms of the data for hydrogen, and this relationship has been used in constructing the planetary models. It has been

TABLE I

Estimated Density Distribution in Jupiter
(*Model* J_1—*heavy elements assumed concentrated at centre*)

r (10^9 cm)	p (10^{12} dyne/cm^2)	ρ (g/cm^3)	$M(r)$ (10^{27} g)
6·99	0	0·09	1902
6·9	0·03	0·17	1895
6·7	0·14	0·24	1871
6·5	0·28	0·28	1842
6·3	0·45	0·31	1812
6·1	0·64	0·33	1781
5·95	0·80	0·35	1757
5·95	0·80	0·77	1757
5·5	2·10	0·99	1595
5·0	4·08	1·26	1401
4·5	6·71	1·54	1203
4·0	10·10	1·84	1012
3·5	14·4	2·17	835
3·0	19·9	2·53	680
2·5	27·2	2·93	551
2·0	37·7	3·43	451
1·5	54·8	4·13	379
1·0	93	5·8	331
0	...	...	303

TABLE II

Estimated Density Distribution in Saturn
(*Model* S_1—*heavy elements assumed concentrated at centre*)

r (10^9 cm)	p (10^{12} dyne/cm^2)	ρ (g/cm^3)	$M(r)$ (10^{27} g)
5·755	0	0·09	569
5·6	0·02	0·15	562
5·4	0·06	0·20	548
5·2	0·11	0·23	534
5·0	0·17	0·25	518
4·5	0·36	0·30	479
4·0	0·62	0·33	443
3·72	0·80	0·35	425
3·72	0·80	0·77	425
3·5	1·15	0·83	397
3·0	2·19	1·01	336
2·5	3·69	1·21	284
2·0	6·01	1·48	241
1·5	10·1	1·85	209
1·0	20·0	2·53	188
0·5	62·2	4·39	178
0	...	...	176

shown in the previous paper (1) that the mean densities of the planets can be explained without central concentrations of heavy material if n is assumed to be 13·0 for Jupiter and 6·4 for Saturn. Smaller helium contents—that is, larger values of n—have been adopted in the present models and, as before, the masses

of the central cores of heavy material have been determined by integrating the hydrostatic equation (3) inward from the surface of the planet. The values of n adopted for Jupiter are 45 and 22, and for Saturn 18 and 9. The results of the calculations are presented in Tables III to VI. The masses of the central cores of heavy material are smaller the smaller the value of n, and the various

TABLE III

Estimated Density Distribution in Jupiter

(*Model* J_2; $n=45$)

r (10^9 cm)	p (10^{12} dyne/cm^2)	ρ (g/cm^3)	$M(r)$ (10^{27} g)
6·99	0	0·09	1902
6·9	0·03	0·19	1895
6·7	0·15	0·26	1868
6·5	0·30	0·30	1837
6·3	0·48	0·33	1804
6·1	0·69	0·36	1770
6·00	0·80	0·37	1754
6·00	0·80	0·81	1754
5·5	2·33	1·08	1558
5·0	4·41	1·36	1347
4·5	7·11	1·66	1133
4·0	10·47	1·97	928
3·5	14·6	2·29	740
3·0	19·6	2·63	577
2·5	25·8	3·00	444
2·0	34·1	3·43	341
1·5	46·7	4·00	271
1·0	70·7	4·93	227
0	...	...	201

TABLE IV

Estimated Density Distribution in Jupiter

(*Model* J_3; $n=22$)

r (10^9 cm)	p (10^{12} dyne/cm^2)	ρ (g/cm^3)	$M(r)$ (10^{27} g)
6·99	0	0·10	1902
6·9	0·03	0·20	1894
6·7	0·16	0·28	1865
6·5	0·32	0·33	1832
6·3	0·52	0·36	1797
6·1	0·74	0·39	1761
6·05	0·80	0·40	1752
6·05	0·80	0·85	1752
5·5	2·56	1·17	1519
5·0	4·74	1·48	1291
4·5	7·50	1·79	1060
4·0	10·81	2·10	839
3·5	14·7	2·42	640
3·0	19·1	2·73	469
2·5	24·0	3·05	332
2·0	29·9	3·39	229
1·5	37·4	3·78	161
1·0	49·7	4·35	120
0	...	...	99

planetary models lead to nearly the same hydrogen contents. The estimated hydrogen contents are smallest if the planets are assumed to be chemically homogeneous and largest if all the heavier elements are assumed to be concentrated at the centre. The extreme estimates for Jupiter are 76 and 84 per cent by mass, and for Saturn 62 and 69 per cent by mass. Thus the spatial distributions of the heavier elements within the planets have little influence on the estimated chemical compositions. The location of the heavier materials affects primarily the computed moments of inertia of the planets and the polar flattenings due to their rotations. The moment of inertia I is greatest if the heavier elements are distributed uniformly and least if all the heavier materials are concentrated at the centre. The extreme values of the ratio I/MR^2 are 0·223 and 0·282 for Jupiter and 0·189 and 0·285 for Saturn, *cf.* Tables VII and VIII. The values of I/MR^2 derived from the polar flattenings of Jupiter and Saturn using the Radau–Darwin approximation are 0·25 and 0·22 respectively, but the approximation may be in error by 10 per cent.

TABLE V

Estimated Density Distribution in Saturn

(*Model* S_2; $n=1.8$)

r (10^9 cm)	p (10^{12} dyne/cm^2)	ρ (g/cm^3)	$M(r)$ (10^{27} g)
5·755	0	0·10	569
5·6	0·02	0·19	560
5·4	0·07	0·24	544
5·2	0·13	0·28	526
5·0	0·20	0·30	507
4·5	0·43	0·35	460
4·0	0·72	0·40	418
3·88	0·80	0·40	409
3·88	0·80	0·86	409
3·5	1·43	0·99	349
3·0	2·47	1·17	277
2·5	3·82	1·38	217
2·0	5·69	1·61	169
1·5	8·63	1·93	134
1·0	14·7	2·46	113
0·5	39·1	3·90	102
0	...	...	96

5. The oblateness of a rotating planet can be calculated on the assumption that the interior is in hydrostatic equilibrium. This assumption is certainly valid in massive planets such as Jupiter and Saturn. Deviations from hydrostatic equilibrium cannot exceed the strength of the material, which is of the order of magnitude of 10^9 dyne/cm^2 for most solids. This pressure is negligible by planetary standards and could not introduce an appreciable error. Even for the Earth the ellipticity computed on the assumption of hydrostatic equilibrium is not in error by more than 0·5 per cent (**5**). A complete theoretical treatment of the figure of a planet requires a knowledge of the internal density distribution which was formerly not available for Jupiter and Saturn. The moments of inertia of the planets had therefore to be derived from the empirical ellipticities by means of the approximate Radau–Darwin formula. This approximation is reliable if the ratio I/MR^2 is not much smaller than 0·4, but it can be seriously in

error when I/MR^2 is as small as for Jupiter and Saturn; *cf.* reference (**6**). Also, second and higher powers of the ellipticity are ignored in the Radau–Darwin formula, which is not justified for Jupiter and Saturn. An accurate numerical treatment will therefore be used in preference to the Radau–Darwin approximation. The ellipticities of the planets will be computed on the basis of the various planetary models in the hope that some of these models can be eliminated by the empirical data. The empirical data for Jupiter are

$$e_s^{-1} = 15{\cdot}4 \pm 0{\cdot}2, \qquad e_s/m = 0{\cdot}73 \pm 0{\cdot}02, \tag{8}$$

and for Saturn

$$e_s^{-1} = 9{\cdot}5 + 0{\cdot}2, \qquad e_s/m = 0{\cdot}65 \pm 0{\cdot}02, \tag{9}$$

e_s being the surface ellipticity and m the ratio of the centrifugal and gravitational forces on the equator.

TABLE VI

Estimated Density Distribution in Saturn

(*Model* S_3; $n=9$)

r (10^9 cm)	p (10^{12} dyne/cm^2)	ρ (g/cm^3)	$M(r)$ (10^{27} g)
5·755	0	0·12	569
5·6	0·03	0·22	559
5·4	0·09	0·28	540
5·2	0·15	0·32	519
5·0	0·23	0·35	497
4·5	0·48	0·41	443
4·00	0·80	0·45	394
4·00	0·80	0·94	394
3·5	1·61	1·12	303
3·0	2·57	1·30	219
2·5	3·66	1·48	153
2·0	4·93	1·66	103
1·5	6·54	1·87	69
1·0	9·08	2·16	49
0·5	16·6	2·84	40
0	...	...	39

6. Darwin (**7**) and de Sitter (**8**) have given a comprehensive treatment of the figure of a planet which is more than adequate for the present purposes; the hydrostatic equations in the interior are treated accurately and only third and higher powers of the ellipticity are ignored. Bullard (**5**) has reduced this treatment to an entirely numerical procedure which is applicable if the internal density distribution is known; this method has been adopted in the present calculations. The equation of a surface of constant pressure is of the form

$$\beta = b\{1 - e\sin^2\phi + (\tfrac{5}{8}e^2 - \kappa)\sin^2 2\phi\}, \tag{10}$$

where β is the distance from the centre of the planet and ϕ the angle of latitude; e is the ellipticity of the surface and the quantity κ allows for the departure from an ellipsoid. As in equation (3), it is convenient to introduce the radius r of the sphere which contains exactly the same volume as the surface (10). The theory is most simply formulated in terms of the quantity

$$e' = e - 5e^2/42 + 4\kappa/7 \tag{11}$$

and its logarithmic derivative

$$\eta = d(\ln e')/d(\ln r). \tag{12}$$

De Sitter (**8**) has shown that η satisfies the equation

$$(1+\eta)^{1/2} = (5/\rho r^5)\int_0^r F(\eta)\bar{\rho} r^4\, dr, \tag{13}$$

where $\bar{\rho}$ is the mean density within the surface defined by r and where

$$F(\eta) = (1 + \tfrac{1}{2}\eta - \tfrac{1}{10}\eta^2 + \Delta)/(1+\eta)^{1/2}, \tag{14}$$

Δ being a small quantity proportional to the ellipticity. The importance of Δ in equation (14) has been examined and its omission alters the calculated ellipticities by less than 0·3 per cent; it has therefore been ignored in these calculations. For values of η less than unity the function $F(\eta)$ does not deviate from unity by more than 1 per cent. In the Radau–Darwin approximation $F(\eta)$ is replaced by unity and equation (13) reduces to

$$(1+\eta)^{1/2} = \tfrac{5}{2}\{1 - \tfrac{3}{2}(I/MR^2)\}, \tag{15}$$

I being the planet's moment of inertia. This approximation is not accurate for Jupiter and Saturn as the values of η are large, $F(\eta)$ being up to 7 per cent less than unity. Equation (13) has been integrated numerically using the internal density distributions derived above; the boundary condition is that η must vanish at the centre of the planet. The surface values of η (denoted by η_s) for the various planetary models are given in Tables VII and VIII. The magnitude of the parameter η_s is all that need be known about the internal density distribution so far as the figure of the planet is concerned. For a given value of η_s and a given angular velocity ω the ellipticity e_s of the planet can be found from the boundary condition at the surface

$$e_s'\eta_s = 5\mu/2 - 2e_s' + 10\mu^2/21 + 4e_s^2/7 - 6\mu e_s/7, \tag{16}$$

where e_s' is the value of e' at the surface and where

$$\mu = (\omega^2 R^3/MG), \tag{17}$$

M and R being the mass and mean radius of the planet. Equation (16) involves the quantity κ indirectly through the parameter e_s', *cf.* equation (11). De Sitter (**8**) has set an upper limit to the magnitude of κ at the surface

$$|\kappa| < \tfrac{5}{16}e_s\mu - \tfrac{1}{4}e_s^2, \tag{18}$$

and even this extreme value leads to an uncertainty of only 1 per cent in the computed ellipticities of the planets. The departure from an ellipsoid is therefore too small an effect to be included in the present calculations and κ has accordingly been put equal to zero. The results of the calculations are presented in Tables VII and VIII.

7. The agreement between the computed and empirical ellipticities of the planets cannot be expected to be better than 4 per cent. Not only are the empirical ellipticities uncertain by about 2 per cent, but the ratio μ defined by equation (17) may be in error by 2 or 3 per cent because of inaccuracies in the adopted values of the radii. The ratio I/MR^2 in best agreement with the empirical ellipticity is 0·267 for Jupiter and 0·262 for Saturn; these values are respectively 8 and 18 per cent larger than those indicated by the Radau–Darwin formula. The empirical data can determine the ratios I/MR^2 only to about 5 per cent. The probable masses of the central concentrations of heavy materials are $11 \pm 10\ M_E$ for Jupiter and $5 \pm 4\ M_E$ for Saturn; the mass M_E of the Earth is $5{\cdot}976 \times 10^{27}$ g. The models $\mathbf{J_3}$ and $\mathbf{S_3}$ give the best representations of the planets, but the chemically homogeneous models $\mathbf{J_4}$ and $\mathbf{S_4}$ cannot be completely excluded.

8. The present calculations were undertaken partly in an attempt to establish or refute the condensation theories of the origin of the solar system. This mode of formation of the planets would require the central concentrations of heavy materials in Jupiter and Saturn to be at least as massive as Neptune, that is, at least 17 M_E; *cf.* reference (**1**). The above calculations show that this requirement is compatible with the empirical data for Jupiter, but the central concentration in Saturn seems to be definitely less massive than Neptune. The discrepancy cannot be attributed to the assumption that the planets are chemically homogeneous, apart from the central concentrations of heavy materials; the estimated masses of the central cores are decreased if the mean atomic weight is assumed to increase gradually with depth. But the condensation theories of the origin of the solar system cannot be dismissed merely on account of this discrepancy for Saturn. The axial rotation of Saturn, and of Jupiter to a lesser degree, exhibit features which are not understood (**9**). The period of rotation adopted for Saturn is $10^h\,38^m$, but the apparent period is $10^h\,14^m$ at the equator and about 11^h in high latitudes. The variation of period with latitude is presumably due to circulation currents in the atmosphere but, in contrast to the Earth, the apparent period of rotation increases with latitude. The estimated mass of the central core in Saturn would be close to the mass of Neptune if the period indicated by equatorial spots were adopted. The observational data cannot be interpreted unambiguously until the nature of the atmospheric circulations is known. Should more reliable estimates of the parameter μ defined by equation (17) become available, the ellipticities corresponding to the various planetary models can easily be found from equation (16) using the values of η_s given in Tables VII and VIII. Second-order perturbations of the planets on their closest satellites may also provide a check on the planetary models (**10**).

TABLE VII

Computed Ellipticity of Jupiter *

Model	η_s	e_s^{-1}	I/MR^2
J_1	1·67	17·4	0·223
J_2	1·50	16·6	0·241
J_3	1·32	15·7	0·260
J_4	1·10	14·7	0·282

TABLE VIII

Computed Ellipticity of Saturn *

Model	η_s	e_s^{-1}	I/MR^2
S_1	1·97	11·5	0·189
S_2	1·67	10·6	0·220
S_3	1·34	9·68	0·256
S_4	1·04	8·79	0·285

* In models J_4 and S_4 the planets are assumed to be chemically homogeneous; the estimated internal density distributions are contained in the earlier paper (**1**).

The aggregation theories of the origin of the solar system relate the chemical compositions of Jupiter and Saturn in an interesting way. On these theories one would expect the central mass M_c of heavy materials to be the same for the two planets. An upper limit to the mass M_c is set by the following consideration. The value of n for Jupiter cannot be less than that for Saturn; that is, the material

captured by the larger planet must be at least as rich in hydrogen as that captured by the smaller planet. The value of n indicated by the mean density is 23 for both planets if M_c is assumed to be $19\,M_E$:

$$M_c = 19\,M_E, \quad n = 23. \tag{19}$$

Larger values of M_c would lead to larger values of n for Saturn than for Jupiter. On the other hand, M_c must be at least $17\,M_E$, the mass of Neptune. The mass of the central concentrations of heavy materials is therefore restricted to narrow limits and the value of n is nearly the same for the two planets. In other words, the difference in the hydrogen contents of Jupiter and Saturn is due mainly to the fact that the central core accounts for a larger fraction of the mass of the smaller planet. The value of n in relations (19) corresponds to 85 per cent hydrogen by mass and this is presumably the hydrogen content of the material from which the planets were formed. This relationship between the chemical compositions of Jupiter and Saturn is a welcome simplification; but it cannot be regarded as a proof that the planets were formed by an aggregation process.

The authors would like to express their appreciation to Professor Harold Jeffreys for much helpful correspondence and to Professor L. Rosenfeld and Professor Z. Kopal for the interest which they have shown in this work.

The Physical Laboratories,
The University,
Manchester, 13:
1952 *January* 22.

References

(1) W. H. Ramsey, *M.N.*, **111**, 427, 1951.
(2) Harold Jeffreys, *M.N.*, **84**, 534, 1924.
(3) Rupert Wildt, *Ap. J.*, **87**, 508, 1938.
(4) K. E. Bullen, *M.N.*, **109**, 457, 1949.
(5) E. C. Bullard, *M.N., Geophys. Suppl.*, **5**, 186, 1948.
(6) Harold Jeffreys, *M.N.*, **111**, 410, 1951.
(7) G. Darwin, *M.N.*, **60**, 82, 1899.
(8) W. de Sitter, *B.A.N.*, **2**, 97, 1924.
(9) H. N. Russell, R. S. Dugan and J. Q. Stewart, *Astronomy*, Ginn and Company, Boston, 1945.
(10) D. Brouwer, *A.J.*, **51**, 223, 1946.

CONTENTS

PAGE

J. A. Rottenberg, Theoretical line profiles for stars of P Cygni type 125

G. L. Camm, Self-gravitating star systems. II 155

H. H. Plaskett, The Oxford solar spectroscope 177

H. Bondi, On spherically symmetrical accretion 195

K. N. Dodd and W. H. McCrea, On the effect of interstellar matter on the motion of a star 205

T. Gold, The alignment of galactic dust 215

G. S. Hawkins and Mary Almond, Radio echo observations of the major night-time meteor streams 219

B. Miles and W. H. Ramsey, On the internal structures of Jupiter and Saturn ... 234

Printed in London by Taylor & Francis, Ltd., 1952 *August*